NAVAL AIR ENGINEERING CENTER
PHILADELPHIA 12, PENNSYLVANIA

AD601447

AERONAUTICAL MATERIALS LABORATORY

REPORT NO. NAEC-AML-1831   DATE 1 April 1964

ANISOTROPIC MECHANICAL BEHAVIOR IN SAPPHIRE
(Al_2O_3) WHISKERS

PROBLEM ASSIGNMENT NO. 10-38 UNDER BUREAU OF NAVAL
WEAPONS WEPTASK RRMA 02 018/200 1/R007 05 01

PREPARED BY:

PAUL J. SOLTIS
PROJECT ENGINEER

APPROVED BY:

WALTER J. FEDYNA, HEAD
PHYSICAL METALLURGY BRANCH

F. S. WILLIAMS, SUPERINTENDENT
METALLURGICAL DIVISION

1

TABLE OF CONTENTS

LIST OF TABLES

LIST OF PLATES

LIST OF SYMBOLS

w - width of cross section

t - thickness of whisker

t_T - sum of bases of a trapezoid

a - length of one side of a hexagon

A - area of cross section

ϵ_{TOT} - total strain

σ_f - fracture strength

σ_y - initial yield point or proportional limit

E - Young's Modulus of Elasticity or the elastic modulus

E_m - measured elastic modulus

$\sigma_{C.R.S.S.}$ - critical resolved shear stress

ϕ - angle normal to slip plane makes with tensile axis

λ - angle slip direction makes with tensile axis

G - shear modulus or modulus of rigidity

b - Burgers vector

γ - stacking fault energy

σ_r - short-range repulsive force

σ_A - long-range attractive force

r - distance between two atoms

r_0 - equilibrium distance between two atoms

ABSTRACT

A method of static tension testing whiskers was described which made it possible to obtain more precise data on the mechanical behavior of sapphire (Al_2O_3) whiskers at 25°C. Anisotropy was detected and measured in tensile properties of a sample of near-micron size whiskers. Measured elastic moduli, whisker cross section geometry, and yield points were useful in identifying whiskers having axes corresponding to simple growth directions in sapphire; i.e., the $<0001>$, $<11\bar{2}0>$, and $<1\bar{1}00>$ directions.

Behavior in whiskers of each orientation ranged from very brittle to very ductile as noted in fractures of tension specimens and stress-strain curves; hence, despite only 0.1% total impurities, heterogeneous growth conditions may result in whiskers showing varying degrees of purity. Impurities are seen as influencing not only the morphology of the whiskers, but also the frequency of stacking defect formation during their growth. A limiting width of cross section, 6.3μ, was found above which whiskers having $<0001>$ orientation were determined to have nucleated and grown by means of a screw dislocation mechanism; below this size, growth is believed to have taken place by way of two-dimensional nucleation.

A pronounced size effect was found in measured elastic moduli and fracture strengths, and trends toward maxima were seen only in the limit of extremely fine size. The maximum measured elastic moduli obtained on the finest whiskers, ascertained to be near structural perfection, are 71.0×10^6 lbs./in.^{2}, 180×10^6 lbs./in.^{2}, and 330×10^6 lbs./in.^{2} corresponding to the $<0001>$, $<11\bar{2}0>$, and $<1\bar{1}00>$ directions, respectively. The large difference found for the $<11\bar{2}0>$ and $<1\bar{1}00>$ directions suggests that elasticity is non-isotropic for whiskers growing in these crystal directions. The highest fracture strength, 3.23×10^6 lbs./in.^{2}, was found in $<11\bar{2}0>$ whiskers. The true cohesive strength can be approached only in extremely fine whiskers having width to thickness ratios near unity where slip plane bending is minimized.

For ductile $<0001>$ whiskers, the primary slip system is basal slip, $(0001) <11\bar{2}0>$; in $<11\bar{2}0>$ and $<1\bar{1}00>$ whiskers, it is prismatic slip, $\{11\bar{2}0\} <1\bar{1}00>$. Although slip planes may be oriented normal to the axis of tension in unstrained whiskers, slip plane bending accounts for the plasticity observed. The forces required to nucleate dislocations in the basal and prismatic slip systems of structurally perfect whiskers was found to be about G/88 and the Peierls-Nabarro forces required to move them about 3.0×10^{-3} G where G for two whisker

orientations, $\langle 0001 \rangle$ and $\langle 11\bar{2}0 \rangle$, are i.   he same proportion as the measured elastic moduli. A rough calcul.   n of stacking fault energy in basal slip yielded 98 ergs/cm . Jog formation accounts for the high work hardening rates observed in ress-strain curves.

I. INTRODUCTION

The phenomenon of fibrous or whisker growth of a solid is one about which many instances could be cited; the first reported dates back several centuries. A comprehensive review of the growth of crystal whiskers which includes a classification of whiskers according to growth conditions, and a theoretical treatment of growth mechanisms was made by Nabarro and Jackson, reference 1. It was only recently, however, that Herring and Galt, reference 2, brought attention to the fact that various materials in the form of whiskers exhibit exceptionally high strengths, approaching the theoretical, as compared to the much lower strengths shown by these materials in bulk form. This behavior in whiskers is attributed to a high degree of structural perfection. Since whiskers are known to grow along preferred crystallographic directions, usually simple directions such as the crystallographic axes of the reference crystal, it should be possible to detect mechanical anisotropy in whiskers whose axes are parallel to such directions. In the light of the above, an investigation was made of the anisotropy in Young's Modulus of elasticity as well as the mechanical strength of sapphire, $\propto Al_2O_3$ (corundum)*, using static tension tests of ultra-fine whiskers having different orientations. Because of the relatively high purity of the whiskers used in this investigation, it was also possible to study their dislocation structure and to make observations concerning their plastic behavior.

Background of Past Research on Sapphire (Al_2O_3)

A. Crystal Structure

According to existing crystallographic specifications, reference 3, the structure of sapphire belongs to the space group $D_{3d}^6 = R\overline{3}C$. It can be described in terms of either a hexagonal unit cell or a rhombohedral unit cell which is triply primitive with respect to the hexagonal unit cell. Sapphire is trigonal and has been assigned, reference 4, to the point group $\overline{3}m$ whose symmetry elements consist of three vertical planes of symmetry intersecting in an inversion triad axis, three

---

*The terms sapphire and $\propto Al_2O_3$ (corundum) are used here synonymously. According to texts on mineralogy, sapphire is regarded as a distinct variety of gem corundum in that it contains a small quantity of impurities which impart color to it. Also, commercially produced Al_2O_3 may often be referred to as alumina.

horizontal diad axes normal to the symmetry planes, and a center as shown in Plate 1 (a). In crystallography, the trigonal system also has been regarded as a hexagonal subsystem.

Past studies, references 5 and 6, indicated that both Al_2O_3 and zinc (hexagonal close-packed) could undergo plastic basal bending and subsequent polygonization by closely related dislocation mechanisms. Kronberg, reference 7, noting from previous work, references 8 and 9, that the oxygen ions in sapphire are very nearly in hexagonal closest packing, with aluminum ions occupying octahedral interstices of the oxygen framework, correlated the sapphire structure with metals having hexagonal closest packing. To satisfy valency requirements, only one out of every three octahedral sites is unoccupied so that each aluminum ion is surrounded by six oxygen ions and each oxygen ion is surrounded by four aluminum ions.

In Plate 1 (b), the hexagonal morphological unit cell shows the distribution of aluminum ions and empty octahedral sites, and the smallest rhombohedral unit cell which correctly describes the positions of cations alone. The true structural unit cell determined by x-ray data has a C_O lattice parameter of 12.97 A° with a c/a ratio of 2.730; whereas C_O for the morphological unit cell based on measurements made on real crystals with well-developed plane faces is actually half this value giving a c/a ratio of 1.365. The C_O translation for the morphological unit cell is accomplished by 3 layers of oxygen ions with 3 sheets of contiguous aluminum ions and holes. A top view illustrating the arrangement of aluminum ions and holes between the two layers of oxide ions as described by Kronberg is given in Plate 1 (c).

Although it appears logical that a structural unit cell should be used instead of the morphological unit cell, Kronberg points out that use of the morphological unit cell could have advantages in studies of mechanical properties. Morphological unit cells have surfaces parallel to well-developed growth faces which are usually planes of high atomic density. Mechanical properties are frequently described in terms of such planes since these are specified by simple indices and well known morphological faces. Hence the morphological unit cell has been taken in this study as a frame of reference.

B. Dislocation Systems

Two common modes of plastic deformation in sapphire are basal and prismatic slip. Basal slip has been observed by McCandless and Yenni, reference 10, at 1300°-1400°C in rods stressed in bending with basal planes oriented 30°-75° to the cylindrical axis. Also, Wachtman and Maxwell, reference 11, tensile crept Al_2O_3 at 900°C at a resolved shear stress of 10,000 lbs./in.^{2} but could not induce creep in specimens

at 1000°C when the basal planes were oriented parallel to the rod axis.
Wachtman determined the slip direction at 1300°C to be $<11\bar{2}0>$ which
was later confirmed by Kronberg, reference 12, for dynamical tensile
loading in the temperature range 1300°-2000°C. The second slip system,
prismatic slip, was found by Klassen-Neckliudova, Ikornikova, and
Tomolovskii, reference 13, who deformed sapphire above 2000°C and by
Scheuplein and Gibbs, reference 14, who bend tested sapphire in an
oxygen gas flame, presumably at about 2000°C. The observed slip direc-
tion was $<1\bar{1}00>$. Gibbs, reference 15, reported the following
concerning the dislocation systems in sapphire: Basal slip involves (0001)
slip planes and $[11\bar{2}0]$, $[\bar{1}2\bar{1}0]$, $[\bar{2}110]$ Burgers vectors; prismatic slip
involves (11$\bar{2}$0), ($\bar{2}$110), ($1\bar{2}$10) slip planes and $[1\bar{1}00]$, $[01\bar{1}0]$, $[\bar{1}010]$
Burgers vectors; and a slip system involving an unspecified slip plane
and $[0001]$ Burgers vector possibly gives rise to spiral growth of
whiskers on the basal plane.

     Kronberg, reference 16, who made a comprehensive study of basal
slip and twinning in Al_2O_3 suggests that although the crystallographic
elements for basal slip in Al_2O_3 are the same as for zinc; i.e., $\{0001\}$
$<11\bar{2}0>$, there is a structural difference between them. In zinc, the
closest packed direction is parallel to a $<11\bar{2}0>$ direction; whereas,
in sapphire the $<11\bar{2}0>$ direction is at 30° to a close packed row of
oxygen ions. A net slip translation of a close packed layer of atoms
in zinc involves only shear over an identical underlying layer of close
packed atoms while in sapphire, it involves shear over an intervening
layer of interstitial ions as well. A comparison of the $<11\bar{2}0>$ slip
directions in zinc and sapphire as formalized by Kronberg is shown in
Plate 2.

     Using the principle that the self-energy of a dislocation is
proportional to the square of its Burgers vector, references 17 and 18.
Krongberg predicted the existence in sapphire of extended dislocations
composed of half partial and quarter partial dislocations with Burgers
vectors shorter than the original total dislocation whose Burgers vector
is in the $<11\bar{2}0>$ direction. Thus, by comparing self energies of dis-
locations, it can be shown that flow along a $<11\bar{2}0>$ direction is
favored by a factor of 3 over flow along a $<10\bar{1}0>$ direction based on
the B^2 criterion applied to the structural repeat distance of total
dislocations having Burgers vectors in these crystal directions (see
Plate 3 (a)). Also, it can be shown that a total dislocation with a
Burgers vector in the $<11\bar{2}0>$ direction can lower its energy by dis-
sociating into half partials and quarter partials as illustrated in
Plate 3 (b). The total dislocation is split first by dissociation into
half partials with $B = 1/3 <10\bar{1}0> = A_0/\sqrt{3}$, followed by further split-
ting of half partials into quarter partials with $B = 1/3 <11\bar{2}0> = 1/3 A_0$.
The self energy of each quarter partial is thus 1/9 of the total disloca-

tion; and in addition, there would be a decrease in strain energy associated with the elimination of the climbing of oxide ion over oxide ion, as required for the total dislocation. A schematic diagram of the extended ribbon consisting of quarter partials is given in Plate 3 (c).

C. Mechanical Properties

Substantial data on the mechanical properties of polycrystalline alumina, called "sinteralumina," was reported by Singer and Thurnauer, reference 19. In the cold, the compressive strength of sinteralumina is 3×10^4 kg/cm^2 (4.3×10^5 lbs./in.^{2}); the maximum tensile strength is 2.7×10^3 kg/cm^2 (3.9×10^4 lbs./in.^{2}). Using rods of circular cross section, tensile strength was found to increase with decreasing diameter of the rods. Young's Modulus for sinteralumina was reported to be 5.88×10^6 kg/cm^2 (83.5×10^6 lbs./in.^{2}), and this was compared with the value for pure crystals of corundum, 5.2×10^6 kg/cm^2 (74×10^6 lbs./in.^{2}). A size effect was noted again, and for decreasing diameter of the test rod, Young's Modulus rose toward the maximum value found for a single corundum crystal. At the largest diameter (0.0125 cm) Young's Modulus fell to its lowest determined value, 2.8×10^6 kg/cm^2 (40×10^6 lbs./in.^{2}). Although no data was presented, impurities were found to reduce the elastic modulus as expected.

Sets of elastic compliance coefficients, s_{ij}, and elastic stiffness coefficients, c_{ij}, derived from the classical theory of elasticity, also have been determined for sapphire. In the classical theory, a linear relationship is assumed, by reason of Hooke's law, between six independent components of stress and six independent components of strain which leads to 21 independent elastic constants for a crystal having no symmetry and six independent elastic constants for the case of sapphire which has trigonal symmetry, reference 20.

Using a dynamic method based on resonant frequency techniques, sets of six elastic compliance coefficients and six elastic stiffness coefficients were determined first by Sundra Rao, reference 21, on large synthetic crystals of alumina and by Bhimasenschar, reference 22, on large natural crystals of corundum. Later, Mayer and Hiedemann, reference 23, suggested that the method of exciting vibrations used by the Indian workers could give spurious resonances which result in incorrect resonances and therefore redetermined the elastic constants for synthetic sapphire. More recently, Wachtman et al., reference 24, suggested a frequency dependence and redetermined the elastic constants for synthetic crystals of corundum using the low kilocycle per second range but found results that agreed reasonably well with the data of M-H. However, a discrepancy was still found in the value obtained for the C_{14}

constant. Using the data of Wachtman et al., Young's modulus of elasticity for the principal directions in sapphire, the $\langle 0001 \rangle$, $\langle 11\bar{2}0 \rangle$, and $\langle 1\bar{1}00 \rangle$ directions, could be determined using the formula, reference 25,

$$\frac{1}{E} = (1 - \ell_3^2)S_{11} + \ell_3^4 S_{33} + \ell_3^2 (1 - \ell_3^2)(2S_{13} + S_{44}) + 2\ell_2\ell_3$$

$$(3\ell_1^2 - \ell_2^2)S_{14} + 2\ell_1\ell_3(3\ell_2^2 - \ell_1^2)S_{25} \tag{1}$$

where ℓ_1, ℓ_2, and ℓ_3 are direction cosines of a unit vector using orthogonal axes. The S_{33} and S_{11} constants in sapphire are 2.170 x 10^{-13} cm^2/dyne and 2.353 x 10^{-13} cm^2/dyne respectively; hence Young's Modulus of elasticity for the $\langle 0001 \rangle$ direction is 66.0 x 10^6 lbs./in.^{2}, and since elasticity according to rules of symmetry is isotropic in the basal plane, Young's Modulus of elasticity for the $\langle 11\bar{2}0 \rangle$ and $\langle 1\bar{1}00 \rangle$ directions is 61.0 x 10^6 lbs./in.^{2}.

D. Whiskers (Growth and Mechanical Properties)

Webb and Forgeng, reference 26, were first to report information on the growth of sapphire whiskers. The whiskers were produced by heating a small amount of aluminum or the intermetallic compound Ti_3Al containing a small excess of aluminum to between 1300° and 1450°C in a stream of hydrogen for 2 to 24 hours. Subsequently, DeVries and Sears, reference 27, and Brenner, reference 28, also reported data on sapphire whiskers. Generally, much of the information reported was concerned with c-axis whiskers; i.e., whiskers whose axes are parallel to the $\langle 0001 \rangle$ direction in sapphire. The c-axis whiskers showed hexagon cross sections and were found to have an axial pore which was attributed to the presence of a screw dislocation. Frank, reference 29, demonstrated how a hollow core along the axis of a screw dislocation should provide it with an energetically favorable crystallographic configuration. Presence of the axial pore in a c-axis whisker could thus be explained easily by the high elastic constant, and large Burgers vector, about 13A°, reported for sapphire.

Apart from the c-axis whiskers, Sears and DeVries, reference 30, grew Al_2O_3 whiskers at 1800°-2000°C which had axes parallel to the $\langle 1\bar{1}00 \rangle$ direction in sapphire; hence, these were called a-axis whiskers. The a-axis whiskers tended to broaden into platelets at their free-ends. Edwards and Happel, reference 31, were able to control the orientation

of sapphire whiskers by growing them on the surface of an alumina sub-
strate whose orientation was determined by x-ray diffraction. Not only
were c-axis whiskers produced in this way but also a-axis whiskers which
were observed growing in 12 equally spaced directions in the basal plane.
The a-axis whiskers broke into two distinct sets, a $<11\bar{2}0>$ set and a
$<1\bar{1}00>$ set, with each set showing six-fold symmetry about the c-axis.

Brenner, reference 32, reported tensile data on c-axis whiskers
in the range 25°-2030°C. These whiskers were grown by heating a por-
celain boat filled with aluminum in a flowing stream of hydrogen (dew
point - 55°C) at about 1250°C; whiskers formed as a wool over the open
top of the boat. In initial tests, specimens fractured at the grips.
This difficulty was attributed to stress concentration and a weak inter-
face between the whisker and fused beads on its ends which provided
supporting surfaces through which tensile load was applied. To overcome
this difficulty, the midsection of the whisker was thinned by vaporiza-
tion at a temperature of about 1800°-1900°C. Calculations of tensile
strength were made assuming a circular cross section, and since the
whisker was tapered to a minimum diameter at its midsection, only frac-
ture strength could be determined. The highest average tensile strength
at 25°C was found to be 900,000 lbs./in.^{2}, this stands in contrast to
the roughly 38,000 lbs./in.^{2} reported for fine rods of polycrystalline
material, reference 33. By assuming $E = 60 \times 10^6$ lbs./in.^{2} and using
the maximum fracture strength at room temperature, the maximum elastic
strain was estimated to be about 2.5% which is in agreement with that
measured by Webb and Forgeng, reference 34, 1.0-2.3%, in bend tests of
sapphire whiskers.

Advantages of Further Research on Al$_2$O$_3$ Whiskers

Although substantial literature has appeared on the growth of sapphire
whiskers, most of the work done thus far has been concerned with whiskers
of considerably more than micron dimensions. Contrary to what might be
expected, not all whiskers of various materials show a high degree of
crystal perfection. Gorsuch, reference 35, using an etch pit technique
found numerous "grown-in" dislocations in iron whiskers in the size
range 50 to 100μ ; there was some qualitative indication that the
degree of crystal perfection increased with decrease in whisker diameter
and with increase in purity of the halide salt used in their growth.
It was not possible to use the etch pit technique on whiskers less than
10μ ; yet, this is the size range where the tensile strength of whiskers
rises rapidly. Brenner, reference 36, found formulas showing the average
tensile strength of iron and copper whiskers varying inversely as the
diameter of the whiskers.

The present study shows that sapphire whiskers can be grown to
extremely fine size, submicron in thickness, in fairly large quantities,

and with different crystallographic orientations. Also, these whiskers can be grown to relatively high purity, in the region where the crystal shows plasticity, and presumably properties of material in a state of near-structural perfection. An attempt was made, therefore, to test these whiskers in tension in order to determine whether they show consistently high strength and possibly a yield point. The test was designed so that Young's Modulus of elasticity could also be measured. Another objective of the tests was to determine what effect anisotropy would have on tensile properties. The effect of anisotropy on Young's Modulus of elasticity is particularly of interest since data on elastic compliance and stiffness coefficients for comparatively large macrocrystals of Al_2O_3 reported by various investigators still show marked discrepancies. These might be explained by the static tension tests of structurally perfect, submicron, sapphire whiskers. Such tests would not only serve as a check on these data but also on earlier static tension tests of large macrocrystals of Al_2O_3.

II. EXPERIMENTAL PROCEDURES

A. Method of Producing Al_2O_3 Whiskers

The sapphire whiskers, obtained from Horizons, Incorporated, were produced by a method similar to that used by Webb and Forgeng, reference 37. A crucible of molten, high purity aluminum was heated to about 1300°-1450°C in a stream of hydrogen (dew point -55°F) until the whiskers nucleated and grew to sufficient length on an alumina rod suspended above the molten metal. After cooling to room temperature, the alumina rod was removed from the furnace and the whiskers, like a layer of wool, were scraped from its surface. Analysis, reference 38, of a sample of these fine sapphire whiskers indicated that they are $\propto Al_2O_3$ (corundum hexagonal) crystals.

B. Description of Whiskers

A sample of the sapphire whiskers is shown in Plate 4 (a), (b), and (c). The finest whiskers are highly elastic; some which were mounted on a glass slide could be bent to a very sharp radius and still spring back to needle-like straightness on removal of constraining forces. A few submicron whiskers, as evidenced by their transparency to the electron beam, are shown in the electron transmission photomicrograph of Plate 4 (c). The large whisker at center shows many smaller whiskers which had nucleated and grown at its edges. This pattern of growth possibly accounts for striations normal to the axis on the surface of some very large whiskers observed under the light microscope. Although photographic evidence cannot be presented, star-like patterns

of sapphire whiskers were also observed. These patterns consisted of six whiskers, 60° apart, emanating from a central axis normal to the axes of the whiskers. These "star" whiskers fit the description of basal plane whiskers previously described by Edwards and Happel, reference 39. Star-like patterns sometimes occurred in groups forming a mesh or screen with whiskers growing in one plane, presumably the basal plane.

The dislocation structure of the sapphire whiskers was studied in the electron microscope using magnifications at or above 10,000X. Also, the crystal structure of the whiskers was further investigated using electron diffraction techniques.

Spectrographic analysis of a small quantity of the whiskers showed the impurity content, mainly silicon, to be about 0.1%. Iron was the only other trace element detected. A small sample of sapphire whiskers of roughly equal purity was provided by the General Electric Company which were used to lend supporting evidence to conclusions drawn during the present study. Data on these whiskers were labeled to distinguish them from others.

C. Selection of Specimens for Tension Tests

The tension tests performed on the sapphire whiskers were intended to be elaborate since not only was strength to be determined, but also the elastic modulus. Test specimens were selected on the basis of their size, uniformity of cross section, and surface smoothness. Usually, the finest whiskers were selected for the tests. These whiskers showed the smoothest surface finish, appeared to be structurally homogeneous monofilaments, were least susceptible to surface damage during handling, and tended to have fairly uniform cross sections. Most of the whiskers were ribbon-like and had a slight taper which could easily escape notice. The tension specimens were usually broken from longer filaments along sections which showed a minimum of tapering, so that after mounting on the tensile grips, area of cross section at the ends of the gauge length varies only about 5-10%.

Many of the whiskers selected for the tests had thicknesses under 1μ while width varied from slightly above 1μ to 20μ. Since these were expected to exhibit strengths approaching the theoretical, it made them the most desirable for testing purposes. Lengths of the specimens selected for the test were not less than 3/32 inch. A 1/32 inch gauge length was found to yield the best results.

D. The Whisker Tensile Apparatus

The apparatus used to obtain tensile data on the sapphire whiskers was fashioned after a tensile testing device designed by

Emrick and Gegel, reference 40, but with a modified whisker mounting fixture and tensile grips redesigned to further minimize bending and twisting of the whisker near the grips. Also, a Kodak contour pro-jector with a fixed magnification of 100X was used for making strain measurements instead of the elaborate optical system used in the original design. The modified version of the tensile apparatus is shown in Plate 5 and details of its various working components in Plates 6, 7, and 8. Briefly, the test consists of applying an axial tensile load to the whisker mounted on the centerline between two drill rod tensile grips through a calibrated, steel spring which is coupled to a micrometer head capable of measuring spring extension to the near-est thousandth inch. Calibration curves drawn for the steel springs were checked before and after a series of tests to avoid errors from any change in spring constant. The calibration curves are quite linear and do not change significantly during the short period a series of tests are run; hence, fracture load can be measured accur-ately to within one percent of the actual value.

E. Details on Measurements

Strain measurements were obtained directly from the screen on the contour projector. In one method, a sheet of tracing paper was placed over the shadow image of the tensile grips shown in Plate 8 (b) and taped firmly to the screen. Using a sharp, hard-lead pencil, gauge marks as outlined by the ground and lapped, flat tips of the tensile grips were drawn with a straight edge normal to the axis of the speci-men with the movable tensile grip hanging free. A 5X pocket magnifier was found to be useful in positioning the straight edge before each strain increment was drawn. The movable tensile grip usually represented a small percentage of the rupture load, less than 5%. Lines were traced over the flat tip of the movable tensile grip after equally spaced load increments until the specimen ruptured. Distance between penciled lines was measured with a telescopic, micrometer-measuring microscope. Since the whiskers showed a tendency toward brittle-like fracture, speci-men elongation was expected to be elastic strain over a major portion of the stress-strain curve. The error in total specimen elongation was estimated at about 5%.

Another method used in making strain measurements involved substitution of a polaroid camera attachment in place of the tracing paper. This technique has advantages in that a permanent visual record of the entire test can be made except for a fractional load increment near the point of rupture. Thus, not only was a permanent record of strain obtained but also a visual record of the specimen configuration, bond configuration at the tips of the grips, and specimen alignment during the course of the test. If any doubt was

cast on a test result, the visual record could always be reviewed. A few test results were discarded on the basis of observations made on such records. The photographic method is not without disadvantages, however, and care had to be exercised in maintaining constant exposure time for each strain measurement, and allowance had to be made for film response from one roll of film to another. Despite these apparent disadvantages, the error in strain measurements using the telescopic, micrometer-measuring microscope proved to be about the same as in the previous method. Most of the test data was obtained using the photographic technique. The sensitivity of strain measurement was estimated to be about 0.0003. The above methods of strain measurement were therefore sufficiently sensitive to provide reliable data.

Cross sections of tension specimens were measured with a light microscope using an oil immersion objective. The measurements were made near the fracture surface with the whisker axis normal to the optical axis of the microscope objective as well as directly on the fracture surface. Usually, if one method is in error in one of its dimensions, the other method will call attention to it. Overall accuracy of the tests was found to depend very much on the accuracy in measurement of cross sections. Preliminary measurements were made with a micrometer eyepiece, and whenever possible, photographs were taken of fractures on 35 mm film. Projection techniques allowed increased magnifications which were used especially on very thin whiskers where width to thickness ratios were reasonably high, about 10:1. Dimensional ratios obtained from the projected image applied to the preliminary measurements allowed an increase of accuracy in measurements made on the thickness dimension. The resulting error in calculated tensile strength was estimated at about 10%.

In estimating the accuracy of the calculated elastic moduli, it was not only necessary to consider the accuracy in the measurement of cross sections but also the accuracy of elastic strain measurements and amount of specimen tapering. The effect of a slight taper was assumed to be nullified by taking the average area of sections near the ends of the gauge length. Considering that many of the calculated elastic moduli in initial tests were very high, it was presumed that the strain contribution from the bond between the whisker and tensile grips was immeasurably small. Accurate alignment of the whisker with respect to the tensile grips was attained by aligning the grips in two directions at right angles to each other under a binocular microscope with an eyepiece containing cross hairs.

Each whisker was cemented to the tensile grips using a solution of Duco cement in acetone, about a 1:1 ratio, which after evaporization of acetone forms a strong bond between them. The whisker during this process is perfectly straight, resting inside a scribed line along the

axes of the grips, and free of any perceptible strain. A side view is shown in Plate 8 (c). Later observation of the bond between the whisker and grips revealed that the cement covered all sides of the whisker including the flat face adjacent to the grip but did not flow over the gauge length area.

The meniscus between the whisker and the tensile grips was usually very sharp indicating that there was very little tendency for cement to run out along the gauge length section of the whisker. The cementing operation was performed under a binocular microscope where the progress of cement flow along the whisker could be closely watched. Since much of the acetone evaporates in a few minutes, the cement readily becomes very viscous and its flow is soon brought to a stand-still. This is in contrast with epoxy or hard, thermosetting resins which may take hours to set and which usually show a strong tendency to flow, particularly on smooth surfaces. If the gauge length surface should become contaminated even with a superficial layer of cement solution, its presence rapidly becomes evident by the appearance of interference colors similar to those shown by soap films; hence, the specimen could immediately be discarded. Such accidents, however, can easily be avoided after a little experience is acquired in handling the cement. It can be said with certainty that surface contamination on the gauge length section of the whisker was completely avoided except for possibly a monatomic layer of adsorbed air or moisture.

A limiting size for sapphire whiskers, about 10^{-6} in.^{2}, was found where the bond between the whisker and grip failed and resulted in very low calculated elastic moduli; hence, the tests were limited to whiskers in the size range 10^{-10} to 10^{-7} in.^{2} corresponding to very low fracture loads, on the order of a few grams for many tests. The good bonding exhibited for whiskers of this size appears to be related to the high surface to volume ratio of the whiskers. The error in the calculated elastic modulus was estimated at about 15 to 20%.

The elastic modulus or what is formally recognized as Young's Modulus of elasticity, E, is determined by the relation

$$E = \frac{\sigma}{\epsilon} \qquad (2)$$

where σ, the stress in the elastic region of the stress-strain curve, is proportional to the strain ϵ. Substituting the parameters used experimentally,

$$\sigma = \frac{T}{A} \qquad \text{and} \qquad \epsilon = \frac{\Delta \ell}{\ell}$$

where T is the load applied in tension, A is the area of cross section, ℓ is the projected original gauge length, and $\Delta \ell$ is the change in projected gauge length, yields the working formula

$$E_m = \frac{T}{A} \cdot \frac{\ell}{\Delta \ell} \qquad (3)$$

where E_m represents the experimentally measured value of the elastic modulus.

III. RESULTS

A. Examination With the Electron Microscope

1. Electron Diffraction

Electron diffraction from the large face of an a-axis whisker located in the diffraction chamber of the electron microscope yielded the Laue pattern shown in Plate 9 (a). Patterns such as this can be used to study the surface structure of solids as demonstrated by Mac Rae, reference 41. The pattern compares reasonably well with the model of the basal layers in sapphire described by Kronberg in Plate 1 (c). The six bright spots at center can be connected by lines to form a hexagon similar to those connecting the empty octahedral sites in the model. Reflections from the aluminum ions are less intense and cannot be seen near the center of the pattern, but by extending the two-dimensional network of hexagons starting with the one at center, the less intense spots can be detected in regions farther away from center. In the farthest regions away from center, it will be noted that some of the diffraction spots are doubled. This double diffraction is brought about when the whisker is sufficiently fine that the column representing the electron beam overlaps the whisker section at two edges; with whiskers having larger widths, the effect disappears. Diffraction from the sapphire crystal thus indicates that there is a strong concentration of electrons at empty octahedral sites which contribute to atomic binding as suggested by Kronberg.

There is a difference in the Laue pattern of Plate 9 (a) and the model of Plate 1 (c). In the model, a two-dimensional network of regular hexagons can be described; whereas, in the Laue pattern, the hexagons in the network are not regular but slightly distorted so that the diagonals differ in length and the angles are found to deviate by as much as 5°. By slightly rotating the specimen in the diffraction chamber, it was found that many fine spots appeared falling on a line with each bright spot which gradually decreased in intensity with

18

rotation. This effect is seen by the continuation of the line of
bright spots upward to the right in Plate 9 (a) in the top half of the
pattern and downward to the left in the bottom half; its full effect
was similar to that shown in the Laue pattern of (b) which resulted
from using a much thinner specimen where diffraction through the
crystal was possible. In the pattern of (b), however, it should be
noted that the hexagons in the two-dimensional network are regular and
that the diffraction spots corresponding to the positions of aluminum
ions in (a) cannot be found; hence, the patterns shown by (a) and (b)
correspond to a-axis whiskers having slightly different orientations

Selected area diffraction patterns obtained on a-axis
whiskers and a c-axis whisker are shown in Plate 9 (c) and (d), respect-
ively. The Laue pattern in (c) is a result of diffraction from several
a-axis whiskers shown in the background; this accounts for the except-
ionally strong reflections observed. The diffraction spots correspond-
ing to the positions of aluminum ions fail to show in the pattern
presumably because the points in the reciprocal lattice are not as
elongated as those found in (a) and (b). The hexagons in the two-
dimensional network are again distorted but to a higher degree than
that shown in (a) because the plane of the whiskers is but roughly
normal to the electron beam. This effect is also evident in the
selected area diffraction pattern for the c-axis whisker in (d) where
a two-dimensional rectangular lattice of points can be detected at the
lower right away from the bright spot at top which is due to the
primary electron beam. The c-axis whisker has a trapezoidal cross
section which makes it possible to see all four of its lateral edges;
the whisker below it is an a-axis whisker, many of which are found to
have larger width to thickness ratios than c-axis whiskers.

Other electron diffraction effects found in the whiskers
are the Kikuchi lines shown in Plate 10 (a), (b), and (c). The Kikuchi
lines are indicative of the high degree of crystal perfection, refer-
ence 42, attained by the whiskers during their growth. Diffraction
from a group of whiskers in the diffraction chamber of the electron
microscope is shown in (a) and (b), and selected area diffraction from
a large a-axis whisker is shown in (c). It should be noted that many
dark diffracted beams besides being reflected internally off the lateral
face of the whisker may continue beyond it as seen on the right in (c).
The diffracted beams within the whisker could easily be confused with
the extinction bend contours described in the following section.

2. Transmission Electron Microscopy

Apart from the diffraction effects described above, trans-
mission electron photomicrographs of Al_2O_3 whiskers revealed phase

contrast effects other than those due to dislocations, therefore, it is
necessary to describe these first. The most common phase contrast
effects are the extinction contours shown in Plate 11 (a). The extinc-
tion contours are brought about by crystal bending which causes reflect-
ing regions around reciprocal lattice points to become extended thus
resulting in a broader and more diffuse scattering than the thin line
contrast effects caused by lattice strains around dislocations, refer-
ence 43. Another phase contrast effect is illustrated in Plate 11 (b),
by the wavy or interference fringe pattern of the whisker running from
top left to right center. These patterns may be due to warping or
bulging in the ribbon-like filament. It appears that the variations
in thickness of whisker through which the incident electron beam must
pass would bring about this result so that the above phase contrast
effect might more appropriately be called thickness contours.

The transmission electron photomicrograph in Plate 12 (a)
reveals some of the dislocation structure in a bent a-axis or basal
plane whisker. The basal plane whisker is identified as such by the
presence of extended total dislocations consisting of two-fold and
four-fold stacking fault ribbons in agreement with the theoretical
predictions of Kronberg, reference 44, concerning the mechanism for
plastic basal slip in sapphire. An enlargement of the area at the top
right of Plate 12 (a) is given in (b). The enlargement shows a two-
fold stacking fault ribbon at the top and two four-fold stacking fault
ribbons near left center. The dark shaded stacking faults show up
because atoms across the stacking fault plane are out of phase with
respect to the electron waves with the result that electron transmission
does not take place; the electron waves become extinct. It should be
noted that maximum tensile stress is on the broad face of the whisker.

The apparent angle that the two-fold stacking fault ribbons
make with respect to the four-fold stacking fault ribbons in Plate 12
(a) appears to be roughly in agreement with the angle between the two
possible flow directions in the basal plane, the $<11\bar{2}0>$ and $<1\bar{1}00>$
directions. Actually, this angle is somewhat smaller than would be
expected for oxygen ions in a regular hexagon arrangement, and it appears
more likely that the angle would be about right for a slightly distorted
hexagon of oxygen ions such as that previously implied by the diffraction
pattern of Plate 9 (a). It should be noted that further along the bent
whisker, two additional two-fold stacking fault ribbons appear, but
these are of lighter contrast. The loss in contrast is apparently due
to a slight change in the orientation of the whisker; hence, the
stacking faults do not show very well unless the orientation is very
nearly the correct one for Bragg reflection. The width of faulted
regions between partial dislocations in the four-fold stacking fault
ribbons is estimated at about 50-75A°.

The dark bands below the stacking fault ribbons in Plate 12 (a) which are oriented at about 60° to the axis of the whisker are believed to bear some relation to the twinning elements in sapphire. Moving along the bent whisker toward the left, the orientation of the whisker changes and alternate regions of dark and light rectangular figures appear. The rectangular cross-section is a characteristic feature of a-axis whiskers. It was not possible to resolve sufficient detail that would clearly identify extended dislocations; i.e., there is no apparent evidence of the grouping of stacking fault planes such that the spacing between them would be similar to that seen in Plate 12 (b). Many of the dark shaded rectangles appear alone and unpaired; hence, it is presumed that such reflections come from atomic planes which constitute errors in the normal sequence of stacking planes during whisker growth. Since growth normally takes place on planes of high atomic density, it is probable that these "stacking defects" occur along the prism planes in sapphire and at least appear to be located approximately so.

A transmission electron photomicrograph revealing the nature of internal defects in a c-axis whisker; i.e., a whisker whose axis is parallel to the <0001> direction in sapphire, is shown in Plate 13 (a). The whisker is identified as such by the trapezoidal shape of its cross section and by mechanical properties data to be presented later. Dark shaded trapezoids appear along the length of the whisker, and these appear to be accidents in growth similar to the "stacking defects" noted previously in the a-axis whisker of Plate 12 (a). Extinction bend contours noticeable at the sharp cornered apexes of the dark shaded trapezoids are indicative of the strain distribution at these points. The presence of the "fringes" suggests that the whisker is slightly bent; this can be seen also by observing that the ends of the whisker are slightly out of focus. Considering the substantial evidence that c-axis whiskers grow along the axes of screw dislocations, there is also a possibility that the dark shaded trapezoids may actually be spiral defects.

Two a-axis whiskers which show very little bending and which are therefore practically in an unstrained configuration are shown in Plate 13 (b). Being somewhat thick the whiskers are almost opaque to electrons, but sufficient detail is evident on the nature of the stacking defects present. The stacking defects are probably grown-in, but it is possible that some stacking faults might have been introduced during handling. There is a noticeable difference between the two basal plane whiskers in that the one on the right shows many of the dark bands oriented at a small angle to the axis of the whisker; whereas, the one on the left shows them apparently normal to the axis of the whisker similar to those described in the a-axis whisker of Plate 12 (a).

This observation seems to imply that the two whiskers might correspond
to different orientations in the basal plane; i.e., the $<11\bar{2}0>$ and
$<1\bar{1}00>$ orientations.

Plate 14 (a) shows an a-axis whisker bent to a substantial
curvature with maximum tensile stress on a lateral face. An enlargement
of the region where the bent whisker meets the larger whisker at center
is shown in Plate 14 (b). Though the fine detail is not entirely clear,
the stacking defects seen here were noted to act as dislocation sources
generating a hexagonal network of partial dislocations which tended to
be continuous in the basal plane along the length of the whisker unless
stopped by other defects. Basinski et al., reference 45, reviewed re-
cent electron microscope studies of such dislocations in layer structures
which crystallize in the form of plates whose faces are parallel to
the basal plane of the structure. These investigators made a study of
hexagonal dislocation grids lying in parallel and closely spaced basal
glide planes of GaSe and discussed in some detail the contrasts of these
dislocations. It was noted that vague outlines of two-fold and four-
fold stacking fault ribbons tended to show up at the far right end of the
bent whisker in Plate 15 (a). The dislocations along the whisker do
not seem to remain stationary and there is a tendency for a pile-up
and recombination to occur. The point where the fine whisker meets
the larger whisker and where the stress is apparently at a maximum is
marked by a complex dislocation tangle.

Plate 14 (c) shows a c-axis whisker identified by the two
additional edges near the central axis which appear to establish the
cross section as a trapezoid. The whisker has a slight bend in it
which produces maximum tensile stress on one lateral face. Extinction
contours and several structural defects are noticeable along the length
of the whisker. The enlargement in Plate 14 (d) shows the nature of
extinction contours in the vicinity of what is presumably a stacking
defect.

B. Observations Made During Tension Test Program

Previous to the use of the tensile apparatus in its present
form, initial tests on sapphire whiskers were made using a 1/8-inch
gauge length. Much scatter in tensile data was encountered in these
tests. It was found that by scaling down the size of the gauge length,
higher fracture strengths and less scatter in data could be attained.
Long whiskers remounted and tested also showed higher fracture strengths.
A similar observation was made by Brenner, reference 46, in work done
on copper whiskers. The low strengths observed initially in the sapphire
whisker tests were attributed to the presence of surface imperfections,
either grown-in or introduced during handling in the whisker mounting

procedure. Such observations resulted ultimately in the use of the 1/32-inch gauge length in the present tests.

Another phenomenon observed in the earlier tests was the appearance of mechanical kinks in sapphire whiskers strained beyond their elastic limits. Whiskers sometimes fractured near one grip while a kink appeared near the other grip. The whisker on either side of the kink could be bent appreciably in a way that would induce considerable stress in the kink itself, but on releasing this applied stress, the whisker would spring back to its original kinked shape elastically without fracture. Mechanical kinks similar to these have been observed in metal whiskers strained beyond their elastic limits, reference 47. The kinks observed in sapphire whiskers are believed to be due to mechanical twins formed possibly because of a slight amount of twist and small bending moment exerted near the originally used wire loop grips during tensile loading. Subsequently, the whisker mounting fixture and tensile grips were modified to their present design in order to reduce bending and twisting to a minimum. Mechanical kinking disappeared but now most of the whiskers fractured in two places with fractures located not far from the tips of the tensile grips, this despite the fact that the whisker has a small but measureable taper along its length.

Brenner, reference 48, observed delayed fractures in tension tests of c-axis whiskers above 630°C, time being related exponentially to applied stress. Delayed fracture was also observed in the present tests at 25°C. Occasionally, a delayed fracture would occur while strain measurements were being made during increment loading. In one instance where load was reduced slightly from a higher value, fracture occurred after a few minutes delay at the lower load. The duration of the tests usually ran from 10 to 15 minutes. The occurrence of delayed fracture in these tests was quite unexpected; since, in the light of the earlier data, its effect was expected to be small at 25°C. Its appearance in the present tests is attributed to a relatively higher purity level shown by these whiskers.

C. Stress-Strain Curves

The results obtained from tension tests on the sapphire whiskers are summarized in Table 1. In measuring cross sections and evaluating tensile data obtained from various whiskers, it was found that characteristics and properties of three distinct types or sets of whiskers were actually being studied. Based on a previous study, reference 49, of sapphire whiskers, it appears that these types should correspond to the three simple growth directions in sapphire, all screw directions, along which whiskers have been observed to grow; i.e., the $<0001>$, $<11\bar{2}0>$, and $<1\bar{1}00>$ directions. The whiskers therefore were labeled c-axis,

a_I-axis, and a_{II}-axis types corresponding to the above respective growth directions. The whiskers were identified and tensile data broken into three distinct sets of results as described in the following sections.

1. c-axis whiskers

As indicated above, the c-axis whiskers are those whose axes are parallel to the $<0001>$ growth direction in sapphire. Usually, the literature will label whiskers according to the growth direction so that the c-axis whiskers could just as easily be called $<0001>$ whiskers, but the former nomenclature seems to have held. The c-axis whiskers were determined to be such on the basis of their measured elastic moduli which for whiskers of high purity and near structural perfection gave values of about 70×10^6 lbs./in.^{2}. This corresponds closely with previously determined values using static and dynamic methods on large single crystals of sapphire. Also, the cross section geometry of these whiskers appeared to be closely related to the hexagon shapes found in c-axis whiskers described in the literature.

The tension test results obtained on c-axis whiskers could be described best by a range of stress-strain curves as shown in Plate 15 running from brittle behavior, curve (1), to increasing ductility for curves toward the right. Comparisons of the ductile behavior observed in different whiskers were made on the basis of the proportional limit or initial yield point, the stress at which the first deviation from the linear elastic portion of the curve takes place, and on the basis of the rate at which the slope of the curve decreases with increasing strain after yielding. The initial yield point as defined above may be considered to be the stress at which dislocation movement becomes significant. The nature of the test was such that it was not sensitive enough to detect microstrain yielding similar to that found by Roberts and Brown, reference 50, in single crystals of zinc at stresses near zero. The tests nevertheless proved capable of indicating the relative ductility of individual whiskers and seemed to give a fair approximation of the yield points which was in agreement with the overall analysis of the whiskers.

The arrangement of the stress-strain curves in Plate 15 in the order of increasing ductility proved useful because it showed the measured elastic moduli increasing with increased ductility. Since increase in ductility can be interpreted as a sign of increased purity, the results imply that impurities lower the elastic modulus which is in agreement with that found by Singer and Thurnauer, reference 51. These investigators, however, also found a size effect in which the elastic modulus increased with decrease in the diameter of the test rod used; the maximum for the c-direction was approached at the finest size rod

tested, about 0.010 cm. The wide range in the measured elastic moduli shown by the curves suggests that besides impurities, size effect must have influenced the results. Later, it will be shown that size effect could provide a very strong influence on this property. Also, since the test was not sensitive enough to detect microstrain yielding, this must be considered a possibility. However, the low measured elastic moduli shown by brittle whiskers which presumably have a high impurity content tends to discount this as a possibility.

The highest measured elastic modulus for c-axis whiskers shown in Table 1 is 71.0×10^6 lbs./in.^{2}. This closely approximates the value measured for large, pure single crystals of corundum, reference 52, 74×10^6 lbs./in.^{2}. The fact that such high values could be attained indicates that the strain contribution from the bond between the whisker and the grips must have been very small. Also, the total elongation values recorded for c-axis whiskers appear to be in agreement with those measured by Webb and Forgeng, reference 53, in bend tests conducted on sapphire whiskers. In these bend tests, elastic strains of over 1.0% and up to 2.3% were measured. It was indicated, however, that 2.3% may not have been the highest strain attainable.

The most significant result of the tests was the ductile behavior found in many of the whiskers. Brenner, reference 54, in previous tension tests of c-axis whiskers reported brittle behavior in all tests even at temperatures not far from the melting point. This brittle behavior can be accounted for by the fact that the whiskers had a much higher impurity content, 2.0-3.0% as compared to the 0.1% total impurities found in the whiskers of the present work. Silicon was the main impurity element in each case. The now substantial evidence, reference 55, already published on the embrittling effect of small amounts of impurities in ionic crystals apparently lends support to this belief. The effect of increasing purity on ductility can be readily seen in Plate 15 as it is reflected in yield point behavior and the nature of the stress-strain curves in the plastic range.

Whiskers showing brittle behavior gave stress-strain curves similar to curve (1) in Plate 15 where no perceptible yield point could be detected. Fracture strengths of brittle whiskers showed considerable scatter, possibly because of the ease with which surface damage could be inflicted on them during handling, but the highest strength attainable, 0.94×10^6 lbs./in.^{2}, is in good agreement with tensile data reported by Brenner for c-axis whiskers. Consecutive curves to the right of curve (1) show the effect of increasing ductility by a more rapid decrease in the slope of the curve after yielding and by a decrease in the initial yield stress which approaches a minimum in curve (4) at about 0.27×10^6 lbs./in.^{2}. In curves (5) and (6), however, the initial

yield stress increases reaching its highest value at 1.02×10^6 lbs./in.^{2} in curve (6). The highest recorded value is 1.47×10^6 lbs./in.^{2}. Whiskers with such high initial yield stresses are presumably near structural perfection, and probably of the highest purity. The effect of this exceptionally high purity is manifested by a high degree of ductility which shows as a rapid decrease in the slope of the curve after yielding occurs. Also, the overall effect of high purity and nearness to structural perfection becomes evident in a high measured elastic modulus which under the given conditions should approach the true value. The highest fracture strength for c-axis whiskers, 1.58×10^6 lbs./in.^{2}, was found in such ultra fine, high-purity whiskers.

2. a-axis whiskers

The a-axis whiskers are those whose axes are parallel to the $< 11\bar{2}0 >$ and $<1\bar{1}00>$ growth directions in sapphire; hence, these might be termed basal plane whiskers. The a-axis whiskers were readily distinguishable from c-axis whiskers by their rectangular or near-rectangular cross sections and their much higher measured elastic moduli. Unfortunately, the main difficulty in whisker identification arose in differentiating between the two types of a-axis whiskers.

During an early stage of the testing program, the highest measured elastic modulus found for a-axis whiskers was 180×10^6 lbs./in.^{2}. Since elasticity was expected to be isotropic in the basal plane of the sapphire structure, this value was looked upon as a limit for a-axis whiskers. Further testing, however, turned up a few whiskers which yielded much higher measured elastic moduli with the highest being 330×10^6 lbs./in.^{2}. It was not possible to establish the orientation relationship between the above whisker types by electron diffraction from ruptured tension specimens as mounted on the tensile grip. An electric charge developed on the whisker and this charge was sufficiently strong to cause electron reversion thus preventing the possibility of observing important detail. Hence, the a-axis whiskers were classified according to which of the measured elastic moduli given above they came nearest. Those whiskers nearest 180×10^6 lbs./in.^{2} were labeled a_I-axis type, and those nearest 330×10^6 lbs./in.^{2} were labeled a_{II}-axis type.

Table 1 shows that a_I-axis whiskers are the next most common whisker found in the sample studied, and that these show tensile properties, particularly measured elastic moduli, which are noticeably different from a_{II}-axis whiskers. Also, it will be noted that a_{II}-axis whiskers tended to be extremely fine in size. The apparent scarcity of these whiskers suggests that they were difficult to grow and this appears to be related to an extremely high elastic modulus. Edwards and Happel, reference 56, who grew numerous near-micron size sapphire whiskers under

roughly equivalent growth conditions found that more whiskers grew in the $<11\bar{2}0>$ direction than in the $<1\bar{1}00>$ direction. This suggests that a_I-axis whiskers have axes parallel to the $<11\bar{2}0>$ direction and a_{II}-axis whiskers have axes parallel to the $<1\bar{1}00>$ direction in sapphire. It is assumed here that the above is correct. The result at present can be only tentative, but further evidence will be presented later to establish this point. The above assumption implies that elasticity in whiskers that grow in the basal plane of sapphire may be non-isotropic. Some support for this view might be found in the discrepancy noted in the apparent flow directions previously indicated by the stacking fault ribbons and the apparent discrepancies seen in electron diffraction patterns of a-axis whiskers. Hence, a_I-axis and a_{II}-axis whiskers were determined to be such on the basis of their measured elastic moduli and on the basis of the evidence presented above.

As in the case of the c-axis whiskers, the tensile behavior of a_I-axis whiskers could be described best in terms of a range of stress-strain curves as shown in Plate 16 running from brittle-like behavior, curve (1), to increasing ductility for curves toward the right. The pattern regarding change in ductility with measured elastic modulus appears to be the same as for c-axis whiskers. Only the values of various tensile properties changed. The highest measured elastic modulus as noted previously is 180×10^6 lbs./in.^{2}. Again, as in the case of c-axis whiskers, such a high value suggests that the whisker is one of high purity and of near-structural perfection. This view finds added support in the fact that a large increase in the initial yield stress to 1.7×10^6 lbs./in.^{2} occurs which can be interpreted as being due to an absence of slip dislocations. The highest fracture strength for a_I-axis whiskers, and apparently for whiskers of all orientations, was 3.23×10^6 lbs./in.^{2}. Also, total elongation values for a_I-axis whiskers tended to be the highest for all whisker orientations with the highest values being slightly above 3.0%.

Although only a limited number of results could be obtained on a_{II}-axis whiskers, stress-strain curves, as shown in Plate 17, follow a pattern similar to c-axis and a_I-axis whiskers. The highest measured elastic modulus, as noted previously, is 330×10^6 lbs./in.^{2}. The whisker yielding this result also showed the highest initial yield stress, 2.0×10^6 lbs./in.^{2}, not only for a_{II}-axis whiskers but also for all whisker orientations. Fracture strength for the same whisker was 2.22×10^6 lbs./in.^{2}. Thus, the above results, again, are indicative of an a_{II}-axis whisker of high purity and near structural perfection for reasons already explained in the case of c-axis and a_I-axis whiskers. Total elongations for a_{II}-axis whiskers, however, appeared to be generally

27

lower than those for c-axis and a_I-axis whiskers, the highest value being 1.9%. The lower elongation values are attributed to a very high elastic modulus.

The elastic moduli shown by a-axis whiskers are very much higher than that indicated by resonant frequency measurements made on large single crystals which yield values of about 60×10^6 lbs./in.^{2}. The difference in values are too great and beyond the range of error established for whisker measurements; hence, the elastic moduli obtained by the resonant frequency technique are believed to be in error. An explanation is offered in the discussion in the section on "Young's Modulus of Elasticity in Sapphire."

D. Discontinuous Yielding In c-axis Whiskers

The phenomenal increase in yield point shown by whiskers with the highest measured elastic moduli for a given orientation prompted interest in the manner in which the shape of the stress-strain curve varies at slightly lower values. Since c-axis whiskers were most abundant in the test results in the range of interest, stress-strain curves for these were studied more closely and are presented in Plate 18. The curves are in the order of increasing measured elastic modulus. Curves (1) and (2) show the expected trend in the shape of the curve with increasing measured elastic modulus and there appears to be a tendency to show the three stages of plastic deformation observed in metals, reference 57, and more recently in ionic solids, references 58 and 59. In curves (3), (4), and (5), however, discontinuous yielding occurs starting at a fairly low initial yield point, about 0.28×10^6 lbs./in.^{2}.

In curve (3) of Plate 18, the initial yield point is not pronounced but the yield points that follow become very noticeable at the higher stresses. This phenomenon could be interpreted in terms of dislocations locked in by their impurity atmospheres, a mechanism of dislocation locking first proposed by Cottrell, reference 60. Thus, dislocations first begin to move at the initial yield point, most likely in a section of crystal where Cottrell locking is weakest; i.e., where purity is relatively higher than the rest of the whisker. The rate of work hardening however prevents the appearance of a flow stress and the slope of the curve again reaches the value it had in the initially elastic portion. This feature is particularly evident in curves (4) and (5). As stress increases, dislocation movement, probably in a less pure part of the whisker, occurs again and the process repeats at higher stresses until the whisker ruptures. In curve (6), yielding is most pronounced probably because of the exceptionally high stress needed to nucleate a slip dislocation in dislocation-free crystal which once nucleated results in rapid plastic deformation. Work hardening again appears to prevent the appearance of easy glide or stage I deformation.

In curve (5), only one yield point is observed and this may be due to a much lower probability of finding dislocations in whiskers of high purity. This idealized case then could easily be visualized for curve (6) which shows no discontinuous yielding presumably because dislocations are effectively prevented from forming in what might be regarded as intrinsically pure material.

E. Size Effect

Brenner, reference 61, found a dependence of fracture stress on the diameter of sapphire whiskers of the c-axis type. The diameter of these whiskers varied over a size range of about 4-30μ. Since the whiskers used in the present work were ribbon-like, the fracture stress was assumed to be dependent upon whisker thickness. Log-log plots of fracture stress versus whisker thickness showed a definite correlation as indicated in Plate 19 (a) and (b) for c-axis and a_I-axis whiskers, respectively. It was not possible to obtain a result for the a_{II}-axis whiskers because of the limited data on these. The log-log plots seemed to be the only kind that would yield curves showing a strong linear relationship. Log-log plots of fracture stress as a function of area of cross section also seemed to yield a linear relationship as shown in Plate 20 (a) and (b).

Whereas the data of Brenner shows a roughly linear relationship between size and fracture stress, the present data suggests that some other relationship exists between them. It was possible to detect this feature because whiskers in a much finer size range and of higher purity were available in the present study. Equations were derived from the log-log plots of fracture stress versus thickness using an average line, the dashed line drawn in the graphs of Plate 19 (a) and (b). The equations are

$$\sigma_f = 2180 \, t^{-0.588} \qquad \text{(for c-axis whiskers)} \qquad (4)$$

and

$$\sigma_f = 922 \, t^{-0.690} \qquad \text{(for } a_I\text{-axis whiskers)} \qquad (5)$$

where σ_f is the fracture stress and t is the whisker thickness. In the limit where t approaches unit cell dimensions, $t = 5A°$, the fracture stress for c-axis whiskers reaches 76.0×10^6 lbs./in.^{2}; whereas, for a_I-axis whiskers, it reaches 193×10^6 lbs./in.^{2}. It is interesting to note that these values of fracture stress approximate the maximum measured elastic moduli found for the two whisker orientations. Theoretically, the fracture strength cannot reach the value of the elastic modulus, only a reasonable fraction of it. Equations similar to those given above could also be derived from log-log plots of

fracture stress versus area of cross section, Plate 20 (a) and (b). The equations are

$$\sigma_f = 4080 \, A^{-0.270} \qquad \text{(for c-axis whiskers)} \qquad (6)$$

and

$$\sigma_f = 3250 \, A^{-0.310} \qquad \text{(for a_I-axis whiskers)} \qquad (7)$$

where A is the area of the whisker cross section. Again, in the limit where A approaches unit cell dimensions, A = 5A° square, the fracture stress reaches 88.6×10^6 lbs./in.^{2} for c-axis whiskers and 196×10^6 lbs./in.^{2} for a_I-axis whiskers so that the results are roughly the same whether thickness or area of cross section is used as the size parameter.

A size effect could also be detected in log-log plots of measured elastic modulus versus whisker thickness. Plate 21 (a) and (b) show the measured elastic modulus as a function of whisker thickness for c-axis and a_I-axis whiskers respectively. The equation derived from average lines drawn through the plotted points are

$$E_m = (1.68 \times 10^7) t^{-0.102} \qquad \text{(for c-axis whiskers)} \qquad (8)$$

and

$$E_m = (5.02 \times 10^7) t^{-0.082} \qquad \text{(for a_I-axis whiskers)} \qquad (9)$$

where E_m is the measured elastic modulus. In the limit of unit cell dimensions, the calculated elastic modulus is 85.0×10^6 lbs./in.^{2} for c-axis whiskers and 186×10^6 lbs./in.^{2} for a_I-axis whiskers. Similarly, log-log plots of measured elastic modulus as a function of area of cross section also gave linear relationships, Plate 22 (a) and (b). The equation derived from these are:

$$E_m = (2.46 \times 10^7) A^{-0.032} \qquad \text{(for c-axis whiskers)} \qquad (10)$$

and

$$\log E_m = (5.17 \times 10^7) A^{-0.041} \qquad \text{(for a_I-axis whiskers)} \quad .. \quad (11)$$

In the limit of unit cell dimensions, the calculated elastic moduli again turn out to be roughly the same as calculated previously, 76.5×10^6 lbs./in.^{2} for c-axis whiskers and 220×10^6 lbs./in.^{2} for a_I-axis whiskers.

Plots of initial yield point versus size of sapphire whisker failed to show any correlation. Hence, size effect in the sapphire whiskers could be summarized in the following generalized equations:

$$\sigma_f = aA^b \tag{12}$$

$$\text{and} \qquad E_m = cA^d \tag{13}$$

where A is the size parameter, and the constants, a, b, c, and d take on different values for each whisker orientation.

The results indicate that in the limit of very fine size, the measured elastic moduli approach what are believed to be the true elastic constants of the crystal. The results further indicate that fracture stresses show a similar trend and in the limit of fine size, these could also reach very high values, but only a reasonably high fraction of the elastic modulus.

F. Morphology of Whiskers

Fractures depicting the morphology of sapphire whiskers are provided in Plate 23 (a) to (e). Cross sections of c-axis whiskers generally assumed the shape of a parallelogram with included angles of about 60° and 120° and with base to altitude ratios varying from about 1:1 to 8:1, Plate 23 (a) and (b). Some cross sections, however, did show slightly different geometry as illustrated in Plate 24 (a) to (f). In Plate 24 (c), the sharp cornered apices of the parallelogram are missing. The normally observed whisker edges appeared to be replaced by well developed prism plane faces which apparently tended to complete the hexagonal form of the crystal. The two new crystal faces actually were seen only as slight, barely perceptible bevels in cross sections, well defined in only a few instances. In Plate 24 (d), the whisker cross section takes the shape of a trapezoid representing a section of a hexagon. Plate 24 (e) shows a further development of this shape which consists of two trapezoids having a common base; i.e., an elongated hexagon.

The hexagonal cross section in Plate 23 (c) is the most common form for c-axis whiskers encountered by investigators in previous studies made of sapphire whiskers. Whiskers with hexagonal cross sections however were not common to the sample studied; in fact, only one specimen was found during the course of the tests. In order to complete the data on c-axis whiskers, the whiskers of hexagonal cross section were obtained from the General Electric Company. A comparison of tensile data obtained on the various whiskers described above indicated that these have quite similar properties.

The single c-axis whisker with a hexagonal cross section on which tensile data was obtained, specimen 18 of Table 1, was found to

be brittle. Only one test result was possible since other whiskers with hexagonal cross sections were actually found in a much larger size range. These whiskers could not meet the requirements of the test because of the limitation on the load allowed by the bond between the whisker and tensile grip. Several tests were run, however, in which strain measurements were made on arbitrarily selected gauge lengths defined by naturally or artificially made markings on the surface of the whisker. Calculated elastic moduli in these tests turned out to be in the range of c-axis whiskers, usually on the low side indicating brittle-like behavior.

A review of Table 1 shows that c-axis whiskers having cross sections other than that of a parallelogram are in the minority, and it is believed that the varying morphology of these whiskers is an effect due to the extent to which impurities are present in individual whiskers. Some support for this belief can be found in the fact that these whiskers tended to be the finest and exhibited tensile properties characteristic of whiskers near structural perfection, a condition already associated with good ductility and therefore high purity.

As noted previously, basal plane whiskers generally showed cross sections in the form of a rectangle. The rectangular shape could be established with a fair degree of certainty in a_I-axis whiskers but not without uncertainty in the a_{II}-axis type. This difficulty is attributed to the extreme fineness of a_{II}-axis whiskers and the slight amount of ductility and irregular fracture noted in some of the specimens. There was some indication of a slight deviation from 90° in the rectangular sections. Typical fractures showing rectangular shapes of basal plane whisker cross sections are given in Plate 23 (d) and (e).

G. Fracture Appearance

1. c-axis whiskers

The c-axis whiskers showing brittle behavior in stress-strain curves at 25°C always tended to exhibit cleavage-type fracture. Cleavage was found to occur along the basal plane as shown in Plate 25 (a). But if the whisker is not totally embrittled, fine slip lines can usually be seen by focusing on points below the fracture surface as shown in (b). The shape of the original fracture section is clearly evident in this view. It should be pointed out that transmitted light was used to reveal this feature. The sapphire whiskers are transparent to light; therefore, this technique can be useful, especially for observing the geometry of cross sections if fracture is irregular.

32

Some evidence of cleavage along prism planes was also found in c-axis whiskers. As noted previously, many whiskers broke in two sections along the gauge length, usually near the grips. A ductile fracture often occurred near one grip while a cleavage fracture was noted near the other grip. The cleavage fracture normally propagated along a basal plane, but in a few instances, the whisker cleaved along a prism plane. An example of this behavior is shown in Plate 25 (c) and (d) where (c) shows the ductile fracture in which extensive basal slip resulted in a layer-like structure; near the other grip in (d), there are cleavage fractures along both prism and basal planes. A segment resulting from prismatic cleavage is seen normal to the upright stem running along the direction of the tensile axis. Also, a broken gauge length section resulting from basal cleavage can be seen at the top of the photograph. Cleavage along the basal and prism planes occurs presumably because of the sudden release of elastic strain energy after the whisker ruptures by plastic deformation. It probably originates in the vicinity of structural defects, possibly along planes where dislocation nucleation occurred.

Plate 26 (a) to (f) further illustrates the plastic and fracture behavior observed in fine c-axis whiskers. Generally, basal slip in the more ductile c-axis whiskers appeared as very broad slip bands which were noticeable, especially near the fracture surface. Focusing at points below the fracture surface sometimes revealed that a Luders band propagated over an appreciable length of the whisker. The slip bands became increasingly finer at greater distances from the fracture surface. Some signs of prismatic slip were also noted in fractures of c-axis whiskers, but pronounced only in a few specimens. Prismatic slip traces were always very fine and difficult to photograph. The slip traces noted in fractures occurred parallel to a broad face of the whisker, and became more evident when focused at a point below the fracture surface. A more interesting example of prismatic slip took the form of multiple slip on parallel prism planes giving the whisker the appearance of a structural laminate. The fractures of individual lamellae showed a saw-toothed or jagged appearance. The above observations seem to suggest that prismatic slip is possible in the $[000\bar{1}]$ direction in sapphire since the $<1\bar{1}00>$ direction for prismatic slip is normal to the tensile axis of the whisker.

In the most ductile c-axis whiskers, both basal and prismatic slip could take place simultaneously resulting in intersecting slip. Intersecting slip was fairly difficult to resolve in photographs. Perhaps the best example of intersecting slip could be found in the fracture of Plate 26 (e). At the lower end of the fracture surface, basal slip could be identified by a broad slip band normal to

the axis of the whisker; prismatic slip could be identified as a fine slip trace parallel to a broad face of the whisker running through the step caused by basal slip.

2. a-axis whiskers

Many of the a_I-axis whiskers failed in a brittle-like manner along a plane normal to the tensile axis as shown in Plate 27 (a) and (b). This suggests that prismatic cleavage is the predominant mode of fracture, analogous to the result found in the case of c-axis whiskers. Only a few whiskers showed extremely fine slip traces indicative of slip on prism planes; also, only a few showed evidence of slip on basal planes. The more ductile whiskers showed a tendency toward irregular fractures. Some fracture had a jagged appearance along with a slight degree of necking. One of the more interesting irregular fractures is shown in Plate 27 (c) and (d). The face of the fracture reveals a lamellar-type structure suggesting that both basal and prismatic slip might have occurred. A cleavage whisker of submicron thickness is seen clinging at one end to the midpoint of the fracture edge in Plate 27 (c).

Fractures of a_{II}-axis whiskers tended to be ductile and one or two exhibited fractures which had a jagged appearance. Because of the extreme fineness of these whiskers, it was very difficult to obtain photographs showing fine detail. The a_{II}-axis whisker with the highest measured elastic modulus, 330×10^6 lbs./in.^{2}, was found to have sharp, cleaved surfaces which permitted fairly accurate measurement of cross sections. The area of cross section turned out to be the same at both ends of the gauge length indicating that the whisker was of uniform cross section. A later check on these measurements yielded practically identical results; hence, much credence is given to the high value of the calculated elastic modulus found in this whisker.

H. Plastic and Fracture Behavior at 900°C

The evidence of intersecting slip found in sapphire whiskers at 25°C prompted interest in what the deformation characteristics might be at elevated temperature. Some whiskers were subsequently strained in tension at 900°C. The whiskers were heated by a 0.020" diameter platinum coil for 15 minutes and strained to rupture at a constant rate; time to rupture was estimated at 10 to 20 seconds. Although the tests were makeshift, the fracture strengths of some whiskers could be roughly estimated at about 0.25×10^6 lbs./in.^{2}.

Sample whiskers ruptured at 900°C are shown in Plate 28. These specimens show that extensive plastic deformation is not limited

to just one section of the whisker; this was suggested to be the case for those ruptured in tension at 25°C. Instead, plastic deformation occurs at numerous points along the stressed section of the whisker, this despite the fact that the whisker may have a small but measure-able taper along its length.

The c-axis whisker in Plate 28 (a) and (b) indicate consider-able ductility, and necking is evident at several points, particulary at center, of the whisker. Moreover, it is evident that basal slip is the primary slip system operating. Basal slip causes the necked regions of the whisker to have a rumpled appearance. Prismatic slip, however, probably operates after appreciable basal slip takes place; this accounts for the necked appearance of the section at center and the apparent loss in the sharpness of slip bands along the basal planes. It should be noted that the basal planes on which slip takes place are bent, as indicated by the curvature in the slip bands at right in (b).

Deformation in the a-axis whiskers of Plate 28 (c) and (d) was quite different. Necking was not evident, and plastic deformation appeared to take the form of pure slip on what are presumably prism planes. The slip bands tend to be narrow and have sharp outlines. Small groups of slip bands, two or more, are noticeable in (c); also, some evidence of a Luders band was noted in the edge of the whisker shown in (d). The fineness of the slip bands in a-axis whiskers, attributed to prismatic slip, appears to be in agreement with earlier data which shows prismatic slip operating at a much higher temperature than that for basal slip, assuming the difference in temperature is a measure of the difficulty of operating these slip systems.

Fractures of c-axis whiskers ruptured in tension at 900°C are shown in Plate 28 (e) and (f). The fracture in (e) shows necking as a narrow border outlining the perimeter of the original section; whereas, the fracture in (f) shows the region of the neck outlined by a very narrow blade with sharp edges within the perimeter outlined by the original section. Both fractures can be compared to the cup and cone fractures often observed in tensile fractures of cylindrical speci-mens of polycrystalline metals. The cup and cone configuration is indicative of good ductility, and it clearly involves both the basal and prismatic slip systems in the case of the sapphire whiskers.

IV. DISCUSSION

A. Anisotropy in Tensile Properties

Anisotropy in the elastic modulus and fracture strength of sapphire whiskers was evident in the study of size effect. The measured

elastic modulus for whiskers of a given orientation was shown to
approach the true value for the given orientation in the limit of
very fine size, and the fracture stress similarly showed a trend
toward very high stress. Since anisotropy could be found in the above
mechanical properties, it should also be possible to detect it in
yield strength. A general comparison of initial yield stresses for
the three whisker orientations does not give clear evidence of aniso-
tropy presumably because of the influence of impurities. It was
shown previously, however, that for a given orientation, the finest
whiskers tend to be the most ductile indicating they are of high
purity, and showed the highest mechanical properties indicating they
are probably near structural perfection. Hence, these whiskers could
be used generally as a basis for detecting anisotropy in tensile
properties. Table 2 compares tensile properties of whiskers selected
on the basis given above. Anisotropy is readily evident in the
measured elastic moduli, fracture stresses, and initial yield
stresses. The low total elastic strain for a_{II}-axis whiskers, as
previously noted, is apparently due to a high elastic modulus. Although
the results might possibly be influenced by further testing, the tensile
properties tabulated in Table 3 appear to approach maximum values for
each whisker orientation; hence, it is felt that these satisfactorily
demonstrate the anisotropy in sapphire whiskers of near structural
perfection.

In Table 2, column 3, the initial yield stresses represent the
forces required to nucleate slip dislocations in dislocation-free crystal;
but, it should also be possible to detect anisotropy in the force required
to move slip dislocations already present in whiskers of relatively
high purity. Such anisotropic behavior was actually revealed in a
semi-log plot of the measured elastic modulus, E_m, versus the initial
yield stress, σ_y, shown in Plate 29. In the curve obtained for
c-axis whiskers, it is seen that E_m varies over a fairly wide range,
running as low as 26.5×10^6 lbs./in.^{2}. The c-axis whiskers with E_m
near this value showed brittle behavior. This feature is indicated
by vertical arrows atop plotted points where such behavior was observed.
It will be noted that all such points fall to the left of the bucket-
shaped curve. The slope of the curve on the left side tends to be
high, and since brittleness is caused by impurities, the steepness of
the slope suggests that Al_2O_3 is highly sensitive to impurities and can
be embrittled at relatively low impurity concentrations.

At the bottom of the bucket-shaped curve for c-axis whiskers,
the yield point reaches an almost constant value of 0.27×10^6 lbs./in.^{2}.
Impurities are probably at a very low value in this range of E_m and do
not appear to exert any locking action on dislocations responsible for
the yield point. It must be concluded that at this value of the yield

point, there is a true Peierls-Nabarro force, reference 62, a direct
measure of resistance the crystal lattice offers to the movement of
slip dislocations, free from the effect of impurities. The small
fluctuations observed in the plotted points along this portion of the
curve are attributed to error in measurement of the yield points which
are enhanced at the low value for c-axis whiskers.

At the highest E_m value for c-axis whiskers, about 69×10^6
lbs./in.^{2}, the yield point may increase abruptly to very high values,
1.47×10^6 lbs./in.^{2}. The abruptness of this change suggests that a
sharp change took place in the structure of the whiskers; i.e., the
whiskers may be free of slip dislocations and approach structural per-
fection. The few points at lower initial yield stress indicated for
whiskers near the highest E_m for c-axis whiskers further suggests that
there is still some small probability of a grown-in dislocation occurr-
ing in what is presumably nearly pure material.

Using Plate 29, the yield point behavior in c-axis whiskers can
be interpreted in the following way: At the lowest E_m, the whiskers are
brittle probably because of a relatively high impurity content. The
brittle whiskers are readily susceptible to damage during handling and
will generally rupture long before their true fracture strengths are
realized. As impurity content decreases, the elastic modulus increases,
but only slightly according to the left side of the bucket-shaped curve,
and a slight amount of ductility becomes evident. The whiskers begin
to show ductility because dislocations are no longer locked tightly by
their impurity atmospheres, and sufficiently high stresses are able to
move them. As impurity content decreases still further, less stress is
required to move dislocations until a point is reached where impurities
no longer have influence on the stress required to move them in the
crystal. The yield point then remains constant over an extended range
of E_m in which the whiskers are of relatively high purity and in which
dislocations are moved by the minimum Peierls-Nabarro force free from
the effect of impurities. As the whiskers approach structural perfec-
tion higher yield points are observed. The higher yield points are
attributed to the high stresses required to nucleate dislocations to
promote slip in dislocation-free crystal. Once dislocation loops of
sufficient size are generated, slip could be very rapid since only the
minimum P-N force is needed to move them. Failure, however, is not
abrupt and this is attributed to the fact that intersecting slip from
a prismatic slip system exerts a braking action on basal slip.

A similar analogy can be drawn for the case of a_I-axis, and a_{II}-
axis whiskers. Hence, although the data was limited, bucket-shaped
curves were purposely drawn to conform to the general pattern found for
c-axis whiskers. The initial yield stresses for the "structurally
imperfect whiskers" are also recorded in Table 2.

B. **Dislocation Structure in Al₂O₃ Whiskers**

A description of the internal structure of the Al_2O_3 whiskers first requires some knowledge of the mechanism of their growth. Most previous investigations of sapphire whiskers indicated that growth takes place along the axes of screw dislocations. Sears and DeVries, reference 63, however, discussed in some detail growth of c-axis sapphire whiskers by two-dimensional nucleation and growth instead of by the screw mechanism which, as noted previously, results in hexagonal prisms, usually showing an axial pore. These investigators showed experimental evidence of c-axis whiskers which grew in the form of a hexagonal prism without an axial pore and which were determined to have grown by two-dimensional nucleation and growth on the clean surface of the substrate crystal. Two-dimensional nucleation was attributed to a condition in which the supersaturation of Al_2O was much higher than the critical for growth along screw dislocations, thus making two-dimensional nucleation easier.

As noted previously, the c-axis whiskers used in the present work showed fracture sections, mainly in the form of a parallelogram; therefore, it naturally caused interest in the mechanism of their growth. It was possible to resolve sufficient detail of dislocation sources in fractures of the larger c-axis whiskers, about 10^{-7} in.^{2}. In Plate 30 (a), (b), and (c), where the focus is adjusted to several points at or near the fracture surface, the vague outline of a Frank-Read dislocation source, reference 64, can be detected. Other evidence of an F-R source was also found in a whisker having a much larger width to thickness ratio. Only one F-R source was observed and this was located near one end of the fracture section. It thus appeared that the whisker could grow first along two axial screws followed by lateral growth at one edge. Aside from the F-R sources, one of the larger whiskers with a low width to thickness ratio revealed only one axial screw dislocation which acted as a spiral source.

The presence of F-R or spiral sources in the c-axis whiskers indicates that there must be a critical size whisker below which such sources may not operate. An estimate of the critical radius of a central loop at a spiral source, references 65 and 66, needed for free, continuous generation of dislocations shows that it should be about $10^4 b$ where b is the Burgers vector of the dislocation. A calculation of the critical radius for a total dislocation in the basal plane of the sapphire structure where b for a total dislocation is 4.75×10^{-8} cm. yields 4.75μ . In the log-log plots of E_m versus t, Plate 21 (a), a sharp change in E_m could be detected at a whisker thickness of about 5.5×10^{-5} in. This feature is emphasized in the semi-log plot shown in Plate 31 where despite some wide scatter in the points, a line could

be drawn through the more dense groups of points. Since the width dimension of the whisker would be expected to determine the limiting size, a subsequent plot of width versus E_m was made, and this is shown by the dashed curve in Plate 31. The critical size thus turns out to be 2.5×10^{-4} in. $(\sim 6.3\mu)$ which appears to be in good agreement with that calculated above.

From the observations made above, it is concluded that most of the larger size whiskers must have nucleated and grown by means of one or two axial screw dislocations which could act as a source from which dislocations could be generated when the whiskers are strained in tension. Whiskers finer than 6.3μ probably grew by two-dimensional nucleation and growth. These could contain stacking defects such as those noted in Plate 14 (c) and (d) with the finest whiskers apparently practically structurally perfect whiskers free of dislocations. The fact that most of the whiskers in the sample studied are in a very fine size range indicates that supersaturation of Al_2O vapor was probably higher than the critical for growth along screw dislocations to the extent that it made two dimensional nucleation easier.

The a-axis whiskers, according to Table 1, are generally in a much finer size range than c-axis whiskers; hence, it is not likely that many of these grew by means of a screw mechanism. Whiskers in a much larger size range were present in the sample, but these were beyond the limits allowed by the tension test. Fractures of a few large a-axis whiskers in preliminary work failed to reveal screw sources. The fracture surfaces tended to be smooth and cleavage-like in character. In the case of fine a-axis whiskers, structural imperfections, as noted in electron photomicrographs, occur mainly in the form of stacking defects running either normal or at a small angle off normal to the axes of the whisker. This small difference in angle implies that the whiskers correspond to different orientations in the basal plane, presumably the $<11\bar{2}0>$ and $<1\bar{1}00>$ directions. The observation made previously, that more a-axis whiskers grow in the $<11\bar{2}0>$ direction than in the $<1\bar{1}00>$ direction, suggests that the above stacking defects develop along the $\{11\bar{2}0\}$ prism planes, and this might account for the fact that most of the a-axis whiskers cleaved along a plane normal to the axis of the whisker. A further implication is that a_{II}-axis whiskers corresponding to the $<1\bar{1}00>$ growth direction might not necessarily grow on planes normal to the axis of the whisker but on $\{11\bar{2}0\}$ prism planes with the growth direction fixed during the nucleation stage.

The stacking defects noted in fine a-axis whiskers did not appear to have a spiral-like character thus indicating that these probably did not form by a screw dislocation mechanism but by two-

dimensional nucleation and growth. Not all these whiskers showed stacking defects and it appears that some are actually near structural perfection. The evidence of two and four-fold stacking faults in electron photomicrographs were observed only in plastically bent whiskers and, therefore, are not considered to be part of the original dislocation structure of these whiskers.

C. Dislocation Movements in Ductile Whiskers

Based on observations of fractures, plastic deformation in c-axis whiskers can be described in a general way with the dislocation models in Plate 32. In (a), a schematic drawing of a c-axis whisker is given which shows known crystallographic elements for slip in sapphire along with two symmetrically located axial screw dislocations A-B and C-D. Two axial screws are not actually needed, and the model could just as easily be described in terms of one. The crystal is assumed to be relatively free of impurities so that dislocation movements are not impeded by them. Crystal slip would be expected to involve generation of stacking faults associated with partial dislocations which subsequently recombine to form total dislocations before slipping out of the crystal. To simplify the picture, the model will be described in terms of total dislocations and the presence of associated stacking faults will be implied.

Before crystal slip can take place, dislocation loops of sufficient size must be generated at some source. In a structurally perfect whisker, the absence of such a source accounts for a high yield stress which is needed to nucleate dislocations. Dislocations in these whiskers most likely nucleate at the surface of the crystal due to basal plane bending. In the general case, however, many of the whiskers show much lower yield points and this is attributed to the presence of a dislocation source, grown-in, or introduced during handling.

Several sources may be possible for the generation of dislocation loops in low-yield point whiskers. One source is a cleavage crack, E in Plate 32 (a), located at one of the thin edges of the whiskers which might have been damaged during handling. Another source is a spiral stacking defect, grown-in, along the basal plane. A spiral dislocation could be schematically illustrated by F in Plate 32 (a). Also, since impurities are attracted to the core of a dislocation, reference 67, a crack may develop in embrittled material at one axial screw providing another possible dislocation source. If the axial screws are not symmetrical about the center of gravity of the whisker cross section, which is quite probable, dislocations will always originate at one screw first. As the dislocation line moves along the basal plane, it intersects the second screw axis and winds itself

around it to complete the Frank-Read dislocation source as shown in Plate 32 (b). The diagram illustrates this process as occurring in one plane which might be an oversimplification. Closer inspection of one fracture surface revealed that each node of the F-R source could have a different character. One node appeared as a peak while the other appeared as a dimple. In other words, the spirals turn in opposite directions along the screws indicating that the screws are opposite in sign.

Once an F-R source is completed, a large number of dislocation loops could be generated under the applied tensile force until the configuration at Plate 32 (c) is reached. Slip on the basal plane is possible since the planes near the screw axes may be substantially sloped and basal planes across the whisker cross section become slightly bent, an effect due to lateral contraction of the whisker which increases in significance with increasing tensile force. As the dislocation loops slip out of the crystal, a slip band appears at the surface of the whisker, and jogs A'-B' and C'-D' are formed. Since the two halves of the crystal are displaced with respect to one another, the tensile force applied along the axis of the whisker exerts a torque on the jogs which increases with the amount of slip and with increasing tensile force. When the torque becomes suffi- ciently great that considerable distortion of the slip plane occurs the dislocations near the source are mechanically locked. The distor- tion may be fairly high in the vicinity of the jogs, so that new dislocation sources can be nucleated at a small distance from them along one of the screw axes; hence, basal slip could repeat in the manner described above. A continuous repetition of this process could thus result in the formation of a Luders band throughout the whisker unless it is stopped by harder regions of crystal which con- tain a higher level of impurities. This is illustrated schematically by Plate 32 (d).

The fact that prismatic slip was observed along with basal slip in c-axis whiskers would indicate that the distortion near a jog was sufficiently great to nucleate dislocations on a prism plane. The Burgers vector for prismatic slip, reference 68, 8.22A°, like that for basal slip, is oriented normal to the tension force, therefore, distortion of the crystal must be such that force could be redistributed in a manner that would direct it in the $<1\bar{1}00>$ direction, the direction for prismatic slip. Slip would otherwise have to take place in the $<0001>$ direction. Since the Burgers vector for the $<0001>$ direction is very large, about 13A°, it could conceivably account for the cleavage fracture observed along prism planes. Apart from the notion of harder regions of the crystal stopping Luders band propagation, prismatic slip could also act as a barrier in the manner illustrated in Plate 32 (e) and (f). The operation of this dislocation system is

necessarily limited to less than one slip translation since the shear
strain due to the large Burgers vector, assuming a $<0001>$ slip
vector, may be sufficient to induce cleavage along the prism plane.

In the case of large a-axis whiskers, similar models might
be described. Since observations of tensile fractures on a-axis
whiskers indicated that very little basal slip was active and that
slip occurred essentially on a prismatic slip system, the model des-
cribed in Plate 32 (a), (b), (c), and (d) with the appropriate elements
of slip inserted could then be applied. The near absence of basal
slip in a-axis whiskers is in accord with the fact that prismatic
slip bands always were noted to be fine indicating that the torque on
resulting jogs caused by prismatic slip was fairly small as compared
to those in the case of c-axis whiskers.

Most of the sapphire whiskers tested, as noted previously,
were of much too fine a size to permit growth along an axial screw
dislocation. Hence, growth must have taken place by two-dimensional
nucleation. Plasticity in whiskers containing no axial screw dis-
location must be explained in terms of dislocation nucleation either
at stacking defects or at the surface of dislocation-free crystal. It
was shown previously in the electron photomicrograph of Plate 14 how
stacking defects could serve as dislocation sources for hexagonal
networks of partial dislocations in the basal plane of a bent a-axis
whisker. Stacking defects noted in a-axis whiskers presumably act
in this fashion generating slip dislocations when the whisker is
strained in tension.

D. The Peierls-Nabarro Force

The fact that minimum yield points could be detected and
measured in Al_2O_3 whiskers suggests the possibility of calculating
the Peierls-Nabarro force required to move dislocations in the basal
and prismatic slip systems in sapphire. The P-N force can be cal-
culated by applying Schmid's critical resolved shear stress law.
Schmid's law for a single crystal stressed in tension shows that slip
in the crystal will take place along a given plane when the shear
stress in a given direction in the plane reaches a critical value,
reference 69. From Plate 33, the critical resolved shear stress,
$\sigma_{C.R.S.S.}$, can be expressed mathematically as

$$\sigma_{C.R.S.S.} = \frac{T}{A} \cos \phi \cos \lambda \tag{14}$$

where T is the axial tensile load, A is the area of cross section, ϕ is the angle between the normal to the plane of slip and the tensile axis, and λ is the angle between the slip direction and the tensile axis. The critical resolved shear stress, $\sigma_{C.R.S.S.}$, is strongly orientation dependent and is determined essentially by the orientation factor $\cos \phi \cos \lambda$, applied to the yield stress T/A.

In c-axis and a_I-axis whiskers where the slip planes and slip vectors are oriented normal to the axis of tension, the orientation factor $\cos \phi \cos \lambda$ should equate to zero. This means that the critical resolved shear stress also should equate to zero, and that the tension test should measure, directly, the cohesion between atoms on opposite sides of the slip plane. Evidence of basal slip in c-axis whiskers, however, indicates that the basal planes must be sloped, possibly because of spiral-like defects in some of the whiskers, or otherwise bent as shown by the curved slip bands in Plate 28 (b). Thus, the $\langle 11\bar{2}0 \rangle$ slip vector is no longer normal to the tensile axis and basal slip becomes operable. In a-axis whiskers where width to thickness ratios tend to be higher than for c-axis whiskers, it is quite probable that slip takes place by means of prism plane bending. Slip plane bending could also account for most of the lateral contraction which must occur when the whisker is extended by the tension force. This in turn could account in part for the size effect noted in measured elastic moduli where the values are lowered by the added elastic extension due to slip plane bending.

In a_{II}-axis whiskers where the observed slip planes, $\{11\bar{2}0\}$ prism planes, are oriented at an angle of 60° to the axis of tension, bending in the prism planes is not expected to be appreciable. The minimum yield point for a_{II}-axis whiskers according to Plate 29 is 0.57×10^6 lbs./in.^{2}, and this is in agreement with the fact that the minimum yield point for a_I-axis whiskers is higher, 0.75×10^6 lbs./in.^{2}, where the observed slip planes, $\{11\bar{2}0\}$ prism planes, are oriented normal to the axis of tension. If prism plane bending can be regarded as negligible in the a_{II}-axis whiskers, the Peierls-Nabarro force, the stress required to move slip dislocations in the prismatic slip system can be calculated. Using $\phi = 30°$ and $\lambda = 60°$, Schmid's relation becomes

$$\sigma_{C.R.S.S.} = \frac{T}{A} \cos \phi \cos \lambda = 0.57 \times 10^6 \times \cos 30° \times \cos 60° \quad (15)$$

It turns out that the P-N force is about 0.25×10^6 lbs./in.^{2}. This high value of the P-N force is attributed to the electrostatic drag exerted by the ionic lattice on a dislocation. It is likely that

because of directed bonds the width of the dislocation is very small
and contracted as compared to those in metals. The high P-N force
accounts for the much higher temperature required to obtain prismatic
slip than to obtain basal slip in sapphire as noted in previous in-
vestigations.

Unfortunately, there was no indication of the existence of
sapphire whiskers analogous to the case of a-axis whiskers with basal
planes oriented other than normal or parallel to the axis of tension;
therefore, an estimate of the P-N force for basal slip must be made
using indirect methods. As previously noted, many of the c-axis
whiskers showing the minimum yield point may be near structural per-
fection and contain few dislocations. Assume first, that the whisker
contains a single axial screw dislocation. Based on x-ray evidence
of the Eshelby twist found in c-axis whiskers, reference 70, the slip
plane might be visualized as a spiral ramp winding about the central
screw axis. The slip vector for basal slip is then no longer normal
to the axis of tension. Since the pitch of the spiral ramp is the
same as the Burgers vector for the $<0001>$ direction, about 13A°,
the slope of the slip vector away from the plane normal to the axis
of tension can be estimated for a whisker of say 10μ in diameter,
assuming a cylindrical specimen. The angle of the slope proves to be
negligible and therefore it follows that the critical resolved shear
stress is also negligible. Hence, plastic deformation in c-axis
whiskers must occur essentially by basal plane bending.

Actually, the above description of a c-axis whisker contain-
ing a single axial screw dislocation is somewhat idealized. The core
of the screw dislocation is in a much higher strained condition than
the rest of the crystal and the basal planes may thus show the highest
slope along the axis of the screw. This effect in the whiskers is
made evident by the dimples and peaks marking the nodes of F-R sources
noted in tensile fractures. The effect falls off rapidly with distance
from the core and this appears to be in agreement with theoretical
calculations of the stress field of a screw dislocation, references 71
and 72, which shows stress inversely proportional to the distance.
Hence, the basal planes only a short distance from the screw axis may
be nearly normal to the axis of tension thus lending additional support
to the notion that plastic deformation occurs essentially by basal
plane bending.

The presence of a single axial screw dislocation in a c-axis
whisker should cause it to show a strong tendency to nucleate disloca-
tions below the highest yield stress possible to structurally perfect
whiskers. This behavior is shown by Plate 30 where a few points at
the highest measured elastic modulus for c-axis whiskers show stresses
not much above the minimum of 0.27×10^6 lbs./in.^{2} established for

c-axis whiskers. The tendency to nucleate dislocations at the lower stresses is attributed to the affinity of the core of the screw dislocation for impurity atoms which in sufficient quantity act to embrittle the whisker at one or more sections along the screw axis thus weakening it. Some evidence of impurity migration to the core of an axial screw dislocation of a c-axis whisker is shown at the top of Plate 11 (a). The central axis is marked by a dark diffuse band around which are other spiral-like bands spaced at irregular intervals. The darkening is attributed to electron reversion which in turn is probably due to a valency effect brought about by the presence of the impurity element. Since silicon is the main impurity element and it has a valence of 4 as compared to 3 for aluminum, the electron concentration could be increased above that for the normal structure. The migration of silicon is presumably easy because it is substitutional with aluminum and moves readily through the hexagonal network formed by the interstitial holes of the sapphire structure. Hence, the effect of an axial screw dislocation in a c-axis whisker is to act as a source for the nucleation of dislocations while the slip process resulting in the formation of slip bands can be attributed essentially to basal plane bending.

A rough estimate of the P-N force for basal slip was obtained in the following way. A comparison was made between two ductile whiskers, one of the c-axis type and one of the a_I-axis type in which the slip planes are normal to the axis of tension. Both whiskers showed minimum yield points, were of equally fine size, and had ratios of width to thickness of $w/t \sim 3.5$. It was assumed that if the geometries of the whiskers are similar, the properties of the whiskers would be roughly in proportion to the anisotropy present in each. In Table 1, specimen #7 of the c-axis whiskers and specimen #9 of the a_I-axis whiskers were selected for this comparison. Stress strain curves showed that both had maximum elastic strains of 0.5%, indicating that the extent of slip plane bending in each whisker may have been roughly the same. The ratio of the minimum yield points, 0.25×10^6 lbs./in.^{2} for c-axis whiskers to 0.75×10^6 lbs./in.^{2} for a_I-axis whiskers gives 1/3, and this would be expected to be equal to the ratio of their P-N forces. A previous calculation of the P-N force for prismatic slip in a_I-axis whiskers gave 0.25×10^6 lbs./in.^{2} so that the P-N force for moving dislocations in a basal slip system in c-axis whiskers would be proportionately about 0.09×10^6 lbs./in.^{2}. Hence, the influence of directed bonds in the sapphire structure should be one-third as great in basal slip as it is in prismatic slip.

E. Young's Modulus of Elasticity in Sapphire

A definition for the elastic modulus or Young's Modulus of elasticity perhaps could be illustrated best by using a simple atomic

model. Consider straining in tension a line of identical atoms or two
kinds of ions linked together by atomic forces. Under a condition of
no load, each atom is in equilibrium with its neighbor at a distance
determined by a balance between a long-range attractive force, σ_A,
and a short-range repulsive force, σ_r ; this is illustrated in
Plate 34 where r_0 is the equilibrium distance of atom 2 from the
atom 1 located at the origin, reference 73. The curve outlining the
cross hatched area gives the difference between σ_A and σ_r at all
possible values of the distance r between the two atoms. From the
nature of this curve, it becomes clear that Hooke's law which states
that stress is proportional to strain is only an approximation and
fails after relatively small displacements of atom 2 from its equili-
brium position r_0 . Thus, Young's modulus of elasticity represented
by the slope of the difference force curve at r_0 also varies sig-
nificantly at small strains.

It was found experimentally that nearly, structurally perfect
c-axis whiskers which are believed to contain no dislocations; for
example, specimen #8 of Table 1, will yield after about 2.2% elastic
strain. All the atoms along the axis may be visualized as being
strained out of their equilibrium positions in all basal planes normal
to the axis by roughly this amount of strain which between adjacent
planes may be a small fraction of 1A°. The slight deviation from
Hooke's law as expected from the difference force curve in Plate 34
is not noticeable and a strong yield point appears first. Appearance
of a yield point implies that basal plane bending must have occurred
so that dislocations could be nucleated at the surface of the whisker
for the slip process. Hence, there are two contributions to the
elastic strain used in calculating the elastic modulus, one is due to
the actual strain tending the pull atoms apart and the other is due
to basal plane bending. Slip plane bending tends to reduce the elastic
modulus, particularly for whiskers with large width to thickness ratios.

Since the dislocation-free c-axis whiskers are usually found
in a finer size range and tend to have smaller width to thickness
ratios, basal plane bending does not contribute appreciably to the
elastic strain used in calculating the elastic modulus. A reasonable
estimate can be made of the degree of basal plane bending using
specimen #16 in the list of c-axis whiskers of Table 1. Assuming
that the volume and thickness remain constant and that lateral con-
traction influences only the width dimension of the whisker during
tensile straining, the final width at the yield point of the whisker
was found to be about 6.35×10^{-5} in. as compared to 6.43×10^{-5} in.
for the original width. This small change in width of the cross sec-
tion suggests that the curvature of the basal planes was fairly large.

Hence, using approximation methods, the extension in the direction of tension due to basal plane bending was found to be about 1.0% of the measured elastic strain at the yield point, and the maximum angle that bent basal planes made with the plane normal to the axis of tension was roughly estimated at about 20°. The calculated elastic modulus is thus correspondingly lowered by 1.0% so that the recorded value, 66.0×10^6 psi, is actually 66.7×10^6 psi, and well within the experimental limits of error.

The large deviations shown in the measured elastic moduli of structurally imperfect whiskers, those containing potential slip dislocations, suggest that these might be due to a combination of factors that act to lower the measured values. Even if an error of as much as 10% each could result from the effects of impurities and of basal plane bending, the measured elastic modulus should still be above 50×10^6 lbs./in.^{2}; hence, these cannot account for experimentally measured values running as low as 26.5×10^6 lbs./in.^{2}. Actually, basal plane bending is expected to remain small at the lower yield stresses recorded for these whiskers, despite the possibility that the presence of an axial screw dislocation might make basal plane bending easier. It is inconceivable, however, that impurities could lower the elastic constants of sapphire to the extent that it is observed in the data of Table 1; hence, it must be due to a size effect as noted previously. The effect of whisker size on the measured elastic modulus is real and finds support in the fact that Singer and Thurnauer, reference 74, found a similar relationship in fine rods of "sinter alumina" tested in tension.

There is at present no clear explanation of why the size of sapphire whiskers should exert such a pronounced effect on the elastic modulus. Basal plane bending as noted above apparently provides only a partial answer; therefore, the problem remains open to further investigation. The elastic modulus determined for dislocation-free c-axis whiskers, 69×10^6 lbs./in.^{2}, is in very good agreement with that obtained for the $<0001>$ direction by Wachtman et al., reference 75, using ultrasonics on single crystal, macrospecimens of synthetic corundum, 66×10^6 lbs./in.^{2}. The high values of the elastic moduli obtained for a-axis whiskers, however, are in sharp disagreement with those obtained by these investigators who assuming isotropy in the basal plane obtained a value of 61×10^6 lbs./in.^{2}. This value is but slightly lower than that for the $<0001>$ direction. The whisker tests definitely show that there is mechanical anisotropy in the two types of a-axis whiskers and this finds added support in the fact that discrepancies were found in the symmetry shown by the diffraction pattern for these whiskers in Plate 9. However, the most puzzling

problem to emerge from this situation appears to be why the dynamic tests should show such markedly lower elastic moduli.

Wachtman et al., reference 76, review in detail past challenges to the theory and experimental procedure used in determining the elastic stiffness and compliance coefficients in crystals. Unlike previous experiments, the recent ultrasonic determination of the elastic constants in sapphire made by these investigators involved several additional precautions. Besides conducting experiments in the low kilocycle range, particular attention was given to the sign on crystal direction in the basal plane. Also, the sound waves were transmitted through a taut suspension thread to avoid error from a faulty bond, a difficulty frequently met when a crystal is cemented to a transducer in the usual method. Despite all these precautions, the data still showed discrepancies, particularly in the C_{14} constant. It was indicated that low angle boundaries in the crystals might have affected the results. A later experiment conducted by Bernstein, reference 77, using the same specimens, acquired from Wachtman et al., which was run in the megacycle-frequency range yielded data in good agreement with that obtained in the low kilocycle range.

Because in the resonant frequency techniques, the atoms in a perfect crystal are strained only a small amount from their equilibrium positions, in the region where elastic behavior is expected to be the closest to linear, this method has been looked upon as being the most reliable for measuring the elastic constants in crystals. Most dynamic measurements, however, have been made on macrocrystals presumably containing numerous dislocations. Although, chemical analyses are not usually made available, the crystals used in most previous experiments were probably of fairly high purity; therefore, dislocation movements must have been possible. There is now considerable evidence, reference 78, that dislocations in crystals have the ability to dampen vibrations markedly. Also, Cady, reference 79, suggested that vibrations propagated in a crystal may not always be fully transmitted in the direction intended, and that vibrational energy could conceivably be directed into other paths of lesser resistance. The various data on sapphire appear to lend support to this view.

F. The Theoretical Strength of Al_2O_3 Whiskers

Failure in ductile sapphire whiskers is usually brought about first by shear along a potential slip plane; hence, it is difficult to measure the true cohesive strength of the pure crystal. The lowest estimate, reference 80, of the critical shear stress required to shear two rows of identical atoms past each other in a perfect metal crystal is about G/30 where G is the shear modulus or modulus of rigidity of

48

the crystal. In well-annealed, large single crystals of pure metals, the shear stress needed for plastic deformation is found to be less than 10^{-4} G. This indicates that dislocations must be present which are able to move under very low applied stresses. In the case of ionic solids such as diamond or sapphire, where directed bonds between ions would be expected to influence the results substantially, the critical shear stress, reference 81, for a structurally perfect crystal might very well be near G/5.

Taking G = 2.0 x 10^{12} dyne/cm^2 (29 x 10^6 lbs./in.^{2}) for sapphire, reference 82, one finds that the minimum yield point for c-axis whiskers, 0.27 x 10^6 lbs./in.^{2}, is 9.3 x 10^{-3} G, but the critical resolved shear stress may actually be about 0.09 x 10^6 lbs./in.^{2} or 3.1 x 10^{-3} G which approaches behavior shown by the pure metals. This low value of the critical resolved shear stress indicates that the whiskers are imperfect and contain dislocations which are able to move under low applied stress. It should be noted that at the low yield point for c-axis whiskers, prismatic slip cannot operate unless an appreciable amount of basal slip takes place.

The ease with which basal slip apparently takes place could be detected in the fine detail of a fracture surface on one of the larger c-axis whiskers. A schematic diagram illustrating the morphology of the fracture surface is shown in Plate 35. Although two sets of dislocation nodes are indicated, the whisker has only two axial screw dislocations along which whisker growth took place. The second set is accounted for by the fact that basal slip involved a strong rotation of one half of the crystal with respect to the other near the final stage of rupture. Location of the axis of rotation can be roughly approximated by drawing straight lines through the two sets of nodes; those near the right-hand edge and those near the bottom edge. The intersection of these lines places the axis at the lower right-hand corner of the fracture section. The results of the rotation is that two nodes locate the position of two axial screw dislocations in one half of the crystal while the other two are merely impressions left by nodes locating the positions of axial screws in the other half of the crystal. A left-hand rotation about the axis of rotation moves most points falling in the area between the two sets of nodes, presumably in the $<11\bar{2}0>$ direction, the direction determined for basal slip.

In the case of dislocation-free c-axis whiskers, the maximum yield point, 1.47 x 10^6 lbs./in.^{2}, is found to be about G/20. Only two c-axis whiskers showed such high yield strengths; the other indicated a value of 1.02 x 10^6 lbs./in.^{2} or about G/28. Further

testing could perhaps turn up a few more results higher than these. It should be pointed out that the above two values were obtained on whiskers of the finest size available; hence, if even finer sizes could be found and tested, it is conceivable that yield points closer to the theoretically estimated critical shear stress of G/5 could be attained. The implication is that size effect could play a significant role in the nucleation of dislocation loops at the surface of dislocation-free whiskers.

Taking specimen #16 of the c-axis whiskers; i.e., the whisker showing a yield point of 1.02×10^6 lbs./in.^{2}, it should be possible to estimate the stress required to nucleate dislocations at a lateral face of the whisker. Previously, it was found that the maximum angle that the basal planes make with the plane normal to the axis of the whisker is roughly 20°; this is the angle that the plane tangent to the bent basal plane at the lateral face makes with the plane normal to the axis of the whisker. Applying Schmid's law, the critical resolved shear stress is found to be 0.326×10^6 lbs./in.^{2} or about G/89. It must be understood that the angle used in the above estimate is an approximation, and it is assumed that the basal planes take on a circular curvature. The value obtained above is much lower than that predicted by theory, hence, it is surmised that the basal planes might take on a somewhat larger slope at the lateral face of the whisker.

To show the manner in which size influences the above result, a qualitative comparison can be made with specimen #8 of the c-axis whiskers. First, it should be noted that this whisker is roughly four times larger in cross section than specimen #16; yet, it shows a much higher yield point. This tends to contradict what was stated previously; but, it should be noted further that specimen #8 has a lower w/t ratio, about 2.5, as compared to 5 for specimen #16. It is the higher w/t ratio which causes specimen #16 to have a lower yield point, despite its finer size. The larger width of the cross section appears to offer more leverage making it easier to bend the basal planes at the lateral faces so that lower stress is needed for the nucleation of dislocation loops.

Lateral contraction of the whisker could also contribute to the critical shear stress required to nucleate dislocations by causing basal planes at the lateral faces, which in this instance are assumed to be well sloped, to squeeze out material at center much as paste is squirted from a thin-walled tube. This effect can be visualized more clearly by taking a deck of playing cards in one hand and bending the whole deck between the thumb and fore finger so that all cards bend convex toward the palm; release of the fingers from the

uppermost cards results in a shower of these cards as they seem to shear away from those still constrained by the fingers. Such shearing forces could conceivably be responsible for cleavage fractures observed in the sapphire whiskers. Hence, in whiskers having a large w/t ratio, it is possible to resolve much of the tensile force at the yield point into slip directions in the basal plane so that the yield strength of the whisker approaches the critical resolved shear stress. Assuming specimen #16 meets the above requirement of a large w/t ratio, the critical resolved shear stress required to initiate basal slip for a perfect sapphire crystal could be nearer G/30, or roughly that estimated for a structurally perfect single crystal of metal, rather than G/5 as previously thought.

The dislocation-free c-axis whisker having w/t of about 2.5, specimen #8, has a higher yield point, 1.47×10^6 lbs./in.^{2}, because a smaller fraction of the yield stress is resolved into slip directions along the basal plane and much of the tensile stress is acting against cohesive forces directed normal to the basal planes. If the results obtained in the study of size effect are correct, then still finer whiskers which have w/t values near unity should show higher yield points because basal plane bending would then be at a minimum. The yield point should, therefore, approach the cohesive strength and come more within range of the elastic modulus. The fact that specimen #8 has a yield point of about E/47 where E is the elastic modulus, 69×10^6 lbs./in.^{2}, gives some indication of the proximity of the yield strength to the true cohesive strength. The true cohesive strength, however, cannot reach the value of the elastic modulus because this means that the whisker would have to be strained 100%; a theoretical estimate, reference 83, of the cohesive strength of a metal gives a value in the vicinity of E/10. Further indication of the high cohesive strength in the <0001> direction can be found in the higher fracture strength of specimen #8, 1.58×10^6 lbs./in.^{2} or E/44. Some prismatic slip probably occurred which exerted a braking action on basal slip thus tending to stop failure by shear so that cohesion between atoms provides the main contribution to fracture strength. Shear at such high stress, again, is very rapid and prevents the appearance of a high work hardening rate so that the whisker fails at a lower fracture strength than that actually possible.

Much of what has been described above could be equally applied to a-axis whiskers. Since the strength properties of a-axis whiskers are substantially higher than those for c-axis whiskers, the calculated values for the critical resolved shear stress for nucleating dislocations in dislocation-free crystal and for the cohesive strength would therefore be closer to the theoretically estimated values providing that

G and E remain the same. Because of the new evidence of higher elastic moduli in the basal plane of sapphire, G and E take on new values for the whiskers. Normally, Young's modulus, E, is expected to be a singular constant of the crystal and is usually taken as the maximum measured value for all possible directions in the crystal. This maximum value according to measurements made on various crystals usually turns out to be that for a principal direction in the crystal such as the c-axis in the case of zinc, and it is shown as such on a representation surface for Young's Modulus of elasticity, reference 84. G values for the a_I-axis and a_{II}-axis whiskers were roughly estimated by assuming that they bear the same relation of G to E as in the case of c-axis whiskers. Thus, for c-axis whiskers G is 0.42E so that G is 75×10^6 lbs./in.^{2} for a_I-axis whiskers and 140×10^6 psi for a_{II}-axis whiskers.

Previously, it was shown that the critical resolved shear stress in a-axis whiskers containing dislocations is 0.25 x 10^6 lbs./in.^{2}. In terms of G for a_I-axis whiskers, this stress is 3.0×10^{-3} G which is close to the result found for c-axis whiskers. The fact that G is different in each case simply indicates that the ability to move dislocations in the two type whiskers is related to the elastic properties of dislocations in the basal and prismatic slip systems. In the dislocation-free a_{II}-axis whiskers where $\{11\bar{2}0\}$ prism planes are oriented 60° to the axis of tension and where the yield strength measured 2.0 x 10^6 lbs./in.^{2}, the stress required to nucleate dislocations on prism planes can be calculated. Using Schmid's relation, the critical resolved shear stress is $2.0 \times 10^6 \times \cos 60° \times \cos 30°$ which gives a stress of 0.866 x 10^6 lbs./in.^{2} or about G/87 for a_I-axis whiskers. The closeness of this result to that obtained for c-axis whiskers again indicates that the nucleation of dislocation loops on the basal (0001) and $\{11\bar{2}0\}$ prism planes is closely related to the elastic properties of dislocations in the two slip systems. The relative difficulty of nucleating and moving dislocations in the two slip system, therefore, is roughly in the ratio of the elastic moduli for the < 0001> and <11$\bar{2}$0> directions, or about 3:1.

It is now possible to make an estimate of the stacking fault energy for basal slip. The stacking fault energy, reference 85, is $\gamma = \sigma_r b$ where σ_r is the critical resolved shear stress and b is the Burgers vector of the partial dislocation. Inserting the values $\sigma_r = 0.09 \times 10^6$ lbs./in.^{2} = 6.2 x 10^9 dynes/cm^2 and b = 1/3 <11$\bar{2}$0> = 1.58 x 10^{-8} cm gives a value of 98 ergs/cm^2 which is comparable to that found in metals, reference 86. This apparently anomalous behavior

in sapphire where directed bonds are otherwise expected to contract the width of dislocations is attributed to the movement of aluminum and oxygen ions in groups, like molecules, as proposed by Kronberg, reference 87, who describes it in terms of cooperative movements of two kinds of ions in forming what are termed synchro-shear partials. The details are complex and involve two types of electrostatic-faults; a more detailed description is given in the reference cited above.

V. SUMMARY AND CONCLUSIONS

1. Methods and techniques of testing whiskers in tension were described which were used to obtain new experimental data on the mechanical behavior of near-micron size sapphire whiskers at 25°C. Anisotropy could be detected and measured in mechanical properties of whiskers corresponding to simple growth directions in sapphire; i.e., the $<0001>$, $<11\bar{2}0>$, and $<1\bar{1}00>$ directions.

2. Although spectrographic analysis of a single sample containing a large number of whiskers showed a low level of impurities, about 0.1% total impurities consisting mainly of silicon, whiskers of each orientation showed a wide range of behavior from extreme brittleness to exceptional ductility as observed in fracture appearance and stress-strain curves. This result is attributed to the heterogeneous conditions under which the whiskers grew in that impurity atoms were distributed in varying degree on individual whiskers.

3. Impurities are believed to influence the frequency with which stacking defects are formed in the whiskers during their growth. Stacking defects occurred along basal planes in $<0001>$ whiskers and along $\{11\bar{2}0\}$ prism-planes in $<11\bar{2}0>$ and $<1\bar{1}00>$ whiskers; the stacking defects appeared to have a spiral-like character in some $<0001>$ whiskers thus indicating the presence of an axial screw dislocation.

4. The morphology of $<0001>$ whiskers is strongly influenced by impurities. Brittle specimens which were ascertained to be relatively richer in impurities had cross sections in the form of a parallelogram; whiskers showing high ductility and therefore high purity tended to show additional plane faces characterizing the hexagonal form of the crystal and also tended to show the highest mechanical properties indicating that they were near structural perfection.

5. Most large size $<0001>$ whiskers grew along one or two screw dislocations acting as a source for the generation of dislocations. A limiting size, about 6.3μ , corresponding to the width dimension of

the cross section, was found below which such sources apparently could
not operate and where whiskers presumably formed by two dimensional
nucleation and growth on the substrate crystal. This limiting size
was found to be in agreement with a theoretical calculation for the
critical radius of a central loop near a spiral source below which
operation of the source would be difficult.

6. Most of the a-axis whiskers used in the tests appear to be too
fine to have grown by a screw mechanism; therefore, growth probably
took place by means of two-dimensional nucleation in agreement with
experimental evidence.

7. A pronounced size effect was found in fracture strength, σ_f,
and in measured elastic moduli, E_m, of the whiskers; maximum values
could be approached only in the limit of extremely fine size. General
equations derived from the plotted data showing E_m or σ_f as a function
of size, A, are as follows:

$$\sigma_f = aA^b$$

$$E_m = cA^d$$

8. The maximum values of measured elastic moduli were 71×10^6
lbs./in.^{2}, 180×10^6 lbs./in.^{2}, and 330×10^6 lbs./in.^{2}, corresponding
to the $<0001>$, $<11\bar{2}0>$, and $<1\bar{1}00>$ directions in sapphire,
respectively. The value obtained for the $<0001>$ direction is in
good agreement with those obtained using ultrasonics. The greatly
reduced values shown by whiskers in a large size range can neither be
reasonably accounted for by the presence of impurities nor by slip
plane bending; hence, it must be concluded that a true size effect is
present, and that the above values merely approach the true elastic
constants of the sapphire crystal.

9. The large difference found in the elastic moduli for the two
types of a-axis whiskers indicates that elasticity is non-isotropic
for the two types of a-axis sapphire whiskers. This data is supported
by the finding of lower symmetry in an electron diffraction pattern
obtained by diffraction from the broad face of a-axis whiskers, and by
the unexpected angular relationship found between two kinds of extended
dislocations.

10. The primary slip system operating in $<0001>$ whiskers is
basal slip, (0001) $<11\bar{2}0>$; in a-axis whiskers, it is prismatic slip,
$\{11\bar{2}0\} <1\bar{1}00>$. Although slip planes in the above slip systems may
be oriented normal to the axis of tension in unstrained whiskers,

appreciable slip plane bending may take place as a whisker is strained in tension, thus making the slip system operable since the slip vector is no longer normal to the axis of tension.

11. Intersecting slip noted in very ductile whiskers indicates that both basal and prismatic slip systems can operate simultaneously; this is brought about primarily by the formation of jogs during the operation of the primary slip system, while torque on the resulting jogs initiates slip on the secondary slip system. Jog formation accounts for the high work hardening rate observed in stage II deformation in stress-strain curves.

12. The Peierls-Nabarro force required to move slip dislocations in the prismatic slip system of sapphire was calculated at about 0.25×10^6 lbs./in.^{2}; that required in the basal slip system could be deduced at about 0.09×10^6 lbs./in.^{2}. Also, the force required to nucleate dislocations along the $\{11\bar{2}0\}$ prism planes in structurally perfect a-axis whiskers was calculated at about 0.866×10^6 lbs./in.^{2}; that required to nucleate dislocations along basal planes of structurally perfect $<0001>$ whiskers was deduced at about 0.326×10^6 lbs./in.^{2}.

13. The relative difficulties of nucleating and moving slip dislocations in the two slip systems, $\{11\bar{2}0\}$ $<1\bar{1}00>$ and (0001) $<11\bar{2}0>$, is roughly in the ratio of the elastic moduli for the $<11\bar{2}0>$ and $<0001>$ directions or about 3:1, thus demonstrating the elastic behavior of these dislocations.

14. The true cohesive strength of the whiskers can be approached only in extremely fine sizes and where width to thickness ratios, w/t, are near unity and slip plane bending is at a minimum.

VI. RECOMMENDATIONS

On the basis of the work done thus far on sapphire whiskers, the following recommendations concerning future research are advanced:

1. New experiments should be run on the growth characteristics of sapphire whiskers, particularly on a-axis whiskers since these show exceptionally high mechanical properties and, therefore, exceptional potential in engineering applications. Such experiments should include control of the type, purity, and orientation of the substrate crystals on which the whiskers grow.

2. Further tests, not necessarily tension tests, should be applied to the near-micron size sapphire whiskers. These tests should include, for example, bend tests and torsion tests, which might give a keener insight into the mechanical behavior of these whiskers.

3. Since the elevated temperature tests made in the present study were strictly qualitative, it would be desirable to run further experiments in which quantitative data could be obtained, particularly in regards to short-time elevated temperature strength, creep resistance, and delayed fracture of sapphire whiskers.

REFERENCES

(1) F.R.N. Nabarro and P. J. Jackson, from "Growth And Perfection of Crystals," the proceedings of an international conference on crystal growth held at Cooperstown, New York, on August 27-29, 1958, edited by R. H. Doremus, B. W. Roberts, and David Turnbull (1958), p. 13.

(2) C. Herring and J. K. Galt, Phys. Rev., 85, 1060 (1952).

(3) J.D.H. Donnay and W. Nowacki, "Crystal Data," Geological Society of America, Memoir 60, (1954).

(4) F. C. Phillips, "An Introduction to Crystallography," 2nd ed., Longmans (1960), p. 121.

(5) J. F. Nye, Acta Met. 1, 153 (1953).

(6) M. L. Kronberg, Science, 122, 599, (1955).

(7) M. L. Kronberg, Acta Met., 5, No. 9, 507 (1957).

(8) L. Pauling and S. Hendricks, J. Amer. Chem. Soc., 47, 781, (1925).

(9) W. L. Bragg, "Atomic Structure of Minerals," Cornell Univ. Press (1939).

(10) E. L. McCandless and D. M. Yenni, U. S. Pat. 2,485,979 (1949).

(11) J. B. Wachtman, Jr., and L. H. Maxwell, J. Amer. Ceram. Soc., 37, 291 (1954).

(12) M. L. Kronberg (reference (7)), p. 510.

(13) M. V. Klassen-Neckliudova, N. Ia. Ikornikova, and G. E. Tomolovskii, Trudy Inst. Krist. Shad Nauk SSR, No. 8, 237 (1953).

(14) R. Scheuplein and P. Gibbs, J. Amer. Ceram. Soc., 43, 458 (1960).

(15) P. Gibbs, "Kinetics of High-Temperature Processes," edited by W. O. Kingery, John Wiley, New York, (1959), p. 21.

(16) M. L. Kronberg (reference (7)), p. 511.

(17) W. T. Read, "Dislocations In Crystals," McGraw-Hill, New York (1952), p. 120.

(18) A. H. Cottrell, "Dislocations and Plastic Flow in Crystals," Clarendon Press, Oxford (1958), p. 37.

(19) F. Singer and H. Thurnauer, Metallurgia 36, 237 (1947).

(20) J. F. Nye, "Physical Properties of Crystals," Oxford, (1960), p. 134-141.

(21) R.V.G. Sundara Rao, "Elastic Constants of Alumina," Proc. Indian Acad. Sci. [A] 26, 352-360 (1949).

(22) J. Bhimasenschar, "Elastic Constants of Corundum," Proc. Natl. Inst. Sci. India, Pt. A 16, 241-243 (1950); "Elastic Constants of Corundum," Current Sci. (India) 18, 372-373 (1949).

(23) W. G. Mayer and E. A. Hiedemann, J. Acoust. Soc. Amer., 30, 756-760 (1958); Acta Cryst. 12, 1-6, (1959).

(24) J. B. Wachtman, Jr., W. E. Tefft, D. G. Lam, Jr., and R. P. Stinchfield, J. Research, National Bureau of Standards - A. Phys. and Chem., Vol. 64A, No. 3, 213, (May-June 1960).

(25) J. F. Nye (reference (20)), p. 145.

(26) W. W. Webb and W. D. Forgeng, J. Appl. Phys., 28, 1449, (1957).

(27) R. C. DeVries and G. W. Sears, J. Chem. Phys., 31, 1256, (1959).

(28) S. S. Brenner, J. Appl. Phys., 33, 33, (1962).

(29) F. C. Frank, Acta Cryst. 4, 497, (1951).

(30) G. W. Sears and R. C. DeVries, J. Chem. Phys., 32, 93 (1960).

(31) P. L. Edwards and R. J. Happel, J. Appl. Phys., 33, 826 (1962).

(32) S. S. Brenner (reference (28)).

(33) E. Singer and H. Thurnauer (reference (19)), p. 240.

(34) W. W. Webb and W. D. Forgeng (reference (26)), p. 1451.

(35) P. D. Gorsuch, General Electric Research Laboratory Progress Report No. 6, "Research On the Behavior of Nearly Perfect Crystals," Contr. No. AF-33(616)-6181, WADD Task No. 70627 (July 1960).

(36) S. S. Brenner, J. Appl. Phys., 27, No. 12, 1488 (1956).

(37) W. W. Webb and W. D. Forgeng (reference (26)), p. 1449.

(38) B. C. Raynes, Horizons Inc., Final Report on "Studies Of The Reinforcement of Metals With Ultra-High Strength Fibers (Whiskers)," Bureau of Naval Weapons, Contr. NOw-61-0207-C (November 27, 1961).

(39) P. L. Edwards and R. J. Happel (reference (31)), p. 827.

(40) J. E. Emrich and H. L. Gegel, ASD Technical Report 61-168, Wright-Patterson Air Force Base, Ohio (Sept. 1961).

(41) A. U. Mac Rae, Science, Vol. 139, No. 3553, 379 (1963).

(42) C. S. Barrett, "Structure of Metals," 2nd ed., McGraw-Hill (1952), p. 593.

(43) P. B. Hirsch, J. Inst. Metals, 87, 406 (1959).

(44) M. L. Kronberg (reference (7)), p. 512.

(45) Z. S. Basinski, D. B. Dove, and A. T. Aldred, J. Appl. Phys., 34, 469, (1963).

(46) S. S. Brenner, from "Growth and Perfection of Crystals," edited by R. H. Doremus, B. W. Roberts and David Turnbull, John Wiley, New York (1958), p. 166.

(47) S. S. Brenner (reference (46)), p. 175.

(48) S. S. Brenner (reference (28)), p. 36.

(49) P. L. Edwards and R. J. Happel (reference (31)), p. 827.

(50) J. M. Roberts and N. Brown, Trans. Amer. Inst. Min. (Metall.) Engrs. 218, 454 (1960).

(51) F. Singer and H. Thurnauer, (reference (19)), p. 241.

(52) F. Singer and H. Thurnauer, (reference (19)), p. 241.

(53) W. W. Webb and W. D. Forgeng (reference (26)), p. 1451.

(54) S. S. Brenner (reference (28)), p. 37.

(55) W. J. Luhman and A. E. Gorum, Acta Met. 7, 685 (1959).

(56) P. L. Edwards and R. J. Happel (reference (31)), p. 827.

(57) A. Seegar, from an international conference, "Dislocations and Mechanical Properties of Crystals," edited by J. C. Fisher, W. G. Johnson, R. Thomson, and T. Vreeland, Jr., John Wiley, New York (1957), p. 270.

(58) S. Mendelson, J. Appl. Phys., 33, 2175, (1962).

(59) D. B. Hoover and J. Washburn, J. Appl. Phys., 33, 11 (1962) p. 12.

(60) A. H. Cottrell (reference (18)), p. 133.

(61) S. S. Brenner (reference (28)), p. 36.

(62) A. H. Cottrell (reference (18)), p. 58-64.

(63) G. W. Sears and R. C. DeVries (reference (30)).

(64) W. T. Read (reference(17)), p. 76.

(65) N. F. Mott, Phil. Mag., 43, 1151, (1952); Trans. AIME, 218, 967 (1960).

(66) A. H. Cottrell (reference (18)), p. 84.

(67) A. H. Cottrell (reference (18)), p. 133.

(68) Roger Chang, J. Appl. Phys., 31, 486 (1960).

(69) E. Schmid and W. Boas, "Plasticity in Crystals," (English translation), F. A. Hughes and Co., Ltd., London (1950).

(70) R. D. Dragsdorf and W. W. Webb, J. Appl. Phys., 29, 817 (1958).

(71) A. H. Cottrell (reference (18)), p. 35.

(72) W. T. Read (reference (17)), p. 114.

(73) R. Houwink, "Elasticity, Plasticity and Structure of Matter," Harren Press, Washington, D. C. (1953), p. 23.

(74) E. Singer and H. Thurnauer (reference (19)).

(75) J. B. Wachtman, Jr., W. E. Tefft, D. G. Lam, Jr., and R. P. Stinchfield (reference (24)).

(76) J. B. Wachtman, Jr., W. E. Tefft, D. G. Lam, Jr., and R. P. Stinchfield (reference (24)), p. 213.

(77) B. T. Bernstein, J. Appl. Phys., 34, 169 (1963).

(78) K. Lücke and A. Granato, from an international conference "Dislocations and Mechanical Properties of Crystals," edited by J. C. Fisher, W. G. Johnson, R. Thomson, T. Vreeland, Jr., John Wiley, New York, (1957), p. 425.

(79) W. G. Cady, Piezoelectricity, McGraw-Hill, New York (1946), p. 47.

(80) J. K. Mackenzie (reference (18)), p. 10.

(81) D. Kuhlmann-Wilsdorf, from a series of lectures on dislocation theory given at the University of Pennsylvania (1962).

(82) W. W. Webb and W. D. Forgeng (reference (26)), p. 1454.

(83) W. L. Finlay and J. R. Lane, Metal Progress, Vol. 84, No. 3, 79 (1963).

(84) J. F. Nye (reference (20)).

(85) D. Kuhlmann-Wilsdorf (reference 81)).

(86) H. Suzuki, from an international conference, "Dislocations and Mechanical Properties of Crystals," edited by J. C. Fisher, W. C. Johnson, R. Thomson, and T. V. Vreeland, Jr., John Wiley, New York (1957), p. 380-387.

(87) M. L. Kronberg (reference (7)), p. 512-517.

ACKNOWLEDGEMENTS

TENSILE DATA ON SAPPHIRE (Al$_2$O$_3$) WHISKERS AT 25°C

c-axis Whiskers

Specimen No.	Geometry of Cross Section	Dimensions of Cross Section (in.)		Area of Cross Section (in.^{2})	σ_y (Initial Yield Stress) (10^6 psi)	σ_f (Fracture Stress) (10^6 psi)	$\varepsilon_{TOT.}$ (Total Strain) (%)	E_m (Measured Young's Modulus) (10^6 psi)	Remarks
1	Parallelogram	w = 5.78 × 10^{-5}	t = 2.57 × 10^{-5}	1.49 × 10^{-9}	0.28	0.35	1.1	35.0	Ductile Behavior
2	Parallelogram*	w = 2.43 × 10^{-4}	t = 4.89 × 10^{-5}	1.19 × 10^{-8}	----	0.39	1.0	32.5	Brittle Behavior
3	Parallelogram	w = 2.18 × 10^{-4}	t = 5.14 × 10^{-5}	1.12 × 10^{-8}	0.26	0.47	1.8	40.0	Ductile Behavior
4	Parallelogram	w = 3.14 × 10^{-4}	t = 7.71 × 10^{-5}	2.42 × 10^{-8}	0.30	0.54	1.9	36.0	Ductile Behavior
5	Parallelogram	w = 3.76 × 10^{-4}	t = 9.00 × 10^{-5}	3.39 × 10^{-8}	0.38	0.56	1.7	38.5	Ductile Behavior
6	Parallelogram	w = 3.46 × 10^{-4}	t = 8.30 × 10^{-5}	2.88 × 10^{-8}	0.55	0.68	2.1	33.0	Ductile Behavior
7	Parallelogram*	w = 1.96 × 10^{-4}	t = 5.46 × 10^{-5}	1.07 × 10^{-8}	0.28	0.82	1.7	59.5	Ductile Behavior
8	Double Trapezoid**	w$_T$ = 1.28 × 10^{-4}	t = 2.57 × 10^{-5}	3.30 × 10^{-9}	1.47	1.58	2.4	67.0	Ductile Behavior
9	Parallelogram	w = 2.12 × 10^{-4}	t = 2.90 × 10^{-5}	6.15 × 10^{-9}	0.43	1.23	2.2	71.0	Ductile Behavior
10	Parallelogram	w = 5.78 × 10^{-5}	t = 1.93 × 10^{-5}	1.12 × 10^{-9}	0.30	1.00	1.9	56.5	Ductile Behavior
11	Trapezoid**	w$_T$ = 2.44 × 10^{-4}	t = 1.45 × 10^{-5}	1.77 × 10^{-9}	0.28	1.10	1.6	61.0	Ductile Behavior

*Sharp cornered apices of parallelogram were slightly beveled.
**w$_T$ used in calculating the area of cross-section is the sum of the parallel sides of the trapezoid.

TABLE 1
PAGE 1 OF 4 PAGES

Specimen No.	Geometry of Cross Section	Dimensions of Cross Section (in.)	Area of Cross Section (in.^{2})	σ_y (Initial Yield Stress) (10^6 psi)	σ_f (Fracture Stress) (10^6 psi)	$\varepsilon_{TOT.}$ (Total Strain) (%)	E_m (Measured Young's Modulus) (10^6 psi)	Remarks
12	Parallelogram	w = 2.57×10^{-4} t = 5.78×10^{-5}	1.49×10^{-8}	0.29	0.71	2.6	54.5	Ductile Behavior
13	Parallelogram	w = 2.70×10^{-4} t = 6.44×10^{-5}	1.74×10^{-8}	----	0.94	2.7	31.0	Brittle Behavior
14	Parallelogram	w = 2.62×10^{-4} t = 5.71×10^{-5}	1.49×10^{-8}	--	0.71	2.7	26.5	Brittle Behavior
15	Parallelogram	w = 5.45×10^{-5} t = 3.85×10^{-5}	2.1×10^{-9}	0.65	0.81	2.8	69.0	Ductile Behavior
16	Parallelogram	w = 6.43×10^{-5} t = 1.29×10^{-5}	8.3×10^{-10}	.02	1.18	2.3	66.0	Ductile Behavior
17	Parallelogram	w = 7.85×10^{-4} t = 6.74×10^{-4}	5.29×10^{-7}	----	0.42	1.3	32.0	Brittle Behavior (G.E. Whisker)
18	Hexagon***	a = 1.56×10^{-4}	6.33×10^{-8}	----	0.30	1.1	28.0	Brittle Behavior (G.E. Whisker)
19	Parallelogram	w = 1.86×10^{-4} t = 1.35×10^{-4}	2.51×10^{-8}	0.24	0.64	0.9	52.5	Ductile Behavior (G.E. Whisker)
20	Parallelogram	w = 5.35×10^{-4} t = 3.58×10^{-5}	1.92×10^{-7}	0.28	0.58	2.5	50.0	Ductile Behavior (G.E. Whisker)
			a — axis Whiskers					
1	Rectangle	w = 1.12×10^{-4} t = 1.45×10^{-5}	1.62×10^{-9}	----	1.74	1.6	110	Brittle Behavior
2	Rectangle	w = 5.17×10^{-5} t = 1.29×10^{-5}	6.65×10^{-10}	1.30	2.32	2.2	119	Ductile Behavior
3	Rectangle	w = 2.25×10^{-4} t = 1.61×10^{-5}	3.62×10^{-9}	1.10	2.17	1.9	108	Ductile Behavior

*** a represents the length of one of the six sides of the hexagon.

TABLE 1
PAGE 2 OF 4 PAGES

Specimen No.	Geometry of Cross Section	Dimensions of Cross Section (in.)	Area of Cross Section (in.²)	σ_y (Initial Yield Stress) (10⁶ psi)	σ_f (Fracture Stress) (10⁶ psi)	$\epsilon_{TOT.}$ (Total Strain) (%)	E_m (Measured Young's Modulus) (10⁶ psi)	Remarks
4	Rectangle	w = 2.03 × 10⁻⁴, t = 1.85 × 10⁻⁵	3.76 × 10⁻⁹	----	1.62	1.5	125	Brittle Behavior
5	Rectangle	w = 4.66 × 10⁻⁵, t = 1.45 × 10⁻⁵	6.74 × 10⁻⁹	0.75	2.08	3.2	166	Ductile Behavior
6	Rectangle	w = 6.75 × 10⁻⁵, t = 1.61 × 10⁻⁵	1.09 × 10⁻⁹	1.24	1.58	1.7	119	Ductile Behavior
7	Rectangle	w = 5.79 × 10⁻⁵, t = 1.61 × 10⁻⁵	9.30 × 10⁻¹⁰	1.05	1.17	1.5	127	Ductile Behavior
8	Rectangle	w = 1.80 × 10⁻⁴, t = 1.60 × 10⁻⁵	2.90 × 10⁻⁹	----	3.12	3.1	121	Brittle Behavior
9	Rectangle	w = 7.70 × 10⁻⁵, t = 2.25 × 10⁻⁵	1.73 × 10⁻⁹	0.75	1.75	2.2	150	Ductile Behavior
10	Rectangle	w = 4.18 × 10⁻⁵, t = 9.64 × 10⁻⁶	4.02 × 10⁻¹⁰	1.70	3.23	1.6	180	Ductile Behavior
11	Rectangle	w = 9.15 × 10⁻⁵, t = 1.61 × 10⁻⁵	1.47 × 10⁻⁹	1.20	2.06	2.2	125	Ductile Behavior
12	Rectangle	w = 6.42 × 10⁻⁵, t = 1.29 × 10⁻⁵	8.25 × 10⁻¹⁰	1.40	2.60	2.6	117	Ductile Behavior
13	Rectangle	w = 2.80 × 10⁻⁴, t = 3.85 × 10⁻⁵	1.08 × 10⁻⁸	----	1.12	1.2	100	Brittle Behavior
14	Rectangle	w = 1.77 × 10⁻⁴, t = 1.93 × 10⁻⁵	3.42 × 10⁻⁹	----	1.37	1.5	90	Brittle Behavior
			$a_{||}$ - axis Whiskers					
1	Rectangle****	w = 4.5 × 10⁻⁵, t = 1.93 × 10⁻⁵	8.67 × 10⁻¹⁰	0.57	1.31	1.17	238	Ductile Behavior (Slight Necking Evident)

****The cross-sections of $a_{||}$-axis whiskers appeared to be rectangular but there was some indication that included angles might be slightly off from 90°. Necking in ductile whiskers and irregular fracture in the brittle whisker prevented establishing this feature with certainty.

TABLE 1
PAGE 3 OF 4 PAGES

Specimen No.	Geometry of Cross Section	Dimensions of Cross Section (in.)	Area of Cross Section (in.²)	σ_y (Initial Yield Stress) (10⁶ psi)	σ_f (Fracture Stress) (10⁶ psi)	$\varepsilon_{TOT.}$ (Total Strain) (%)	E_m (Measured Young's Modulus) (10⁶ psi)	Remarks
2	Rectangle****	w = 8.68 x 10⁻⁵ t = 2.02 x 10⁻⁵	1.76 x 10⁻⁹	0.71	1.80	1.93	233	Ductile Behavior
3	Rectangle****	w = 6.1 x 10⁻⁵ t = 1.45 x 10⁻⁵	8.84 x 10⁻¹⁰	----	1.06	0.48	222	Brittle Behavior
4	Rectangle****	w = 7.39 x 10⁻⁵ t = 1.61 x 10⁻⁵	1.19 x 10⁻⁹	2.00	2.22	0.70	330	Ductile Behavior
5	Rectangle****	w = 6.75 x 10⁻⁵ t = 1.45 x 10⁻⁵	9.68 x 10⁻¹⁰	0.58	0.75	0.32	250	Ductile Behavior

****The cross-sections of all-axis whiskers appeared to be rectangular but there was some indication that included angles might be slightly off from 90°. Necking in ductile whiskers and irregular fracture in the brittle whisker prevented establishing this feature with certainty.

TABLE 1
PAGE 4 OF 4 PAGES

ANISOTROPIC TENSILE PROPERTIES OF Al$_2$O$_3$ WHISKERS

Orientation	Measured Elastic Modulus* (10^6 lbs./in.^{2})	Initial Yield Stress* (10^6 lbs./in.^{2})	Fracture Stress* (10^6 lbs./in.^{2})	Total Elastic Strain* (%)	Initial Yield Stress** (10^6 lbs./in.^{2})
c-axis	67.0	1.47	1.58	0.95	0.275
a$_I$-axis	180	1.70	3.23	0.95	0.750
a$_{II}$-axis	330	2.0	2.22	0.60	0.570

*The values recorded were obtained from whiskers believed to be of high purity and near structural perfection.

**The values recorded were obtained from whiskers believed to be of high purity but containing potential slip dislocations.

TABLE 2
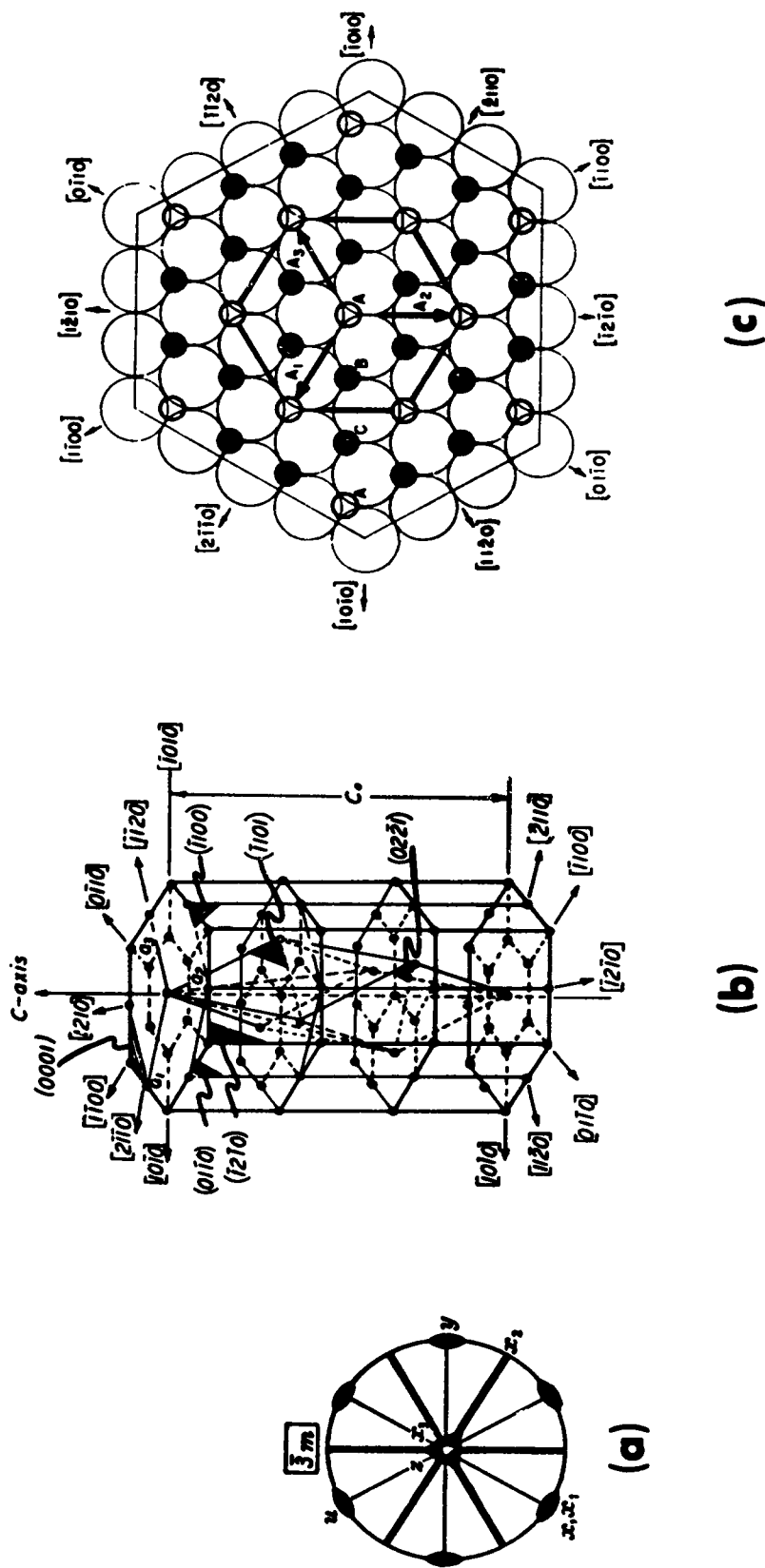
STRUCTURE AND SYMMETRY OF SAPPHIRE (Al_2O_3) - (a) Symmetry elements in point group $\bar{3}m$; diagram shows orthogonal axes used in analyses of crystal properties (Nye, reference 20); (b) Model for crystal structure of sapphire (Kronberg, reference 7); (c) Arrangement of basal layers in sapphire; large open circles are oxygen ions; small solid circles are aluminum ions; small open circles are empty octahedral sites (Kronberg, reference 7).

orientations, $\langle 0001 \rangle$ and $\langle 11\bar{2}0 \rangle$, are i_ _e same proportion as the measured elastic moduli. A rough calcul_ _n of stacking fault energy in basal slip yielded 98 ergs/cm . Jog formation accounts for the high work hardening rates observed in _ress-strain curves.

(b)

(a)
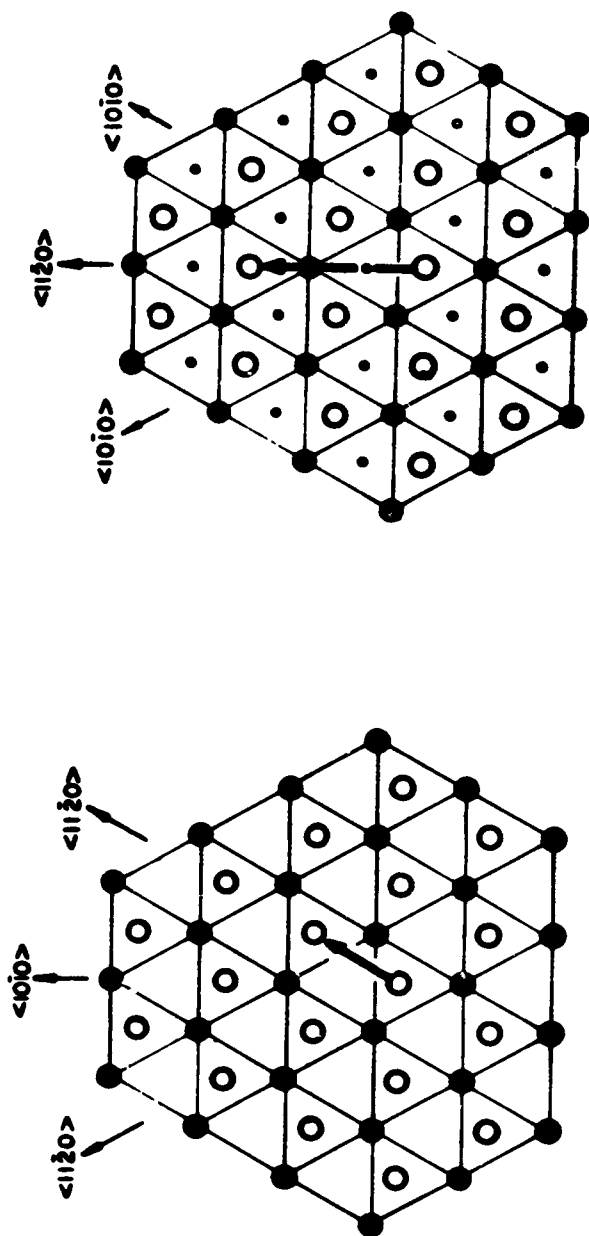
COMPARISON OF ⟨11$\bar{2}$0⟩ SLIP DIRECTIONS IN ZINC AND SAPPHIRE (Kronberg, reference 7) - (a) Zinc; (b) Sapphire; large filled circles represent oxide ions in an underlying basal plane and large open circles represent oxide ions in the plane above; small filled and open circles designate aluminum ions and holes, respectively, lying on the median plane between oxide sheets.

PHOTO NO: CAN-358875(L)-3-64

PLATE 2
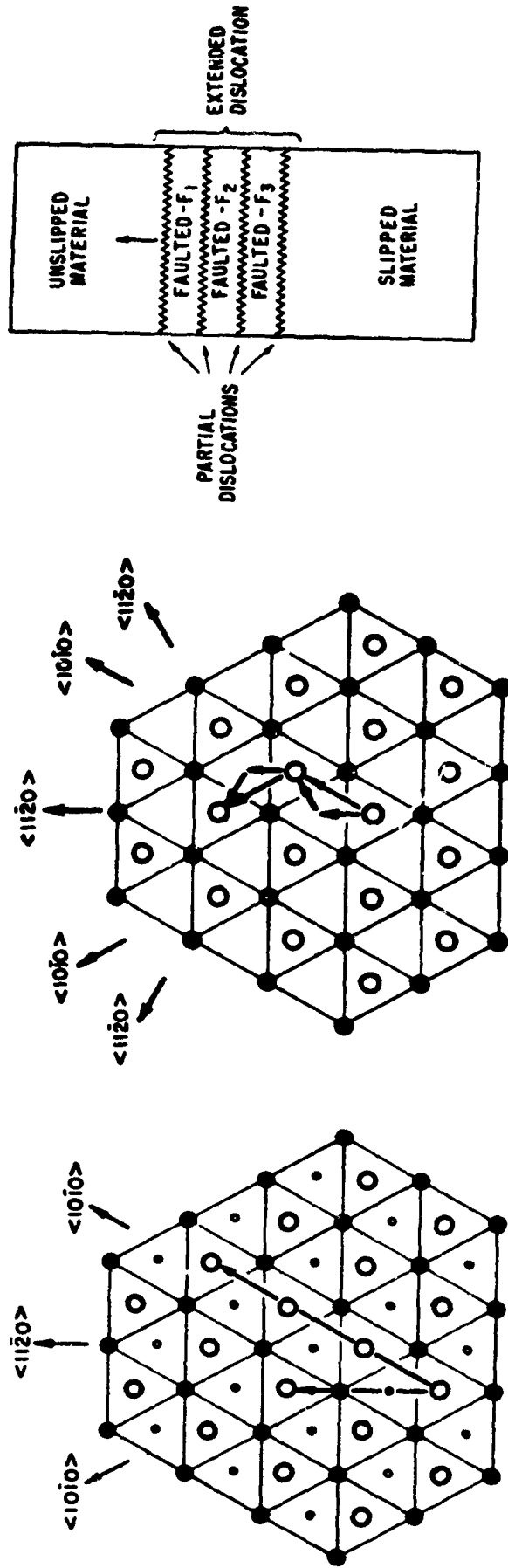
MECHANISM FOR BASAL SLIP IN SAPPHIRE (Kronberg, reference 7); - (a) Comparison of Burgers vectors for $\langle 11\bar{2}0 \rangle$ and $\langle 10\bar{1}0 \rangle$ directions; (b) Splitting of total dislocation with Burgers vector in $\langle 11\bar{2}0 \rangle$ direction into partial dislocations with Burgers vectors $1/3 \langle 10\bar{1}0 \rangle$ and $1/3 \langle 11\bar{2}0 \rangle$; (c) Extended total dislocation as it should appear when actually observed in the crystal.

PLATE 3

PHOTO NO: CAN-358876(L)-3-64

(a)

(b)
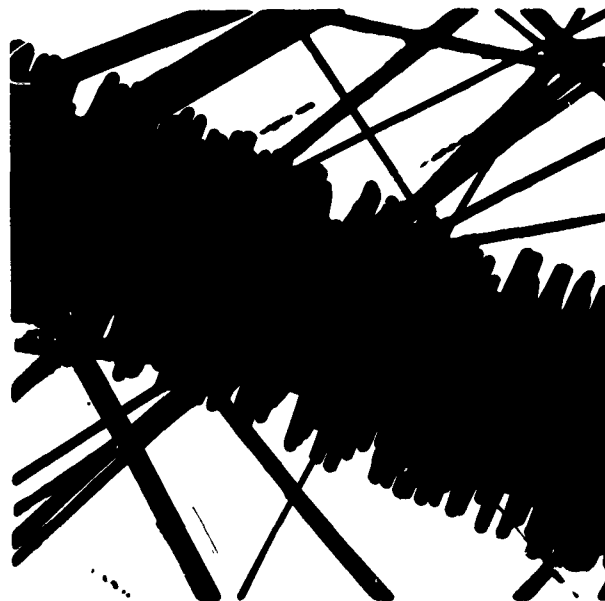
(c)

PICTORIAL DESCRIPTION OF Al$_2$O$_3$ WHISKERS - (a) Sample showing wool-like character of whiskers, 7X; (b) At 40X; (c) Transmission electron photomicrograph showing ultra-fine whiskers; large whisker at center shows many smaller whiskers in the nature of dendrites which nucleated and grew at its edges, 2000X.

PHOTO NO: CAN-358877 (L)-3-64

PLATE 4

WHISKER TENSILE APPARATUS (COMPLETE)

PLATE 6

(b)

(a)
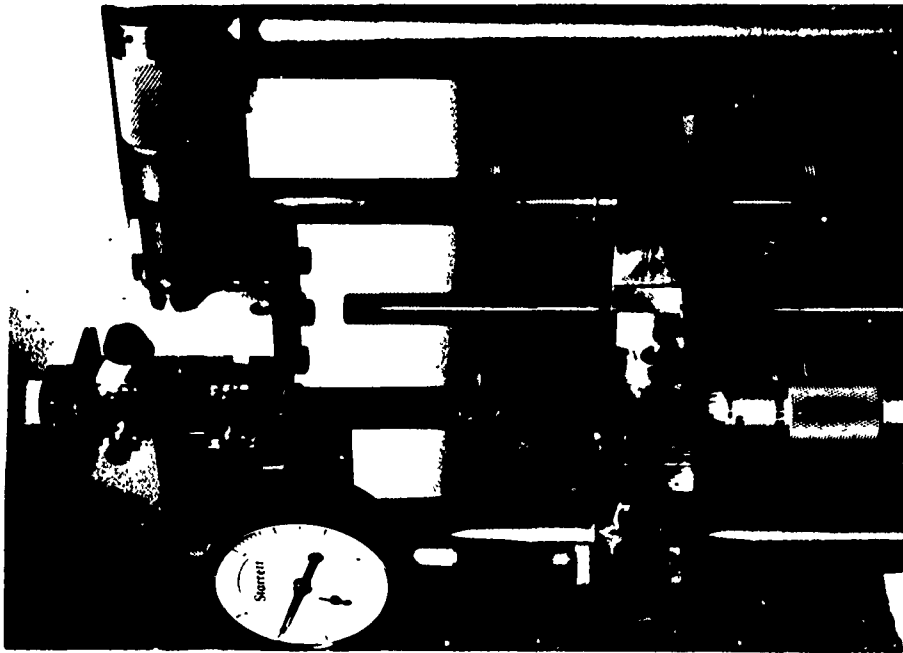
CLOSE-UP VIEW OF WHISKER TENSILE APPARATUS - (a) Loading and load measuring components; (b) Whisker mounting fixture in test frame.

PHOTO NO: CAN-358879(L)-3-64
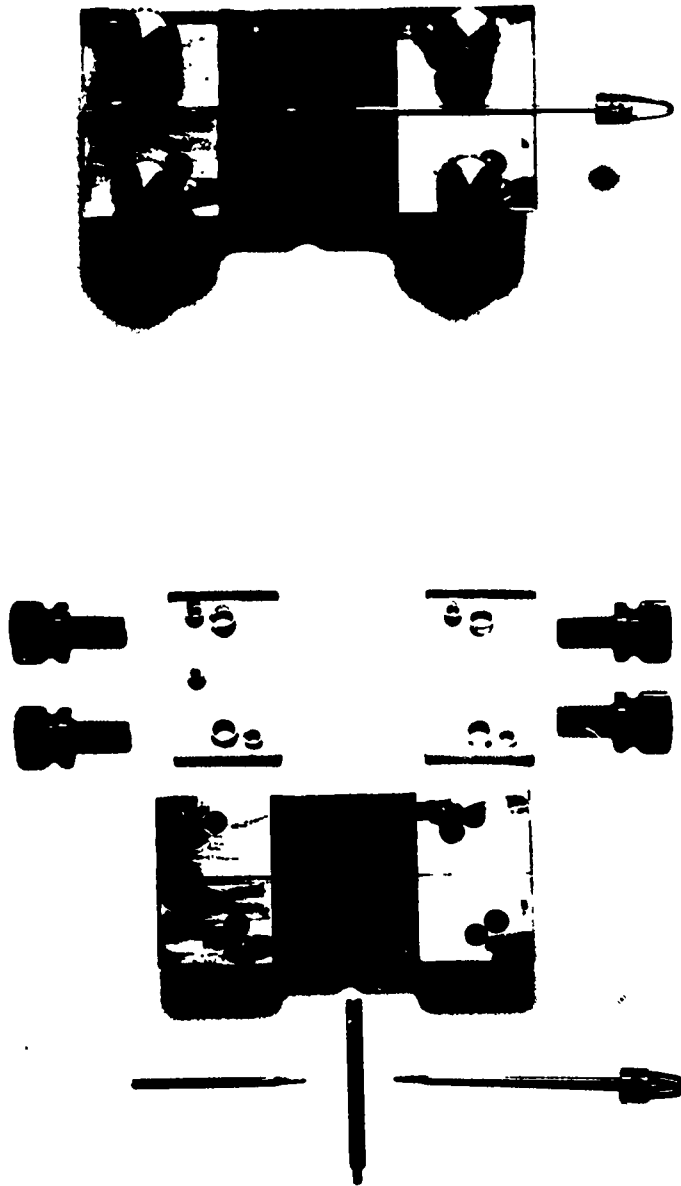
(b)

(a)

WHISKER MOUNTING FIXTURE - (a) Assembly of parts; (b) Assembled fixture with gauge length plate removed.

PHOTO NO: CAN-358880(L)-3-64

PLATE 7

(a)
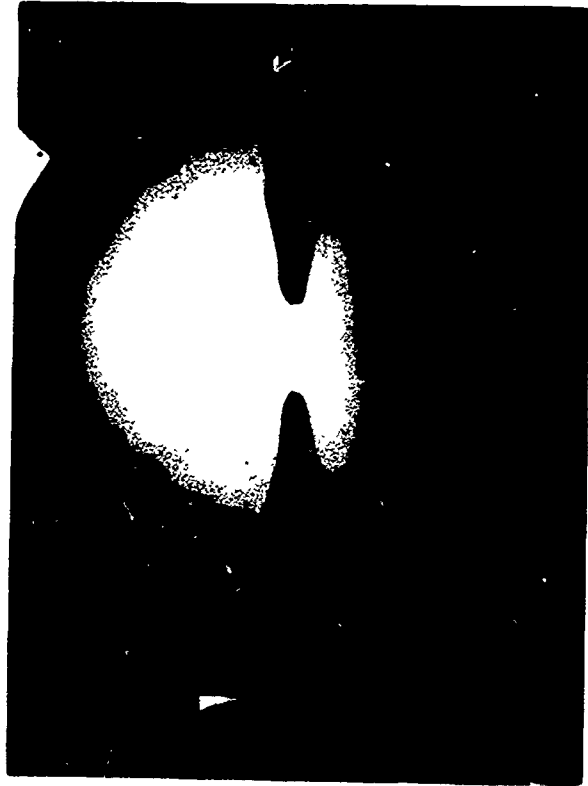
(b)

(c)

MOUNTING AND ALIGNMENT OF WHISKER - (a) Checking alignment of grips on contour projector; grips are magnified 100 times; (b) Nature of bond between whisker and grips; (c) View of whisker mounted on grips before application of cement.

BLANK PAGE
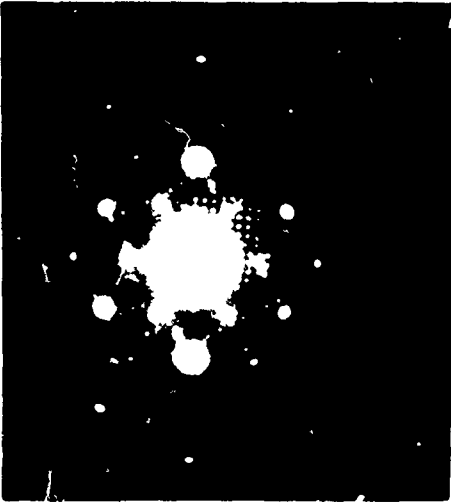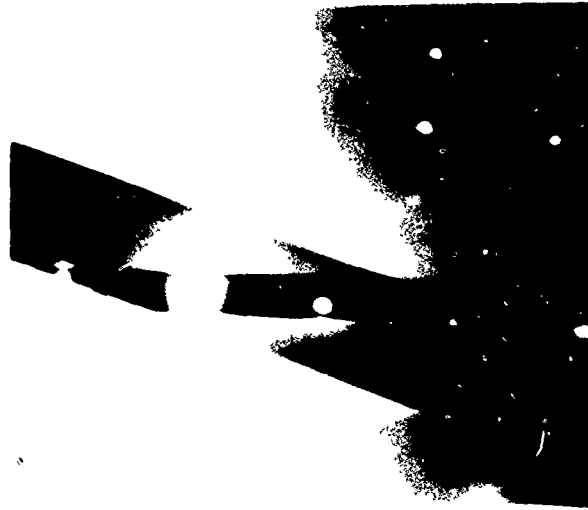
(a)　(b)　(c)　(d)

LAUE ELECTRON DIFFRACTION PATTERNS FOR Al_2O_3 WHISKERS - (a) Thick a-axis whisker; (b) Ultra-thin a-axis whisker; (c) Selected area diffraction from several a-axis, $\langle 11\bar{2}0 \rangle$ orientation, whiskers; (d) Selected area diffraction from a c-axis whisker which rests on top of an a-axis whisker.

PHOTO NO: CAN-358882(L)-3-64

PLATE 9

(c)

(b)

(a)
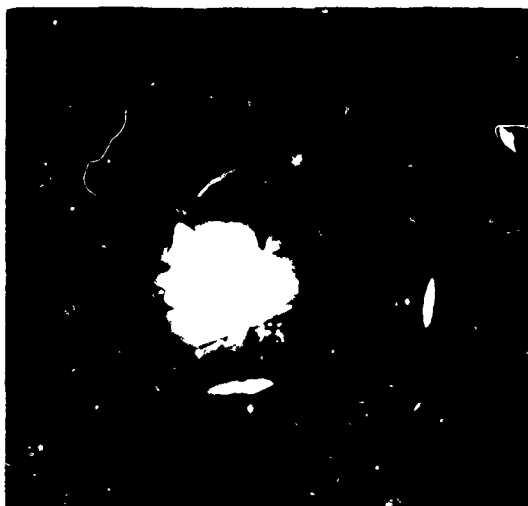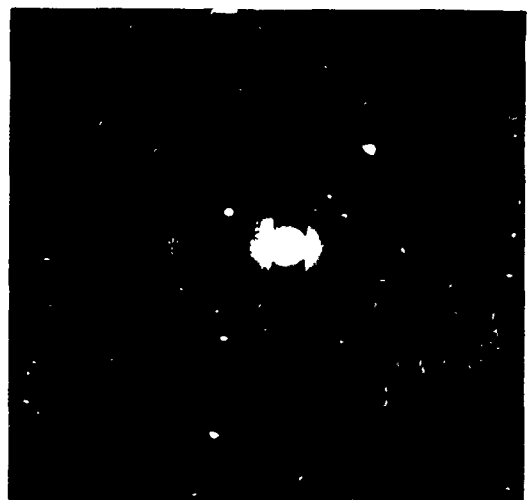
KIKUCHI LINES OBTAINED BY ELECTRON DIFFRACTION FROM STRUCTURALLY PERFECT Al$_2$O$_3$ WHISKERS -

(a) and (b) Diffraction from whiskers located in diffraction chamber of electron miscroscope;

(c) Selected area diffraction from large area face of an a-axis whisker.

PHOTO NO: CAN-358883(L)-3-64

PLATE 10

(b)

(a)

TRANSMISSION ELECTRON PHOTOMICROGRAPHS SHOWING EXTINCTION CONTOURS IN Al_2O_3 WHISKERS - (a) Extinction bend contours are numerous in whisker on right, 33,000X; (b) Bulging; i.e. longitudinal plus transverse bending results in thickness contours in whisker running from top left to right center, 33,000X.

PHOTO NO: CAN-358884(L)-3-64

PLATE 11

(b)

(a)

TRANSMISSION ELECTRON PHOTOMICROGRAPHS OF BENT Al_2O_3 (a-axis) WHISKER WITH MAXIMUM TENSILE STRESS IN THE BROAD FACE - (a) Shows array of stacking faults and growth defects, 33,000X; (b) Shows enlargement of area at top right in (a); Two four-fold stacking fault ribbons are located at center and a two-fold stacking fault ribbon at top.

PHOTO NO: CAN-358885(L)-3-64

PLATE 12

TRANSMISSION ELECTRON PHOTOMICROGRAPHS OF Al_2O_3 WHISKERS SHOWING NUMEROUS GROWN-IN STACKING

DEFECTS - (a) c-axis whisker ; 33,000X; (b) a-axis whiskers; 33,000X.

PHOTO NO: CAN-358886(L)-3-64

PLATE 13

TRANSMISSION ELECTRON PHOTOMICROGRAPHS SHOWING NATURE AND BEHAVIOR OF DEFECTS IN BENT Al_2O_3 WHISKERS HAVING MAXIMUM TENSILE STRESS IN A LATERAL FACE - (a) a-axis whisker; 10,000X; (b) Enlargement of (a); (c) c-axis whisker; 10,000X; (d) Enlargement of defect at right in (c).

PHOTO NO: CAN-358887(L)-3-64

PLATE 14
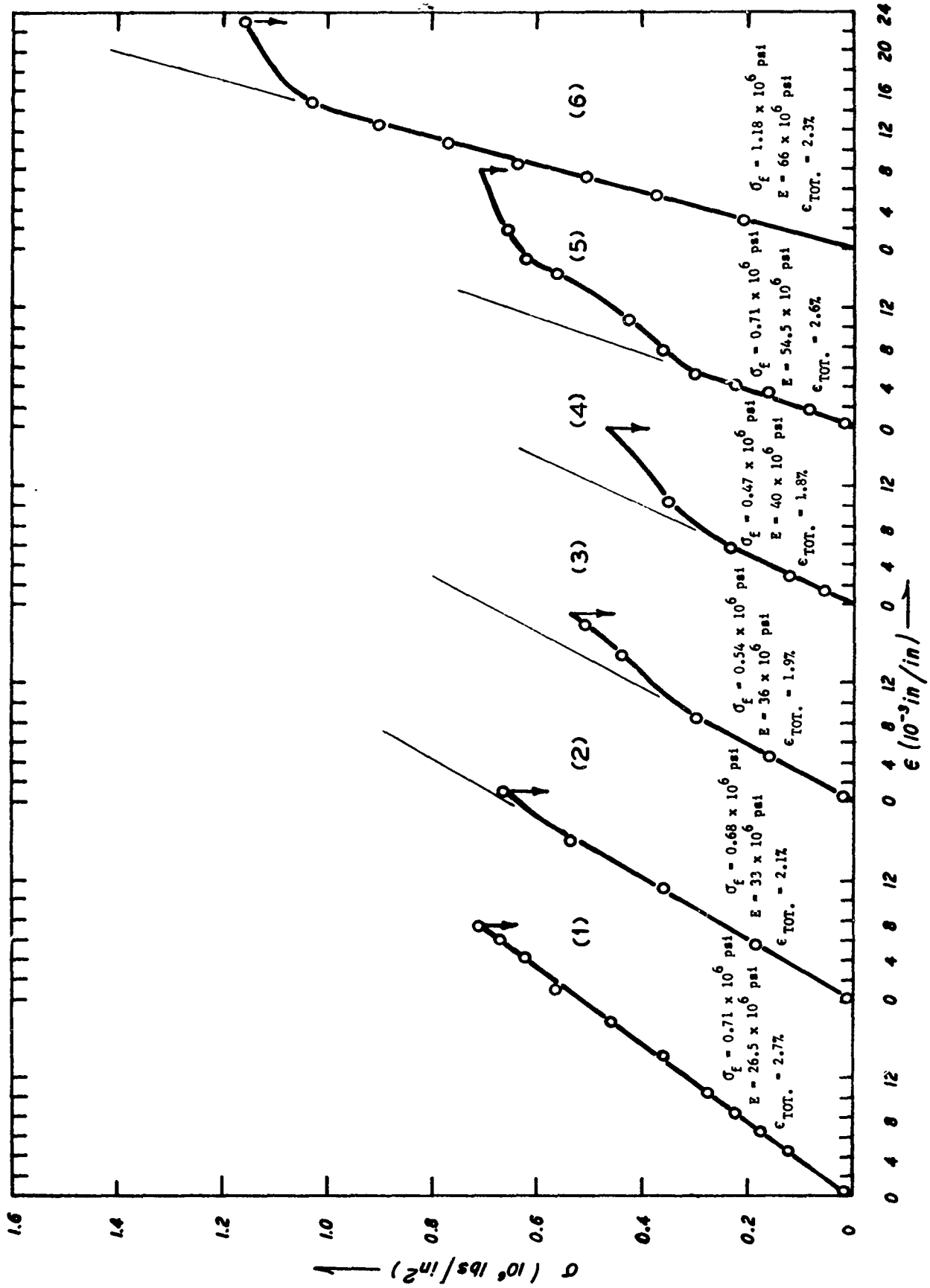
RANGE OF TENSILE STRESS-STRAIN CURVES FOR Al_2O_3 (c-axis) WHISKERS

PLATE 15

PHOTO NO: CAN-358888(L)-3-64
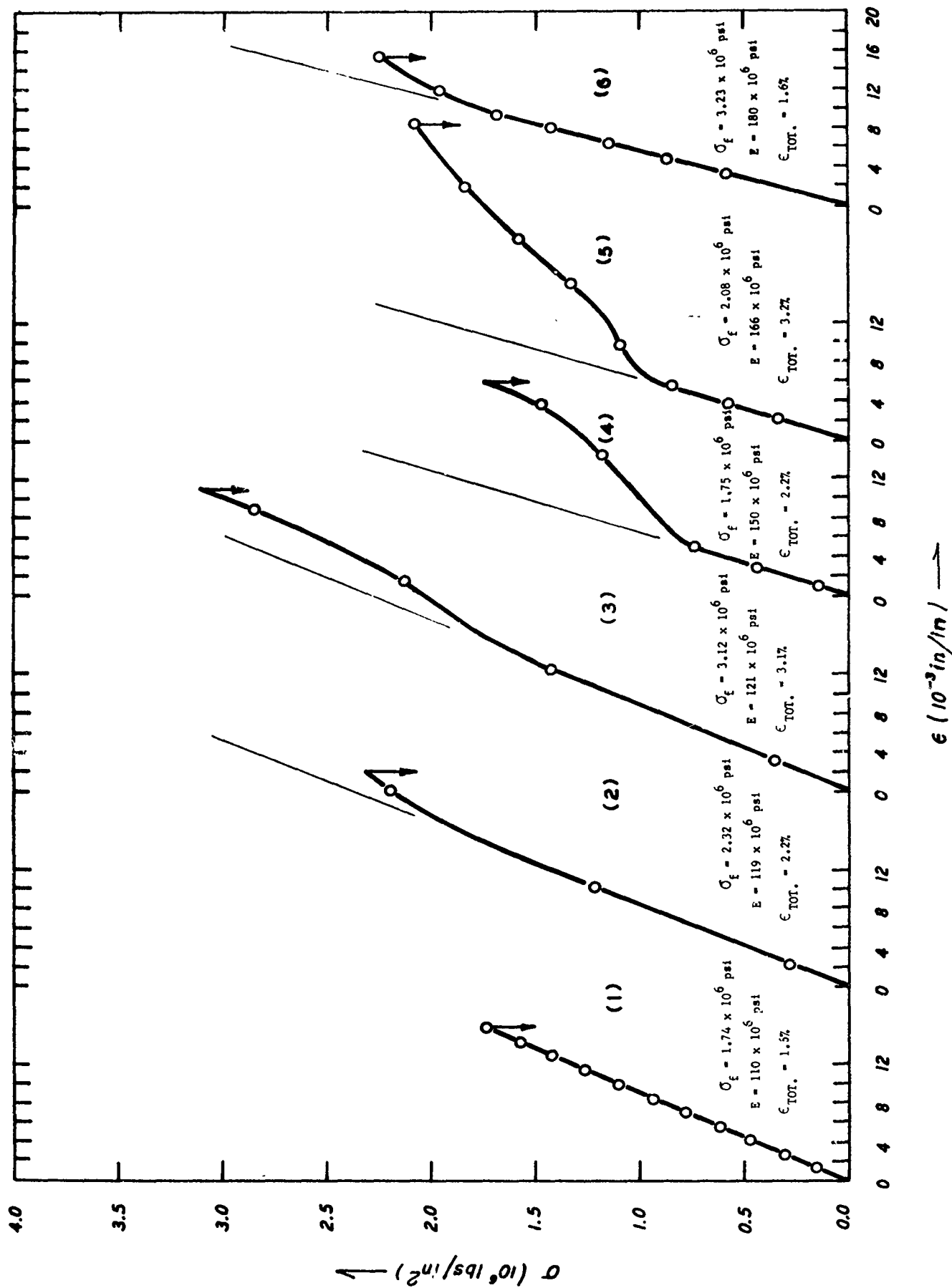
RANGE OF TENSILE STRESS-STRAIN CURVES FOR Al_2O_3 (a_I-axis) WHISKERS

PLATE 16

PHOTO NO: CAN-358889(L)-3-64
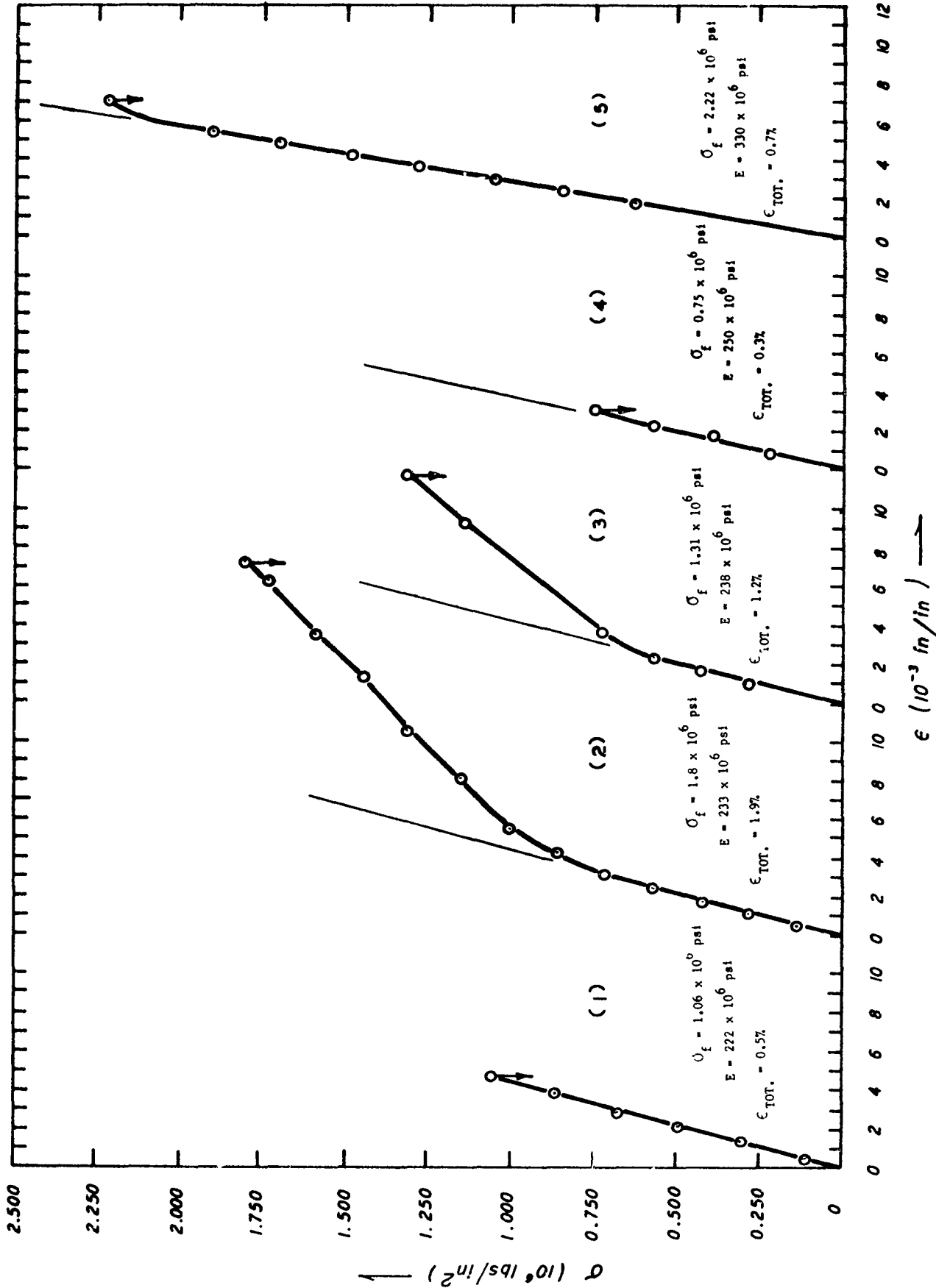
RANGE OF TENSILE STRESS-STRAIN CURVES FOR Al_2O_3 $(a_{II}$-axis) WHISKERS

PLATE 17
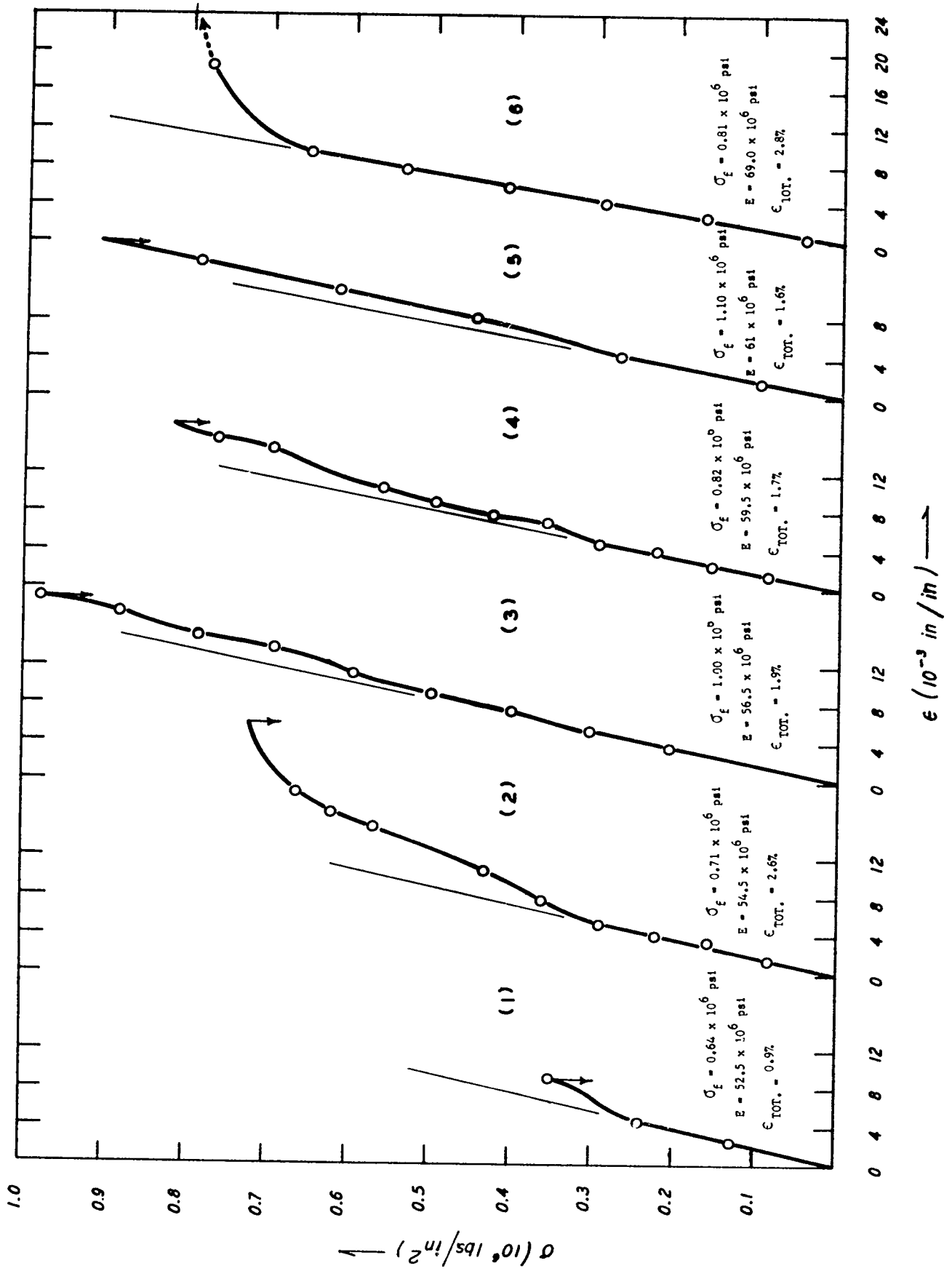
DISCONTINUOUS YIELDING IN Al_2O_3 (c-axis) WHISKERS

PHOTO NO: CAN-358891(L)-3-64

PLATE 18

LOG-LOG PLOTS OF σ_f VERSUS t FOR Al_2O_3 WHISKERS - (a) c-axis whiskers

PLATE 19

LOG-LOG PLOTS OF σ_f VERSUS t FOR Al_2O_3 WHISKERS - (b) a_I-axis whiskers

PLATE 19

PHOTO NO: CAN-358893(L)-3-64

LOG-LOG PLOTS OF σ_f VERSUS A FOR Al_2O_3 WHISKERS - (a) c-axis whiskers

PLATE 20

LOG-LOG PLOTS OF σ_f VERSUS A FOR Al_2O_3 WHISKERS - (b) a_I-axis whiskers

PLATE 20

PHOTO NO: CAN-358895(L)-3-64

LOG-LOG PLOTS OF E_m VERSUS t FOR Al_2O_3 WHISKERS - (a) c-axis whiskers

PLATE 21

PHOTO NO: CAN-358896(L)-3-64

PLATE 21

LOG-LOG PLOTS OF E_m VERSUS t FOR Al_2O_3 WHISKERS - (b) a_I-axis whiskers

PHOTO NO: CAN-358897(L)-3-64

LOG-LOG PLOTS OF E_m VERSUS A FOR Al_2O_3 WHISKERS - (a) c-axis whiskers

PLATE 22

PHOTO NO: CAN-358898(L)-3-64

LOG-LOG PLOTS OF E_m VERSUS A FOR Al_2O_3 WHISKERS - (b) a_I-axis whiskers

PLATE 22

PHOTO NO: CAN-358899(L)-3-64
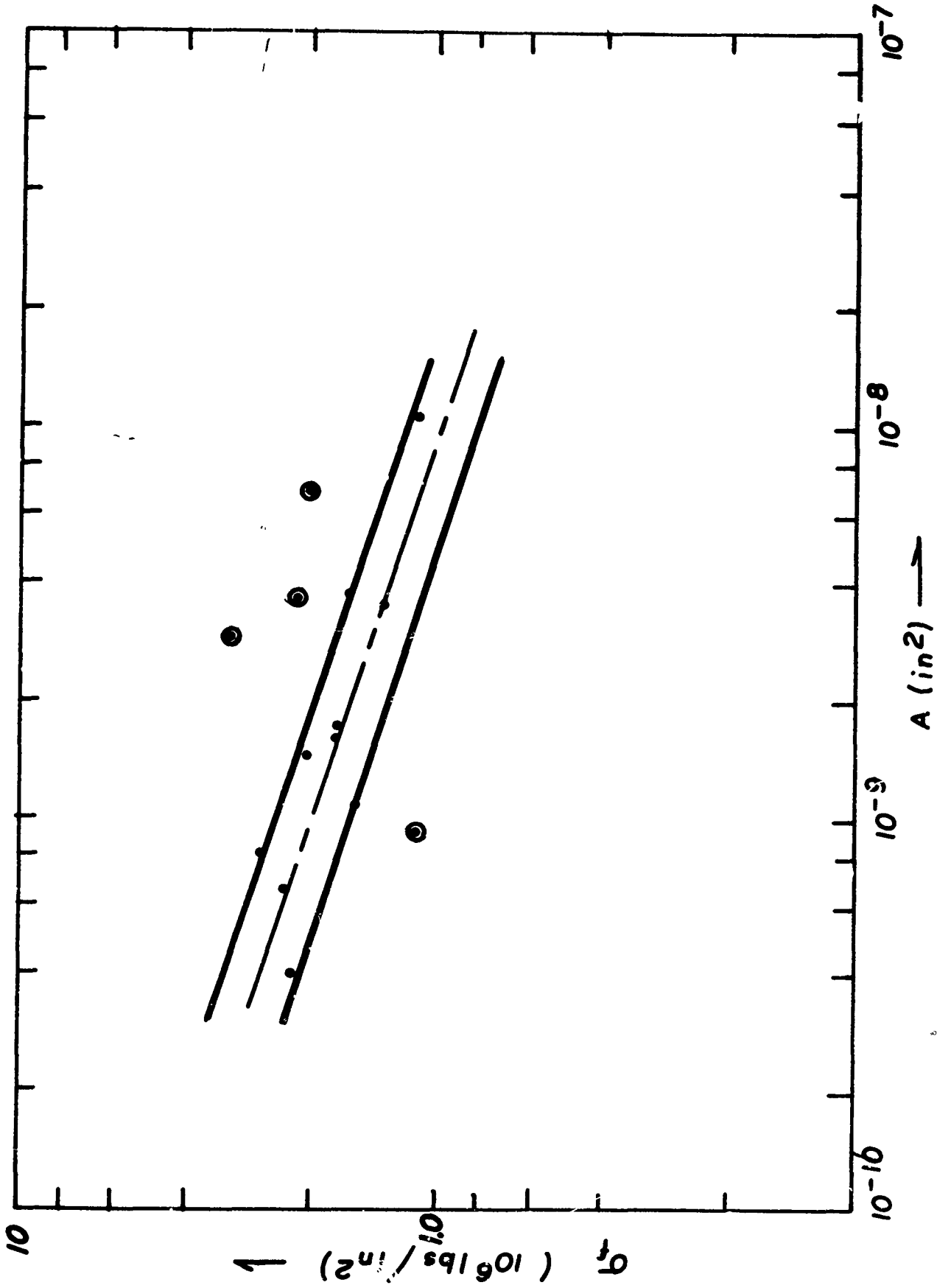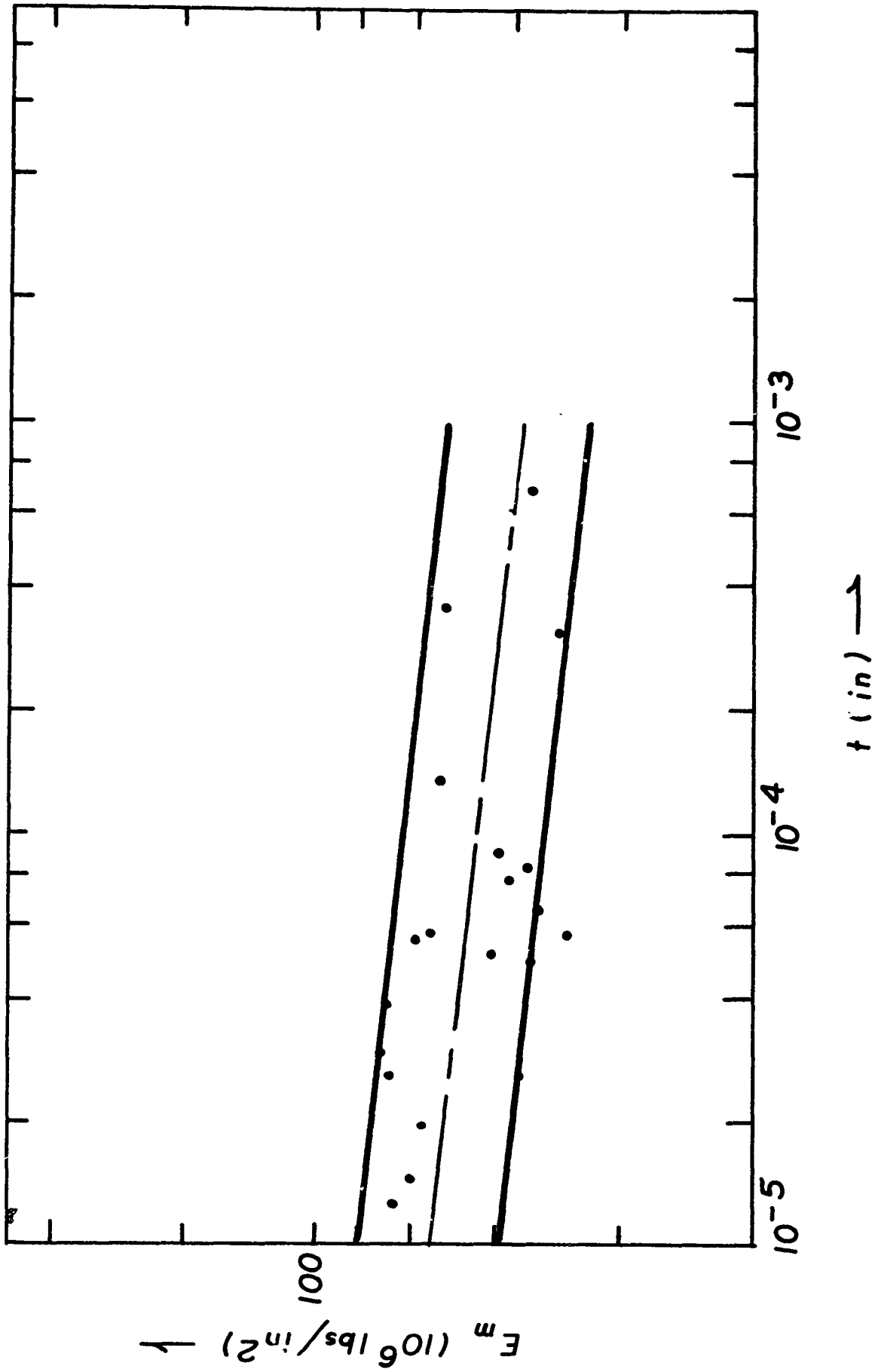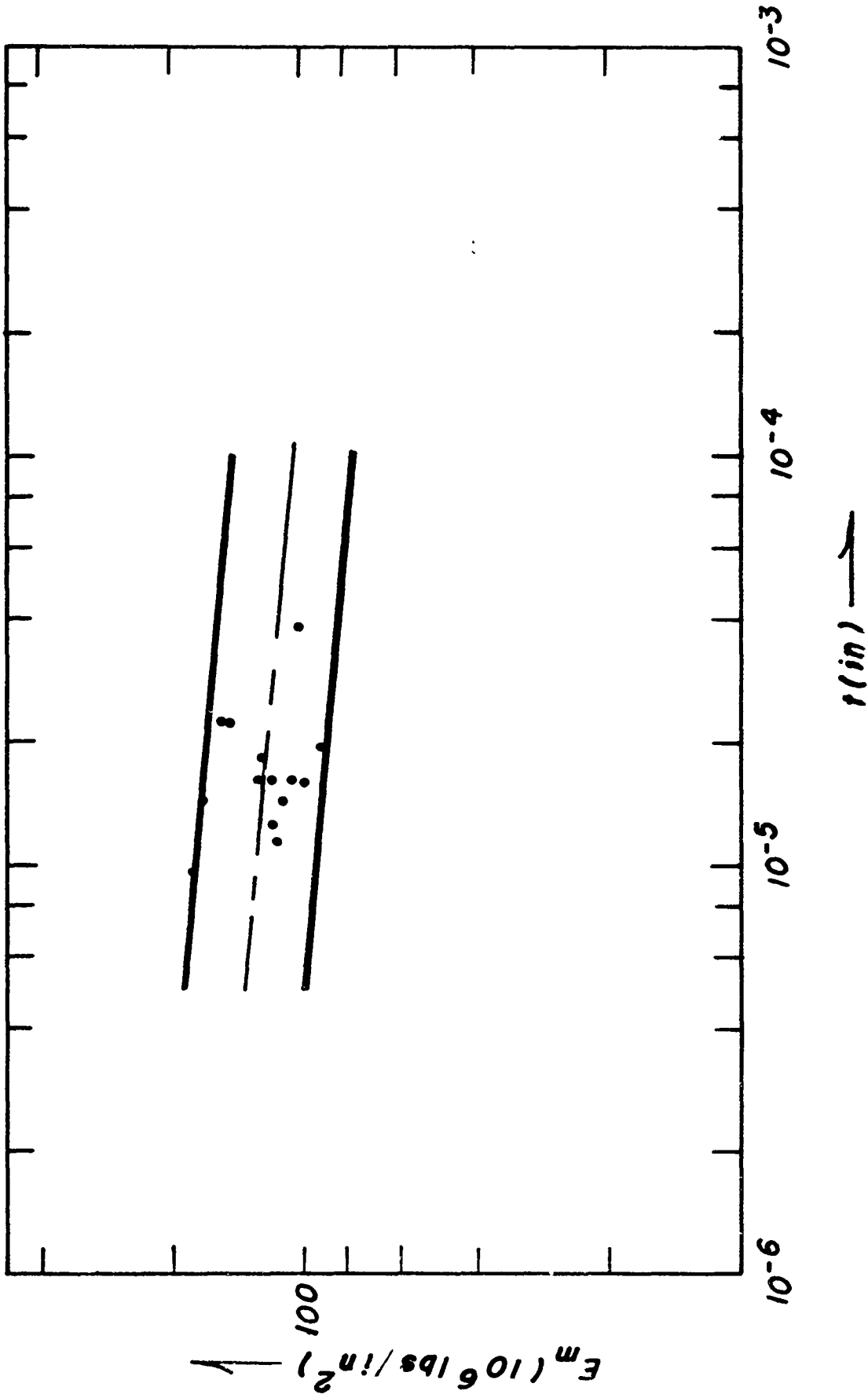
FRACTURES SHOWING GEOMETRY TYPICAL OF Al_2O_3 WHISKERS - (a), (b), and (c) are c-axis whiskers;
(d) and (e) are a-axis whiskers.
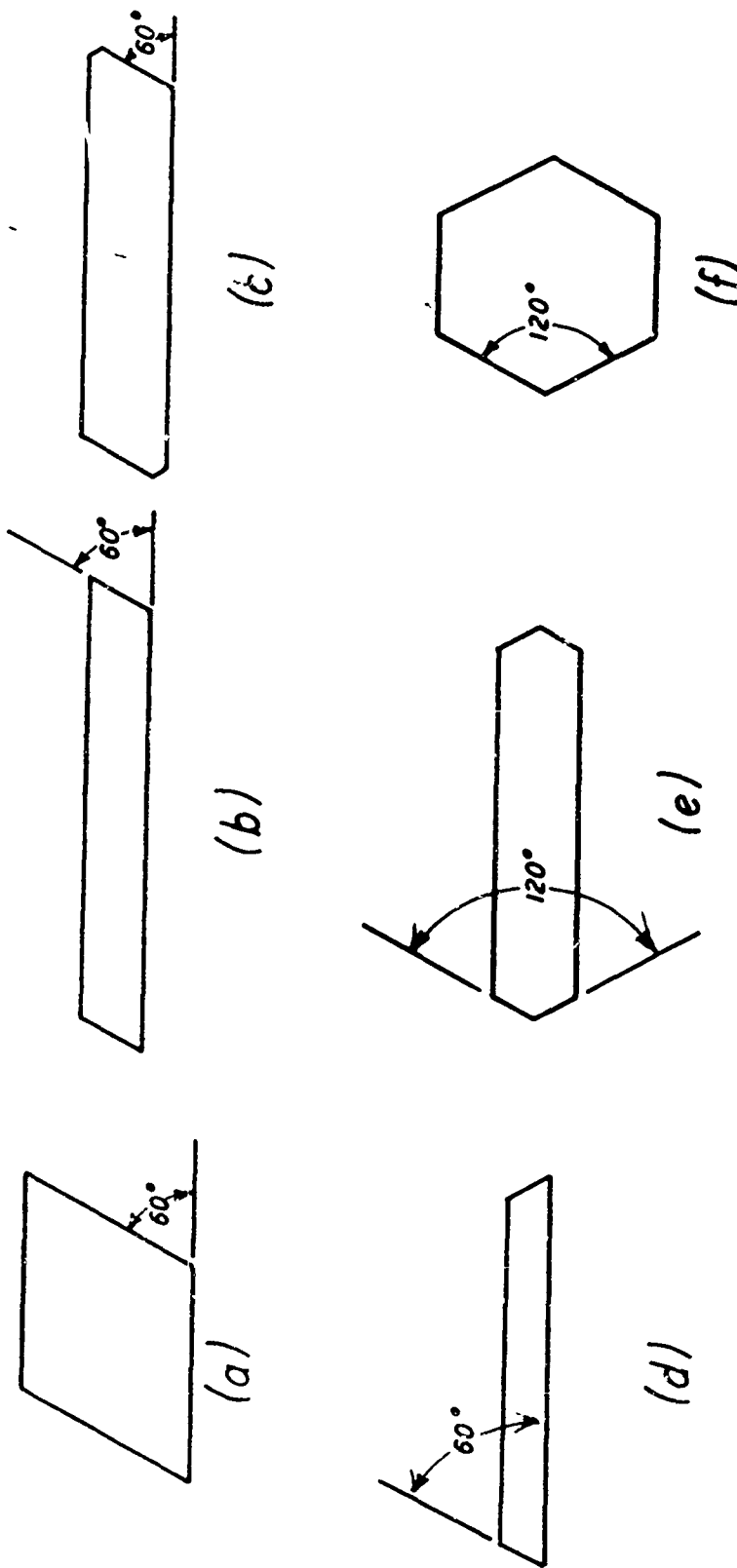
MORPHOLOGY OF VARIOUS Al$_2$O$_3$ (c-axis) WHISKERS

PLATE 24
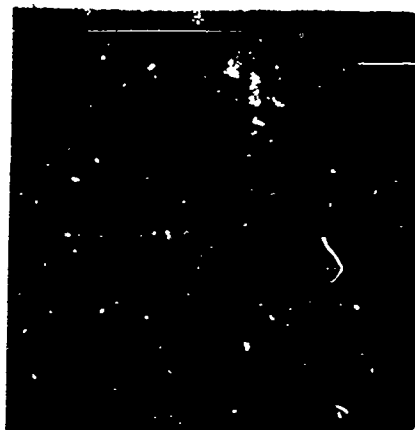
(a)

(b)
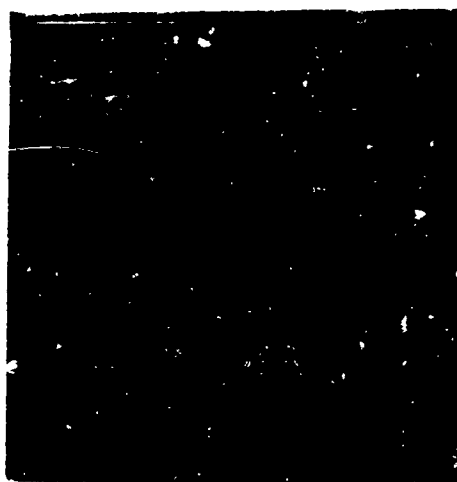
(c)

(d)

CLEAVAGE FRACTURES IN Al_2O_3 (c-axis) WHISKERS - (a) and (b) indicate basal cleavage; (c) shows ductile fracture near one grip while both basal and prismatic cleavage occurred near the other grip in (d).

PHOTO NO: CAN-358902 (L)-3-64

PLATE 25

(a)

(b)

(c)

(d)

(e)

(f)
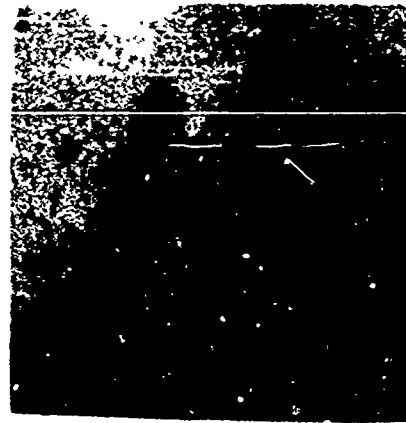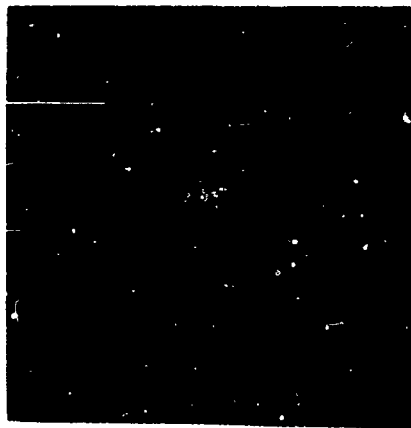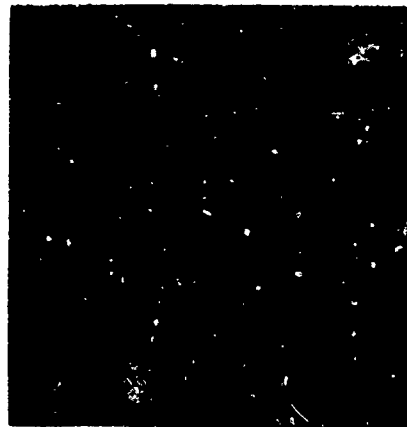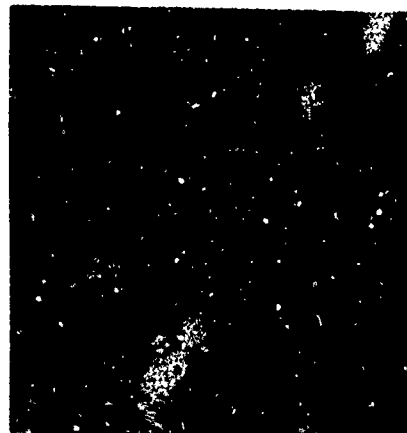
PLASTICITY IN Al$_2$O$_3$ (c-axis) WHISKERS - (a), (b), (c) and (d) illustrate
the nature of basal slip; (e) indicates intersecting slip; (e) and (f)
show laminated appearance suggesting prismatic slip had occurred.
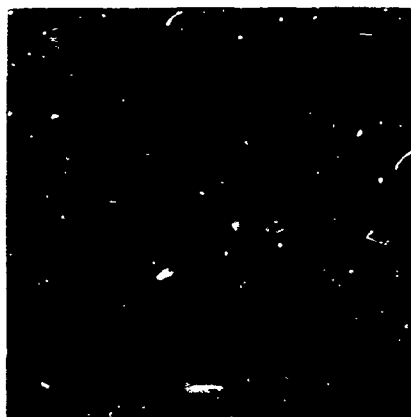
(a)

(b)

(c)

(d)

FRACTURES IN Al_2O_3 (a-axis) WHISKERS

(a)

(b)

(c)

(d)

(e)

(f)
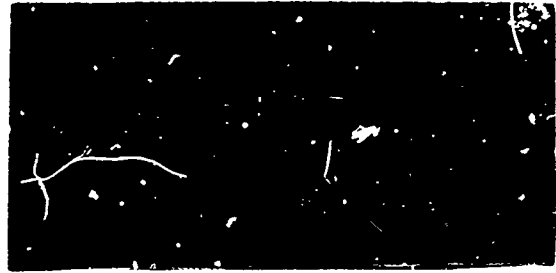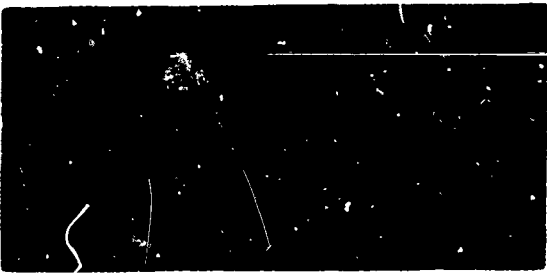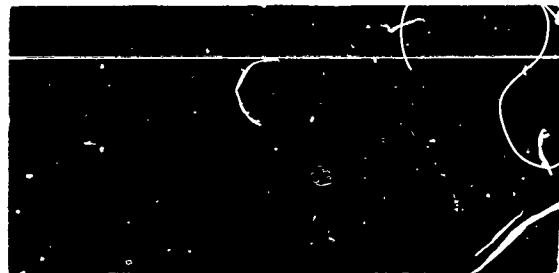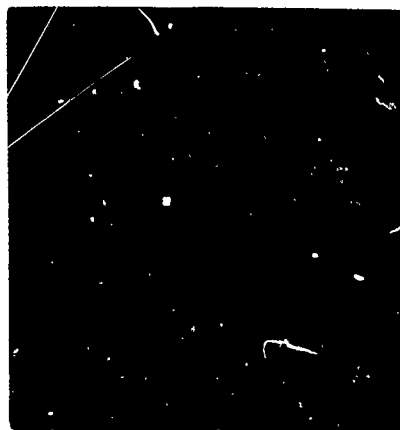
PLASTICITY IN Al$_2$O$_3$ WHISKERS AT 900°C - (a) and (b) c-axis whisker focused at two different points showing necked regions along length of whisker; note curved slip bands at right; (c) and (d) a-axis whisker focused at two different points; note Luders band at right; (e) and (f) show fractures resulting in c-axis whiskers.
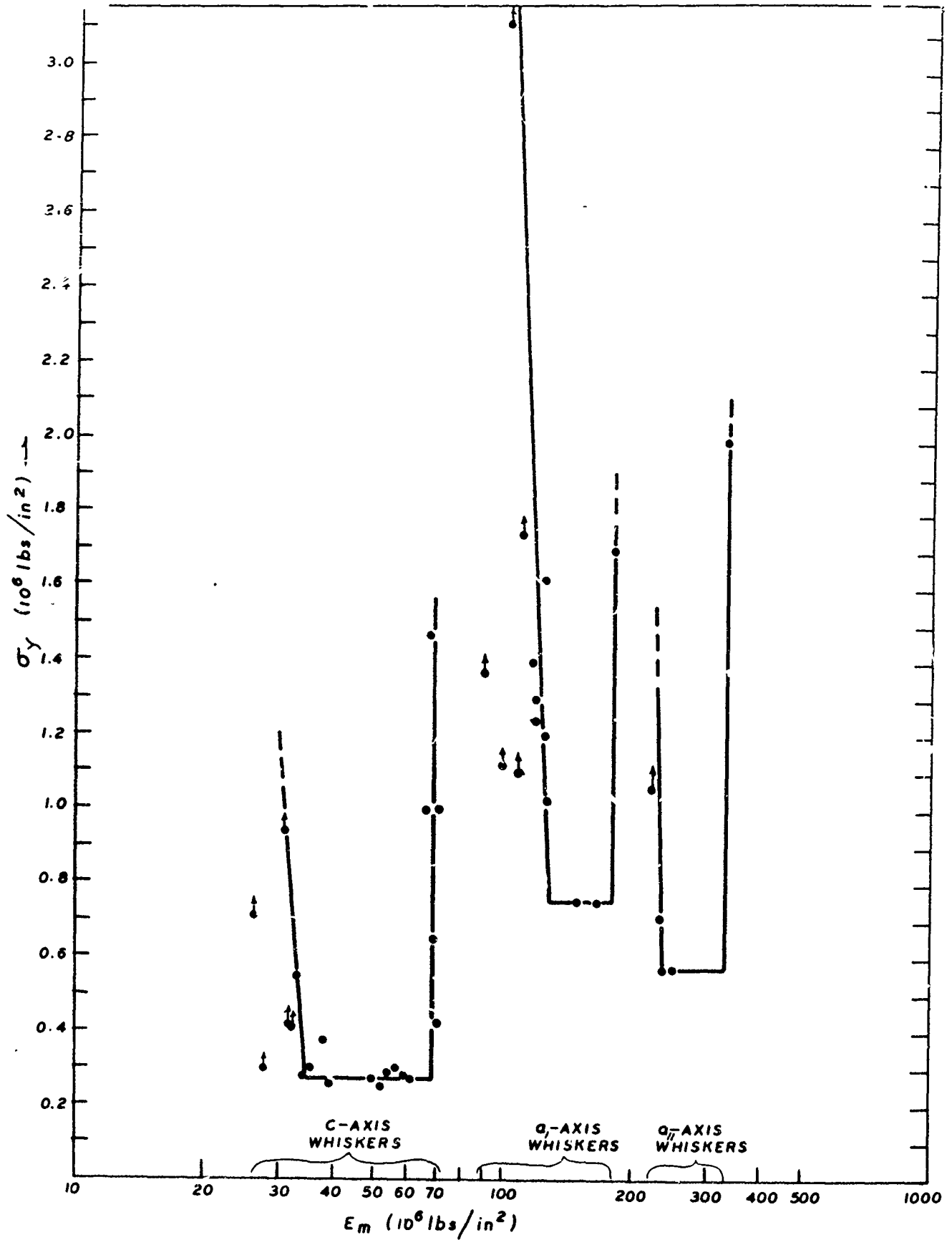
SFM1-LOG PLOT OF σ_y VERSUS Em FOR Al_2O_3 WHISKERS

PHOTO NO: CAN-358906 (L)-3-64

PLATE 29

BLANK PAGE

(a)
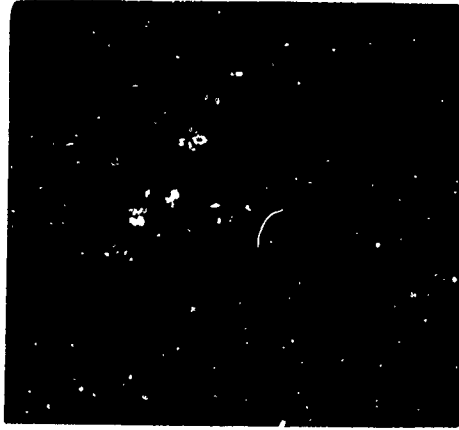
(b)

(c)

FRANK-READ DISLOCATION SOURCE IN FRACTURE SURFACE OF AN Al_2O_3 (c-axis) WHISKER - (a), (b), and (c) are focused at different distances from the fracture surface.

PHOTO NO: CAN-358908(L)-3-64

PLATE 30

O VALUES BASED ON THICKNESS.

• VALUES BASED ON WIDTH.

SIZE (in) ⟶

E_m (10^6 lbs/in^2) ⟵
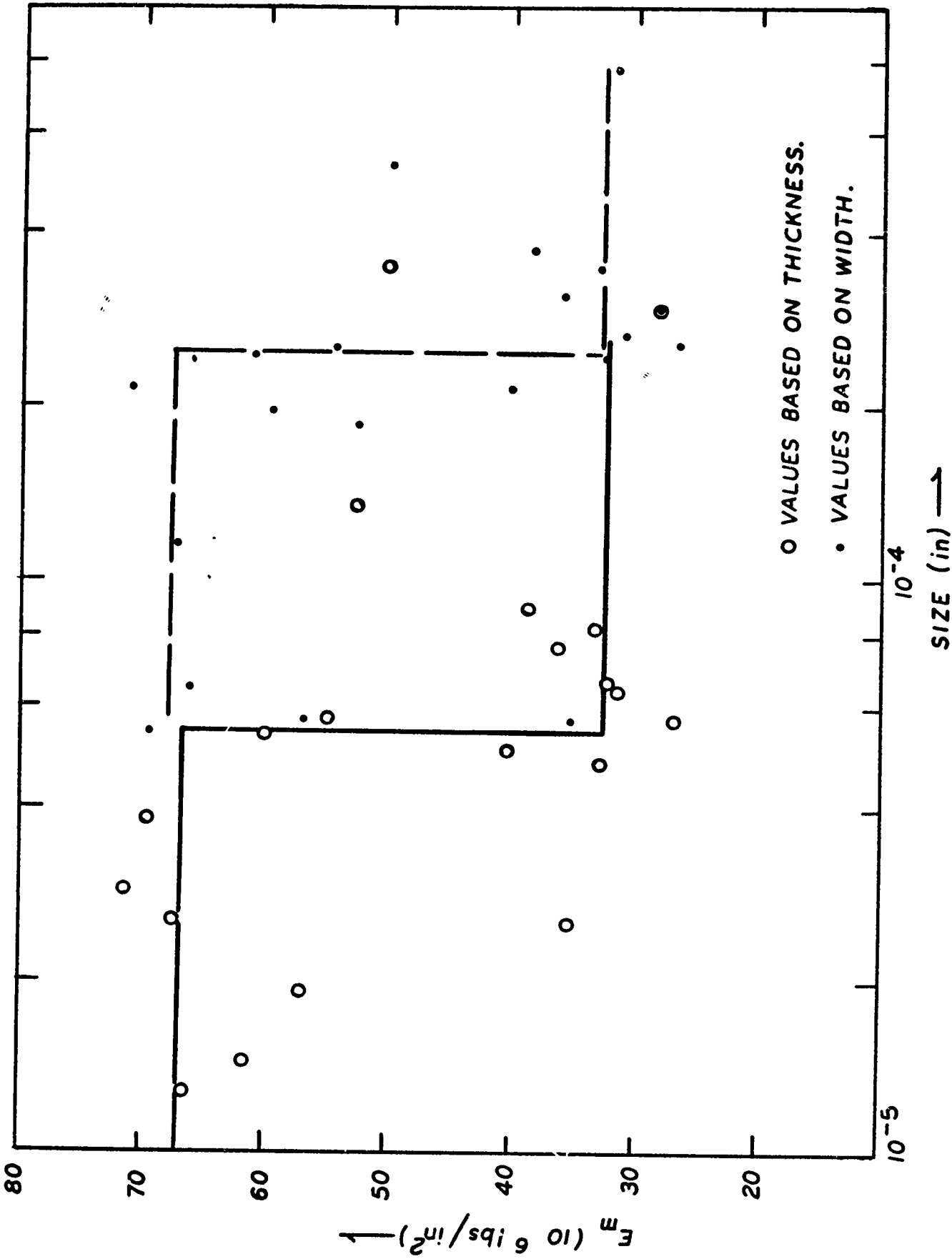
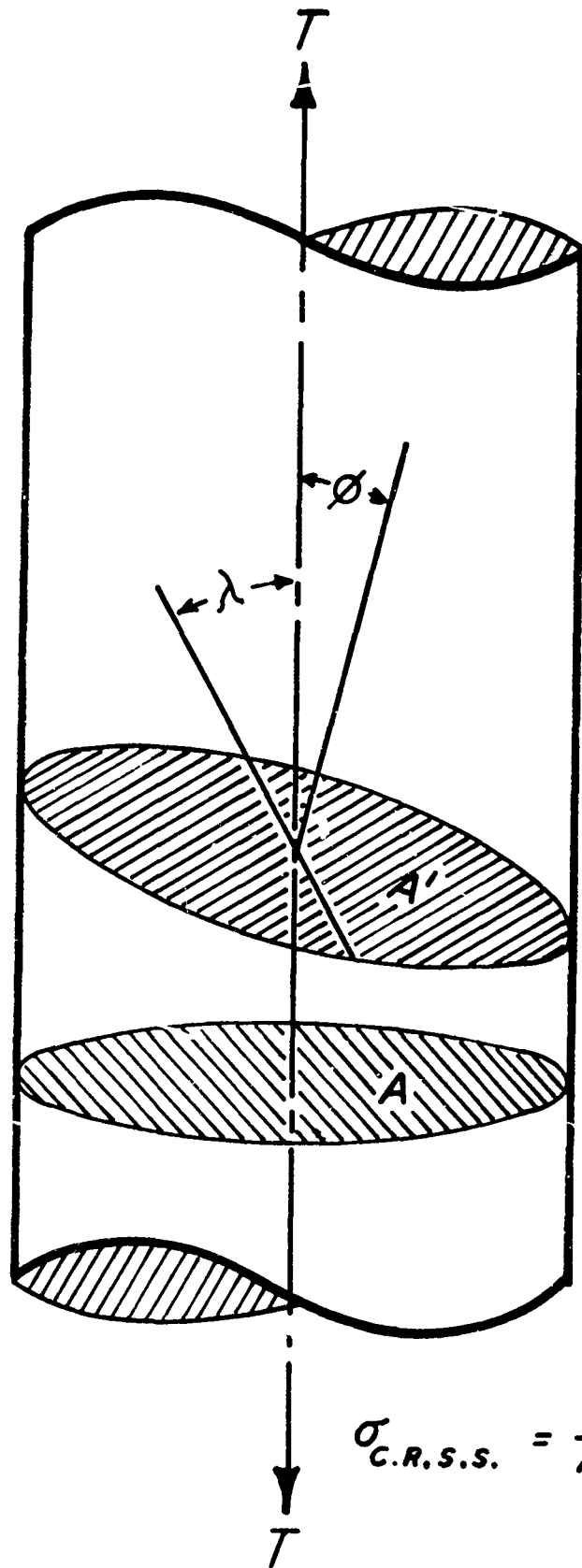SEMI-LOG PLOT OF SIZE VERSUS E_m FOR Al_2O_3 (c-axis) WHISKERS
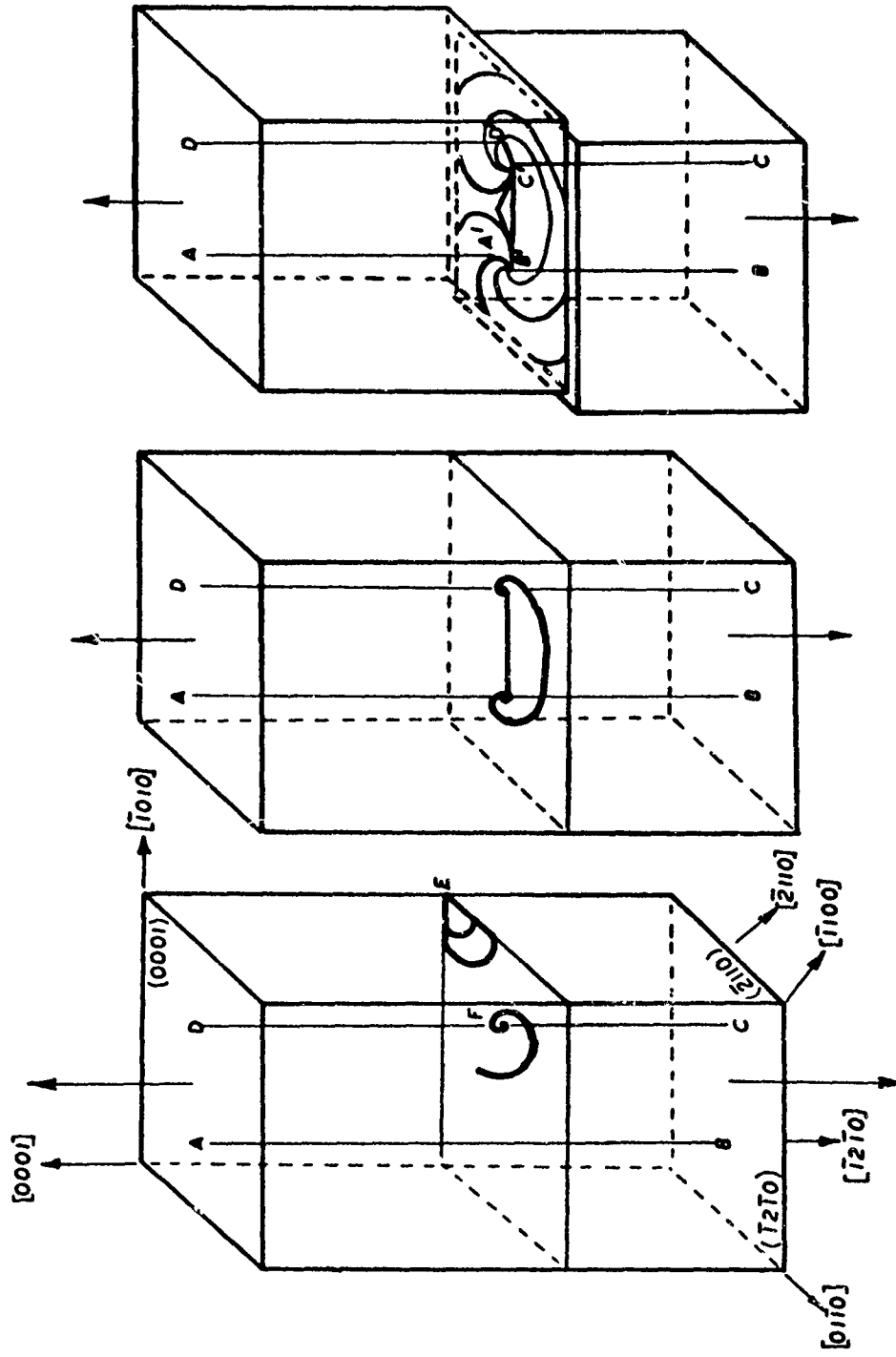
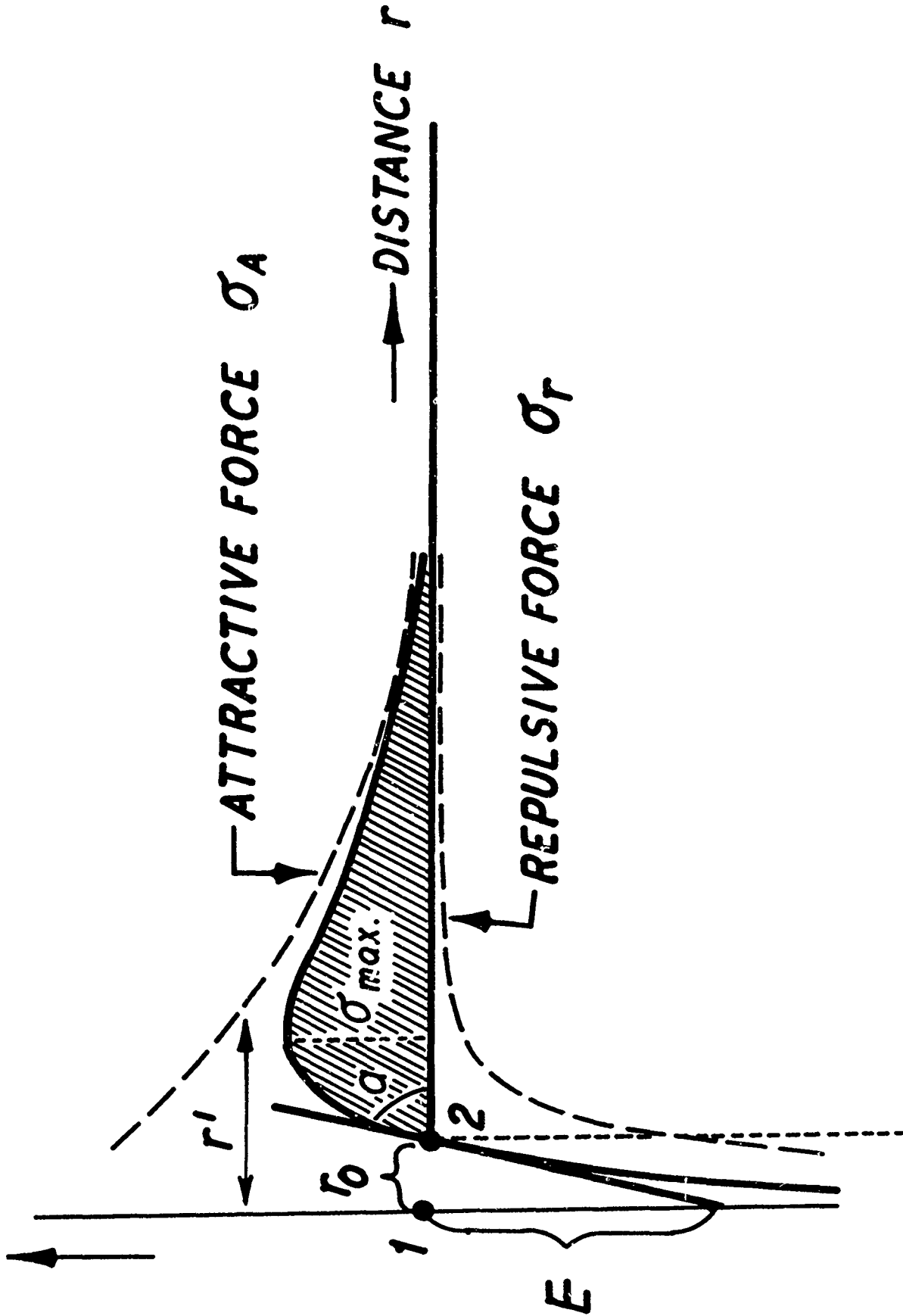DISLOCATION MODEL FOR PLASTIC DEFORMATION IN Al_2O_3 (c-axis) WHISKERS

PLATE 32

(f)

(e)

(d)

DISLOCATION MODEL FOR PLASTIC DEFORMATION IN Al_2O_3 (c-axis) WHISKERS

PLATE 32

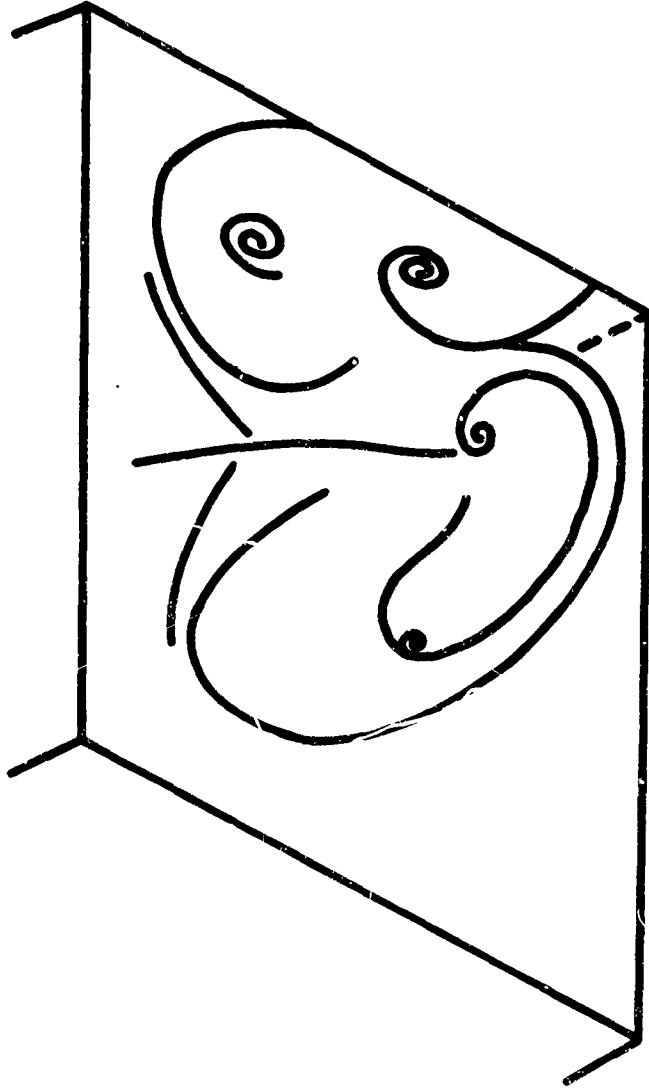$$\sigma_{C.R.S.S.} = \frac{T}{A} \cos \phi \cos \lambda$$
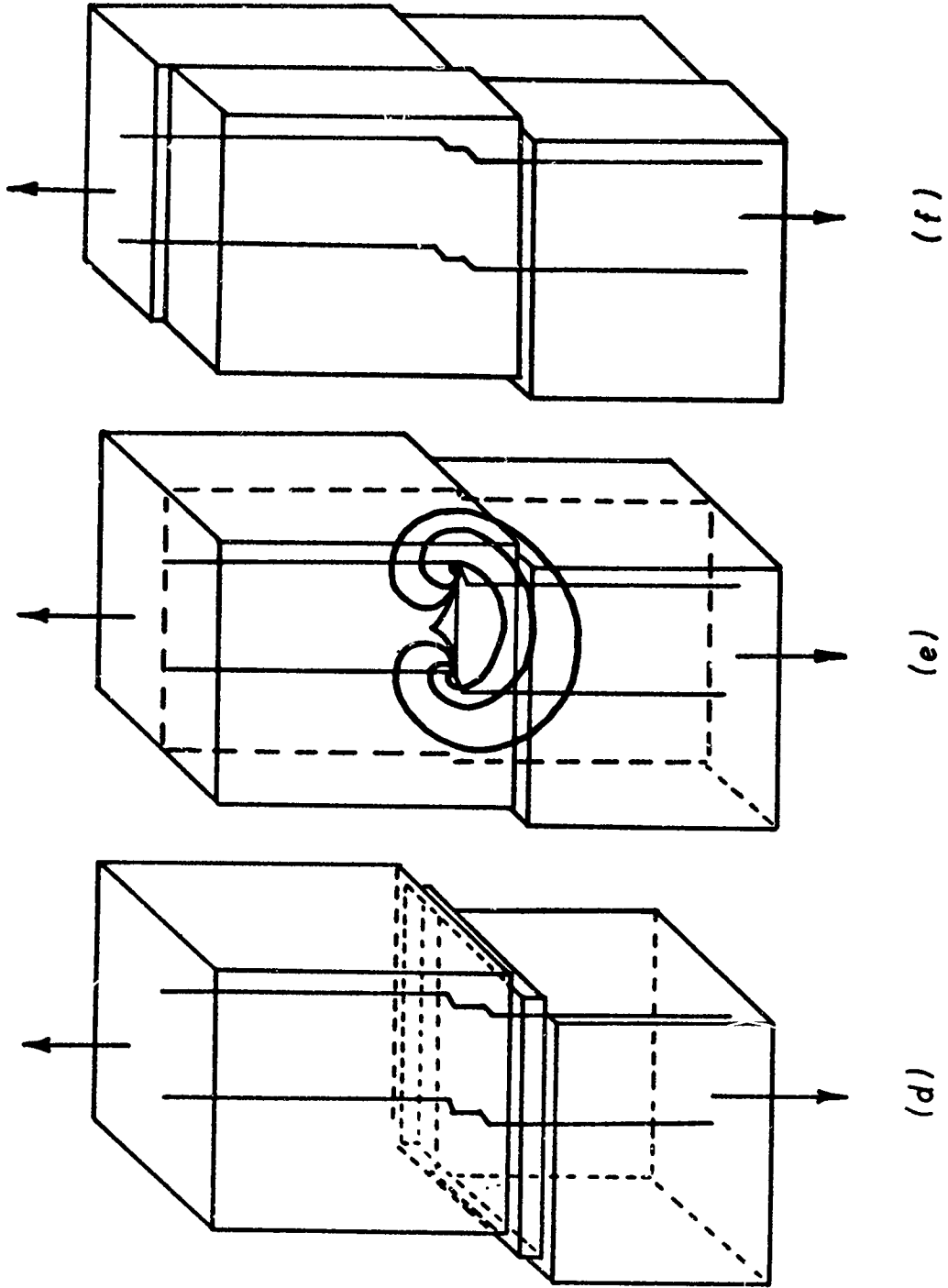
SCHMID'S CRITICAL RESOLVED SHEAR STRESS (Reference 69)

BLANK PAGE

SCHEMATIC REPRESENTATION OF FORCES BETWEEN TWO ATOMS IN A
CRYSTAL (Houwink, reference 73)

SCHEMATIC PATTERN OF F-R SOURCE FOUND IN FRACTURE SURFACE OF AN Al_2O_3 (c-axis) WHISKER

PLATE 35